UNCLASSIFIED

SECURITY CLASSIFICATION OF THIS PAGE (When Data Entered)

REPORT DOCUMENTATION PAGE		READ INSTRUCTIONS BEFORE COMPLETING FORM
1. REPORT NUMBER AFIT/CI/NR 88-30	2. GOVT ACCESSION NO.	3. RECIPIENT'S CATALOG NUMBER
4. TITLE (and Subtitle) ON DERIVING THE THREE-DIMENSIONAL KINEMATIC STRUCTURE OF CONVECTIVE STORMS FROM A SINGLE RADAR		5. TYPE OF REPORT & PERIOD COVERED PhD THESIS 6. PERFORMING ORG. REPORT NUMBER
7. AUTHOR(s) ROBERT MONROE COX		8. CONTRACT OR GRANT NUMBER(s)
9. PERFORMING ORGANIZATION NAME AND ADDRESS AFIT STUDENT AT:		10. PROGRAM ELEMENT, PROJECT, TASK AREA & WORK UNIT NUMBERS
11. CONTROLLING OFFICE NAME AND ADDRESS		12. REPORT DATE 1988 13. NUMBER OF PAGES 142
14. MONITORING AGENCY NAME & ADDRESS (if different from Controlling Office) AFIT/NR Wright-Patterson AFB OH 45433-6583		15. SECURITY CLASS. (of this report) UNCLASSIFIED 15a. DECLASSIFICATION/DOWNGRADING SCHEDULE

16. DISTRIBUTION STATEMENT (of this Report)

DISTRIBUTED UNLIMITED: APPROVED FOR PUBLIC RELEASE

17. DISTRIBUTION STATEMENT (of the abstract entered in Block 20, if different from Report)

SAME AS REPORT

18. SUPPLEMENTARY NOTES

Approved for Public Release: IAW AFR 190-1
LYNN E. WOLAVER
Dean for Research and Professional Development
Air Force Institute of Technology
Wright-Patterson AFB OH 45433-6583

19. KEY WORDS (Continue on reverse side if necessary and identify by block number)

METEROLOGY

20. ABSTRACT (Continue on reverse side if necessary and identify by block number)

ATTACHED

DD FORM 1 JAN 73 1473 EDITION OF 1 NOV 65 IS OBSOLETE

UNCLASSIFIED

SECURITY CLASSIFICATION OF THIS PAGE (When Data Entered)

Robert M. Cox, Capt, USAF

On Deriving the Three-Dimensional Kinematic Structure

of Convective Storms from a Single Radar.

1988

156 page Dissertation for the degree of PhD from

Texas A&M University

ABSTRACT

The objectives of this investigation were to determine the feasibility of deriving vertical velocity patterns, the magnitudes of those patterns, and the three-dimensional wind field in severe convective storms. A technique called Tracking Radar Echoes by Correlation (TREC), also called the NEXRAD Transverse Wind algorithm, and data from a single radar were used to determine the internal storm *motions. The radar data were composed of* National Severe Storms Laboratory (NSSL) Doppler data collected on 19 June 1980.

TREC uses correlation analysis to determine motion within and around a given storm. TREC was used to determine the u and v wind components. These components were gridded using a standard objective analysis technique. It has been shown that in weak reflectivity regions random pattern matching can occur, therefore in areas of reflectivity less than 10 dBZ TREC-derived data were viewed with caution.

Important results of this study are: 1) there was good agreement in both areal extent and magnitude between the TREC-derived vertical velocities and the dual-Doppler velocities; 2) for time increments of 5 min or less between radar volume scans, the horizontal wind field derived by TREC agreed with the dual-Doppler wind field during the multicell and transition phases of the storm; 3) the effects

of the generator level motions on the TREC derived wind field were evident only in the supercell phase and; 4) vertical cross sections indicated regions of updrafts, storm-relative inflows especially in regions of updrafts, updrafts extending through a bounded weak echo region, and an apparent gust front.

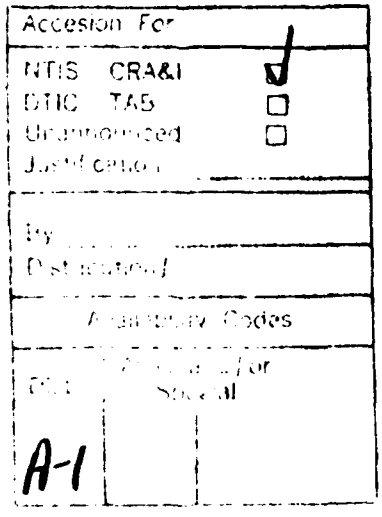

ON DERIVING THE THREE-DIMENSIONAL KINEMATIC STRUCTURE OF CONVECTIVE STORMS FROM A SINGLE RADAR

A Dissertation

by

ROBERT MONROE COX

Submitted to the Graduate College of
Texas A&M University
in partial fulfillment of the requirement for the degree of

DOCTOR OF PHILOSOPHY

May 1988

Major Subject: Meteorology

ON DERIVING THE THREE-DIMENSIONAL KINEMATIC STRUCTURE OF CONVECTIVE STORMS FROM A SINGLE RADAR

A Dissertation

by

ROBERT MONROE COX

Approved as to style and content by:

George L. Huebner, Jr.
(Chairman of Committee)

Kenneth C. Brundidge
(Member)

Phanindramohan Das
(Member)

Rudolf J. Freund
(Member)

Glen N. Williams
(Member)

James R. Scoggins
(Head of Department)

May 1988

ABSTRACT

On Deriving the Three-Dimensional Kinematic Structure

of Convective Storms from a Single Radar.

May 1988

Robert M. Cox, B.S., University of South Florida;

M.S., Saint Louis University

Chairman of Advisory Committee: Dr. George L. Huebner, Jr.

The objectives of this investigation were to determine the feasibility of deriving vertical velocity patterns, the magnitudes of those patterns, and the three-dimensional wind field in severe convective storms. A technique called Tracking Radar Echoes by Correlation (TREC), also called the NEXRAD Transverse Wind algorithm, and data from a single radar were used to determine the internal storm motions. The radar data were composed of National Severe Storms Laboratory (NSSL) Doppler data collected on 19 June 1980.

TREC uses correlation analysis to determine motion within and around a given storm. TREC was used to determine the u and v wind components. These components were gridded using a standard objective analysis technique. It has been shown that in weak reflectivity regions random pattern matching can occur, therefore in areas of reflectivity less than 10 dBZ TREC-derived data were viewed with caution.

Important results of this study are: 1) there was good agreement in both areal extent and magnitude between the TREC-derived vertical velocities and the dual-Doppler velocities; 2) for time increments of 5 min or less between radar volume scans, the horizontal wind field derived by TREC agreed with the dual-Doppler wind field during the multicell and transition phases of the storm; 3) the effects

of the generator level motions on the TREC derived wind field were evident only in the supercell phase and; 4) vertical cross sections indicated regions of updrafts, storm-relative inflows especially in regions of updrafts, updrafts extending through a bounded weak echo region, and an apparent gust front.

DEDICATION

To my loving wife–**Rita**

Without your support I would not have finished. I love you!

ACKNOWLEDGMENTS

I take great pleasure in acknowledging those individuals who have contributed to the successful completion of this effort. My graduate committee deserves to be acknowledged first and foremost. I am indebted to them and appreciated their support and interest. Their doors were always open. Special thanks must go to my chairman, Dr. George Huebner. I could not have asked for a nicer, more supportive mentor. His advice on solving those many problems that seem to occur in a work such as this cannot be over-stated. Also, without his unselfish and unfailing support I might have never finished this project.

I am pleased to recognize fellow students and staff. Discussions with Capt. Mike Walters were very instrumental in the development of a consistent finite differencing technique. Also, discussions with Capt. Jim Schaefer provided insights into the optimization of the interpolation scheme. Mr. David Wolff provided the assistance needed in the inital understanding of the graphics package used by the university computer. Mr. Charles Brenton, Practical Meteorologist, applied his 35+ years of experience to analyze the mesoscale maps presented. He was able to polish them to a level I would have never been able to attain.

A special recognition is due Major Dave Bonewitz. He introduced me to the fundamentals of Doppler weather radar and had the patience with me and my never ending questions. Without his dedication to advancing the state of understanding in Doppler technology I would have never attained the results that follow.

A grateful acknowledgment is made to the staff at the National Severe Storms Laboratory, especially Mr. Ken Wilk and Dr. Ed Brandes. When I was searching for data sets to investigate, they provided valuable suggestions. Also, they provided many helpful hints for analyzing those data sets.

This work was accomplished while the author was assigned to Texas A&M University under the auspices of the Air Force Institute of Technology. This research supports the Next Generation Weather Radar (NEXRAD) program.

Finally, to God, even though I have failed Him, He has never failed me (Psalms 150; Joshua 24:15b).

TABLE OF CONTENTS

TABLE OF CONTENTS (Continued)

LIST OF TABLES

LIST OF FIGURES

LIST OF FIGURES (Continued)

LIST OF FIGURES (Continued)

LIST OF FIGURES (Continued)

CHAPTER I

INTRODUCTION

Overview

In the early 1960's, researchers recognized the ability of the newly developed Doppler radar to help in the observation of the internal kinematics of the thunderstorm (Atlas, 1963; Lhermitte, 1964). Since that time much research has been done using the Doppler weather radar.

Presently, Doppler weather radar has been identified as a tool to enhance the weather forecaster's ability to detect and monitor thunderstorms. A coordinated effort is being made by the National Weather Service (NWS), Federal Aviation Administration (FAA), and the United States Air Force Air Weather Service (AWS) to jointly plan, procure, and operate a new national network of weather radars, which will possess Doppler capability and replace the system currently in use. The program has been named the Next Generation Weather Radar (NEXRAD) program. Along with this new radar technology there has been an explosive development in computer technology which, with proper algorithms, should allow automated analysis of radar data and extraction of pertinent information for use by the meteorologist. According to Doviak and Zrnić (1984) single-Doppler radar offers good promise as a useful operational tool for severe weather warning.

As NEXRAD approaches reality more emphasis is being placed on the development of techniques to analyze the Doppler data in real-time. In this vein, the NEXRAD Joint System Program Office (JSPO) published a series of reports

---

The citations on the following pages follow the style of the *Journal of Atmospheric Sciences*.

documenting existing algorithms and areas needing further research. These areas include analysis techniques for precipitation, turbulence, thunderstorms, and winds (NEXRAD JSPO Staff, 1983; 1984).

Previous Work

General

Ludlam (1963) and Barnes (1976) gave early descriptions of the theory of severe local storms, with Browning and Ludlam (1962) providing an early model of the severe thunderstorm. From these descriptions the meteorologist now classifies thunderstorms into two basic categories, the multicell and the supercell storm.

The multicell storm develops in an ambient wind pattern with light to moderate speed shear and little directional shear. The updrafts tilt very little with height allowing the precipitation to fall through the updraft. The outflow from the precipitation-induced downdraft causes low-level convergence and leads to the development of another cell in a preferred location (Chisholm, 1973; Leary and Houze, 1979). Under certain conditions the multicell storm will undergo extensive development and become a supercell storm (Crawford and Brown, 1972; Vasiloff et al., 1986).

The supercell storm is located in a strongly-sheared environment with the winds usually veering with height. These storms normally move to the right of the mid-level environmental wind. Also, the environmental wind causes the updraft to turn clockwise with height as it slopes over the colder downdraft air (Klemp and Wilhelmson, 1978). The downdraft air originates in the mid-levels and is initiated by the precipitation falling. The surface outflow of the downdraft interacts with

the inflow air of the updraft leading to the formation of the gust front (Goff, 1976). A more complete discussion will follow in the next section.

Multiple-Radar Derived Structure of the Severe Storm

The use of a multiple-Doppler radar system to examine a severe storm event enables the researcher to have an increased areal coverage. Also, the accuracy of the determination of the three-dimensional wind flow is increased, which leads to a more accurate calculation of the internal storm kinematic parameters. This section will review the multiple-Doppler structure of the severe storm.

It is not the purpose of this section to describe how the three-dimensional wind field is reconstructed. The technique is fully described by Armijo (1969), Brandes (1977), Ray et al. (1980), or Doviak and Zrnić (1984). It should be noted that the system of equations used to reconstruct the wind field is different each time another radar is added to the Doppler network. However, Ray et al. (1980) found that the derived horizontal wind field for two to four radars is nearly the same. In fact, the errors were typically less than 3 ms^{-1} for two radars and improved only slightly when compared to the derived field using four radars.

For the calculation of divergence and vorticity, Brandes (1984a, 1984b) found that the errors depended on the storm location relative to the radars and had an uncertainty of $25-50\times10^{-4}$ s^{-1}. This value was based on inspection. He also arrived at three principal conclusions. The first was that vertical vorticity generation in the tornadic thunderstorm results from the tilting of horizontal vorticity. This vorticity is then amplified by pre-existing vorticity and convergence. Next, he found that the vorticity is increased during tornadogenesis by an increase in convergence that comes from the interaction of the rainy downdraft and air inflow. Finally,

after tornado dissipation the vertical vorticity diminishes with height. At this time downdrafts spread throughout the mesocyclone and it becomes increasingly divergent with vertical vorticity rapidly declining.

For the calculation of vertical velocities, the anelastic equation of continuity proposed by Ogura and Phillips (1962) is used. It is solved using finite differencing, which may lead to errors in the calculation of vertical velocities. Vasiloff et al. (1986) stated that uncertainties in the use of this equation result in errors on the order of 5-10 ms^{-1}.

The actual structure of the severe storm has been discussed by many researchers (Browning, 1964; Brandes, 1977, 1984a, 1984b are examples). However, the most detailed work was presented by Lemon and Doswell (1979). They began their discussion by saying that the supercell normally begins as a multicell, non-severe storm. During the initial stage of development a cell on the right rear flank develops a weak echo region (WER). Next, a bounded WER (BWER) forms. This is an indication of increasing water and ice forming around the core of the updraft. At this time the mesocyclone forms. A mesocyclone is defined as a circulation larger than a tornado, that acts as a vorticity-producing source. The average mesocyclone will last for over an hour, and will have a diameter of 5 km or more, a vertical extent of at least 8 km, and an outer rotational velocity across the storm of 23 ms^{-1} or more (Hennington and Burgess, 1981).

As the storm evolves the mesocyclone core is separated from the BWER and is displaced upwind of the BWER. The mesocyclone is now positioned between the updraft and the rear flank downdraft (Brandes, 1978). It descends to the surface along with the rear flank downdraft. At this point the mesocyclone has a basic change in nature. It now has a divided structure with strong cyclonically curved

updrafts in the warm inflow sector to the east and a strong cyclonically curved downdraft in the cool outflow sector to the west. Lemon and Doswell concluded that most tornadoes reach the surface only after the mesocyclone has developed a divided structure.

The final stage of the supercell life is its collapse. This can be seen by increasing radar reflectivity in the BWER. The storm's downdrafts increase while the updrafts decrease. This is the phase in which the strongest downbursts and tornadoes occur.

Prior to tornado touchdown the Doppler data can reveal a small region of strong horizontal shear, the tornado vortex signature (TVS). The TVS first develops in the mid-levels on the upwind side of the BWER and eventually replaces the mesocyclone core. Lemon and Doswell stated that, with the one exception of a weak tornado, each tornado has an associated TVS.

The above discussion was derived from data taken by two or more Doppler radars. However, as mentioned earlier, the NEXRAD program, which will be complete in the early 1990's, will have only single-Doppler coverage (Wilk, 1986). Therefore, the meteorological community needs to intensify its research efforts concerning the analysis of single-Doppler data.

At this time techniques to detect mesocyclones and the TVS with a single-Doppler radar have been developed and tested. Techniques to determine divergence, vorticity, and vertical velocity have been proposed (Wood et al.,1986; Hogue and Zawadzki, 1986); however, these techniques underestimate the magnitude of the desired kinematic parameter and occasionally improperly analyze the pattern. Thus, an effective technique to determine these parameters with a single radar needs to be developed.

Statement of Problem

The objectives of this research were to determine the feasibility of deriving vertical velocity patterns, the magnitudes of those patterns, and the three-dimensional wind field in severe convective storms. A technique called Tracking Radar Echoes by Correlation (TREC) and data from a single radar were used to accomplish the objectives. A correction for raindrop fall velocity was employed in the calculation of vertical velocity magnitudes. The data used in this study were chosen because the kinematic parameters in question have been calculated and published in a multiple-Doppler study (Vasiloff et al., 1986).

Present Status of the Problem

There are presently five potential approaches that attempt to determine the wind field inside a storm using data from a single radar. These approaches are 1) velocity-azimuth display (VAD), 2) velocity-volume processing (VVP), 3) simulated dual-Doppler, 4) echo tracking, and 5) TREC. Of these the first three are based on single-Doppler velocities, whereas, the rest can be used with conventional radar data also. Of the latter two, only TREC can be used in and around convective activity.

Lhermitte and Atlas (1961) first proposed using VAD as a way to obtain the true wind field from single-Doppler radial velocity data. However, this technique is severely limited to operation in a region of a uniform wind field. The statistical regression technique of VVP was originally developed by Waldteufel and Corbin (1979). Once again as in VAD, VVP must be used in a uniform wind field. Another restriction of VVP is that it requires a full volume of data. Echo Tracking computes storm motion, which may provide the environmental winds (Bjerkaas and Forsyth,

1980). This technique is restricted by echo growth and decay. Peace et al. (1969) originally described the simulated dual-Doppler technique. It requires two scans of radial velocity data separated by approximately 5 min. The two scans provide two different views of the storm in question. If the assumption of steady-state is made the two scans should provide the same perspective of the storm as a dual-Doppler analysis at a given instant would provide. This technique was modified by Bonesteele and Lin (1978) to model storm flow. Battan (1973) pointed out that for longer periods of time the steady-state assumption may be unreasonable.

TREC was proposed as a method for determining internal storm motions by Rinehart and Garvey (1978). As mentioned earlier this technique can be used on data from a conventional as well as a Doppler radar. From work accomplished by Rinehart (1979) and Hamidi et al. (1983), TREC was adopted as a possible technique to be implemented in the NEXRAD program (NEXRAD JSPO, 1983).

TREC follows reflectivity patterns rather than air motions and uses correlation analysis to determine the movement of the reflectivity pattern. While tracking reflectivity patterns it is possible to have random matching patterns, thus leading to erroneous vectors, Bonewitz (1986) found that in the case of a significant meteorological event, a gust front, TREC was able to track its movement even though reflectivity values were on the order of 1 dBZ. In general Bonewitz concluded that reflectivity values less than 10 dBZ often lead to erroneous vectors.

Rinehart (1979) studied the effects of grid interval or box size and the success of TREC to accurately model the wind field. He found that with very small box sizes TREC was matching reflectivities, not patterns. With large box sizes the effects of small scale motions decreased and TREC modeled the general motion of the storm. A rapid increase in success rate was found with increasing box sizes from 1 to 4 km.

A general decrease in success was noted beyond 10 km.

Because TREC matches reflectivity patterns, two separate reflectivity fields are needed. When the time increment between reflectivity fields is too large, TREC may not detect air motions, but instead track precipitation generators that are at heights above the analysis level (Hamidi et al., 1983; Smythe and Harris, 1984). However, Bonewitz (1986) claimed he was able to detect the movement of a gust front and, by having a shorter time increment, he was able to restrict the effects of the generator-level motions. This observation agrees with Rinehart (1979), who stated that a tornado would itself never be detected by TREC, but the larger scale rotation might show up quite well since it is several kilometers across. Rinehart also found that the success of TREC to model accurately the wind field decreased after 5 min, thus leading to tracking of the generator-level motions.

Rinehart (1979) concluded his work by mentioning the possible utility of TREC for determining vertical velocity patterns and their magnitude. His primary interest was the derivation of the horizontal wind field at low radar elevation angles. Therefore, he left the area of deriving vertical velocity patterns and their magnitude as future research.

When considering the derivation of vertical velocity values by the use of radar data, care must be taken to include the effects of the terminal fall velocity of raindrops. To do this the raindrop spectra in the thunderstorm needs to be known. Sekhon and Srivastava (1971) did such a calculation and derived an empirical dropsize distribution for a thunderstorm. By using such a distribution the dropsize of a precipitation particle can be calculated from the average radar reflectivity. When raindrops are involved the terminal fall velocity can be calculated by the use of an equation derived by Gunn and Kinzer (1949).The terminal fall velocity of hail

can be calculated from a formula derived by Douglas (1964). Pruppacher and Klett (1980) showed the variation of terminal fall of water drops with the change in drop diameter. With larger raindrops the terminal fall velocity can be as high as 10 ms^{-1} at sea level.

There have been several recent studies that have used multi-Doppler data to determine vertical velocity patterns and their magnitudes in thunderstorms (Brandes, 1977, 1978, 1984a, 1984b; Heymsfield, 1981; Vasiloff and Brandes, 1984; Vasiloff et al., 1986). The data obtained for this study are of the same storm investigated by Vasiloff and Brandes (1984) and Vasiloff et al. (1986), hereafter referred to as VBDR. Therefore, to determine the success of TREC in finding vertical velocity patterns and their magnitudes the results of the VBDR study will be used as ground truth. The other studies will be used to point out areas of interest.

CHAPTER II

SINGLE RADAR DATA AND HANDLING PROCEDURE

Introduction

This research involves the study of weather radar data in and around convective storms. These data require special handling techniques. Therefore, this section will discuss first the radar data, its format, and the various computer programs that were needed to manipulate the data. Once the reader has a fundamental knowledge of the data used in this research, the complete procedure used to evaluate and interpret the computer output will be presented. Thus, the purpose of this chapter is to present the techniques used to solve the objective of this research.

Data Handling

The radar data used in this research were collected using the National Severe Storms Laboratory (NSSL) Doppler radar located in Norman, Oklahoma. This radar is a modified FPS-18 weather radar operating at a wavelength of 10.52 cm. The specific radar parameters can be found in Table 1.

The NSSL Doppler radar system employs a narrow beamwidth of 0.81 deg and uses a dual pulse repetition frequency (PRF) processing system. The dual PRF system allows reflectivity data to be taken during a long pulse repetition period with velocity data taken in a short period at the same time. Thus, one is able to have a longer unambiguous range for reflectivity while keeping the unambiguous range for velocity shorter, resulting in a higher Nyquist interval. Burgess et al. (1978) described how the velocity estimates are effectively positioned in space by comparing the reflectivity and velocity sample. This technique is accomplished

Table 1. NSSL Norman Doppler radar parameters.

PARAMETER	VALUE
General	
wavelength (cm)	10.52
peak power (kW)	750
beamwidth (deg)	0.81
antenna gain (dB)	46.8
antenna rotation rate (deg s^{-1})	6.0
pulse length (μs)	1
radar constant	70.42
Reflectivity	
pulse repetition frequency (Hz)	325
maximum unambiguous range (km)	460
range gate spacing (m)	600
number of range gates per radial	762
Velocity	
pulse repetition frequency (Hz)	1300
maximum unambiguous velocity (m s^{-1})	$\pm$34
maximum unambiguous range (km)	115
range gate spacing (m)	150
number of range gates per radial	762
velocity resolution (m s^{-1})	1
spectral width resolution (m s^{-1})	0.5

electronically within the radar hardware and effectively filters out multiple trip echoes.

Doviak and Zrnić (1984) described the three Doppler moments and how they are computed. The NSSL Doppler radar uses an autocovariance processor called a pulse-pair processor (PPP). A complete description of the PPP can be found in Groginsky (1972) or Doviak and Zrnić (1984). It is sufficient to say that the PPP converts a pair of power spectral density functions for each range gate into the reflectivity and radial velocity values for that given range gate. The spectrum width is obtained from the standard deviation of the samples of radial velocity in that pulse volume.

Data Format

Once the data had been collected they were converted to the common Doppler format, otherwise known as the universal format (UF), developed to create a standard for Doppler radar data storage on computer tape. A description of the UF has been given by Barnes (1980).

Bonewitz (1986) developed a computer program called Disk Write (DISKW) to read the UF tapes. DISKW is able to find a specific volume sector of data by specifying a given beginning and ending elevation angle, azimuth, and range. All necessary conversions of data (e.g. reflectivity data from dBm to dBZ) are made by DISKW, which then stores all the needed data on a computer disk by range bin, radar field, azimuth, and elevation angle for a full volume.

Reflectivity Plots

Figure 1 is an example of a reflectivity plot which is obtained through graphical plotting routines that convert from polar to cartesian coordinates in plotting the Doppler radar data. The contours were drawn by linear interpolation between grid points through the grid domain. Reflectivity plots were used to display the intensity of radar echoes in the area of interest.

TREC

The TREC program, which generates u and v wind components, was originally developed by Rinehart (1979). The current implementation follows the NEXRAD algorithm description for the transverse wind algorithm (NEXRAD JSPO Staff, 1984) and was programmed by Bensinger (1986). The technique was described in Chapter I and the procedure detailing its use will follow later in this chapter.

TREC requires several data inputs. These inputs include two data sets separated by some time increment, a pattern area size or box size, estimated storm speed, box overlap, azimuth separation in the data sets, and the azimuth/range boundaries of the data sets. The selection of values for these data inputs are crucial to the success of TREC to analyze accurately the wind field. The selection of these inputs will be discussed in the procedure section of this chapter.

As mentioned earlier TREC provides the user with the u and v wind components for a given x-y location. It also provides the horizontal wind direction, speed, and as its name implies, the value of the largest correlation coefficient of the pattern from the second data set that matches the original pattern from the first data set.

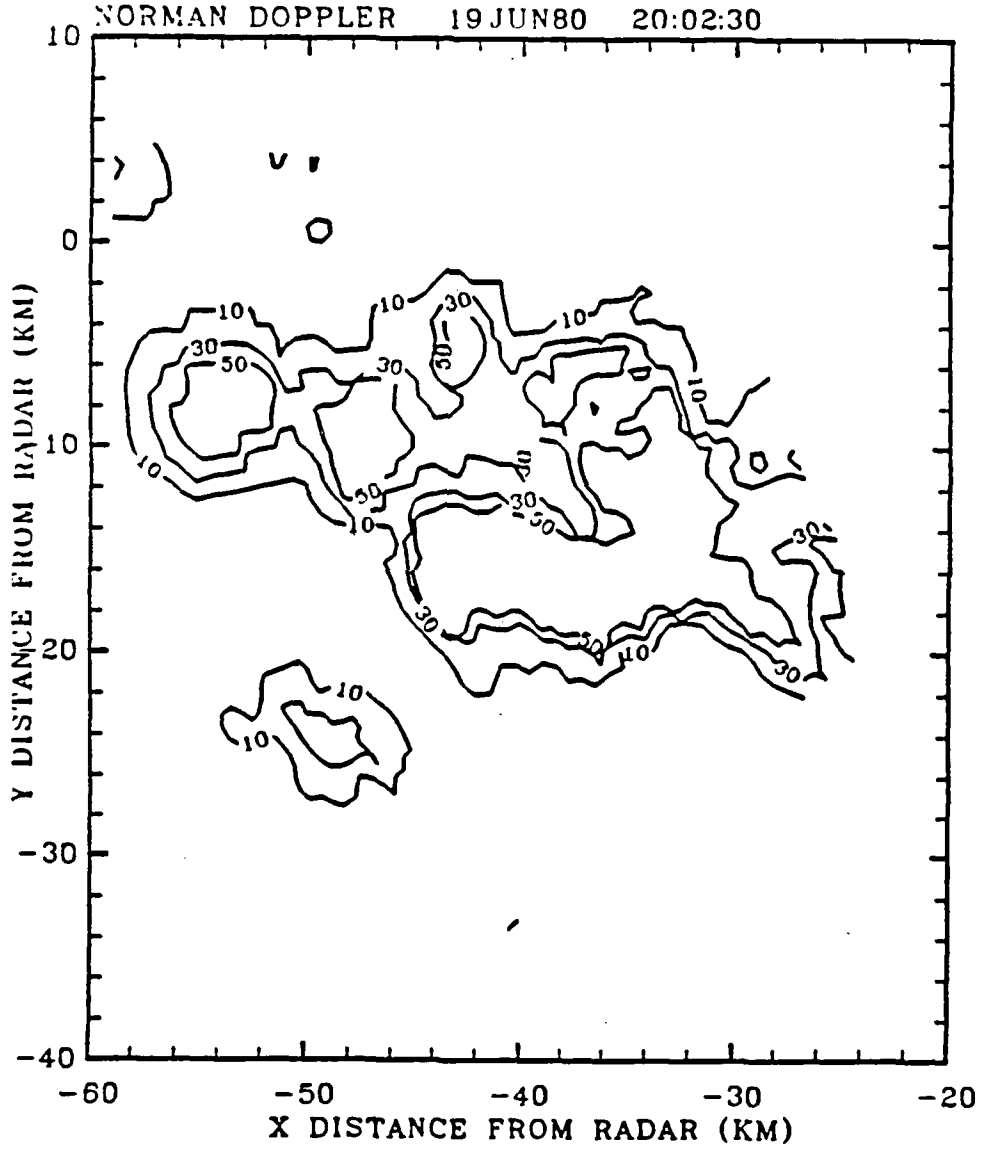

Fig. 1. Example of contoured Doppler radar reflectivity data.

Vector Wind Plots

Two programs were written to produce a graphical representation of the vectors produced by TREC. Those programs were called WPLOTV. for vertical motion patterns, and WPLOTG, for gridded horizontal wind field. Both of these programs used the graphical routine package called DISSPLA.

WPLOTV was written to determine graphically the vertical motion patterns (VMP). The full technique to determine the VMP will be discussed later in this chapter; however, at this time it is sufficient to say shorter vectors represent a VMP. An example of output from WPLOTV will be shown and discussed later in this chapter.

WPLOTG was written to display graphically the horizontal wind field derived by TREC. Once again as with WPLOTV output, an example of WPLOTG output will be shown later. To produce this type of graphical output the u and v wind components as determined by TREC were gridded using a Barnes (1964, 1973) analysis. Once the fields were gridded the vectors were scaled and plotted for a given radar elevation angle.

Vertical Motion Calculations

A program called VERTMT was written to calculate numerically the vertical motions within the VMP identified earlier by using WPLOTV. It should be emphasized that WPLOTV only identifies a region which is experiencing vertical motion. By using VERTMT an actual magnitude can be assigned to that pattern.

Initially, the u and v wind components obtained from TREC were gridded using a Barnes (1973) analysis. Next, the horizontal divergence was calculated. Special care was taken to make certain the finite difference technique was numerically

consistent (Haltiner and Williams, 1980). The wind components were gridded and the horizontal diverence was calculated every 2 km. This calculation uses the finite difference method for calculating divergence given by Holton (1979). Once the divergence was obtained, the anelastic equation of continuity for deep convection (Ogura and Phillips, 1962) was solved giving estimates of the vertical motion through the storm. The derivation of the computational form of this equation is given in Appendix B. A correction for the terminal fall velocity of the hydrometeors was used to correct the final estimate of the vertical motion.

Vertical Cross Sections

To have a complete three-dimensional veiw of the thunderstorm, vertical cross sections were constructed. As with the wind plot graphs, these diagrams were generated using the DISSPLA graphics package. The cross section requires the data to be gridded in the same fashion as before.

Procedure

General

The objective of this research was to determine the feasibility of deriving vertical velocity patterns, their magnitudes, and the three-dimensional wind field in the severe storm environment using data from a single radar and a technique called TREC. This technique derives the horizontal wind field using pattern matching and correlation analysis. TREC can use either reflectivity or radial velocity data from a Doppler radar to derive the wind field. To accomplish the objective this research was divided into three phases. First, TREC was used to derive the VMP between

two adjacent elevation angles within a single volume scan of radar data. Next, the horizontal wind field was derived using TREC and radar data from two separate volume scans at the same elevation angle. This provided the needed u and v wind components required to accomplish the third phase, the derivation of the vertical motion magnitudes within the VMP. All results were compared first to the results published by VBDR, who did a multi-Doppler analysis of the same event and second to known meteorological conditions that occur in the severe storm environment.

Before the procedure used to accomplish the three phases of this research is discussed, a brief overview will be presented to familiarize the reader with how TREC determines the velocity vector and how the variables needed as input to TREC were selected. A more complete discussion can be found in Rinehart (1979). Also, a brief summary of the selection of the test data sets is given.

Determination of the Velocity Vector

TREC's operation is dependent on digitized reflectivity or radial velocity data with specified range and azimuth values. An area of interest from an initial radar scan, or time 1, is first identified. This area is then divided into boxes, which for time 1 are called BOX1's. At this point, a radius of search is defined around the first BOX1. The search radius is dependent upon the storm speed and the time increment between the two radar scans. A correlation coefficient (CC) formula (Equation 1) is used to compare the BOX1 from the first radar scan with all boxes in the second radar scan (BOX2's), whose centers fall within the search radius.

$$CC = \frac{A - B}{(C \times D)^{\frac{1}{2}}}, \tag{1}$$

where,

$$A = \sum_n dBZ(1)_n dBZ(2)_n, \tag{2}$$

$$B = \frac{1}{N} \sum_n dBZ(1)_n \sum_n dBZ(2)_n, \tag{3}$$

$$C = \sum_n (dBZ(1)_n^2 - N(\sum_n \frac{dBZ(1)_n}{n})^2), \tag{4}$$

$$D = \sum_n (dBZ(2)_n^2 - N(\sum_n \frac{dBZ(2)_n}{n})^2). \tag{5}$$

The variables dBZ(1) and dBZ(2) are the reflectivity values in BOX1 and BOX2, respectively. The summation is over all pulse volumes, n, making up BOX1 and BOX2. A vector is drawn from the center of the BOX1 and the location derived from a second order curve fit across the center of the BOX2 with the highest correlation coefficient. Figure 2 is a graphical representation of how TREC determines BOX1's and BOX2's. To determine the magnitude of the velocity vector, the distance between the two boxes is divided by the time increment between the two scans as shown by equation 6.

$$| \vec{V} | = \frac{\Delta d}{\Delta t}. \tag{6}$$

Selection of TREC Variables

The effective use of TREC depends upon the values of three variables. These variables are box size, box overlap, and the time increment between scans.

An important variable to the success or failure of TREC is the box size. Rinehart (1979) studied this variable comparing results using box sizes ranging from 1.2 km to 19.2 km. He found a rapid increase in the success rate of TREC to model storm motions as box sizes increased to 4 or 5 km. Beyond that the box size

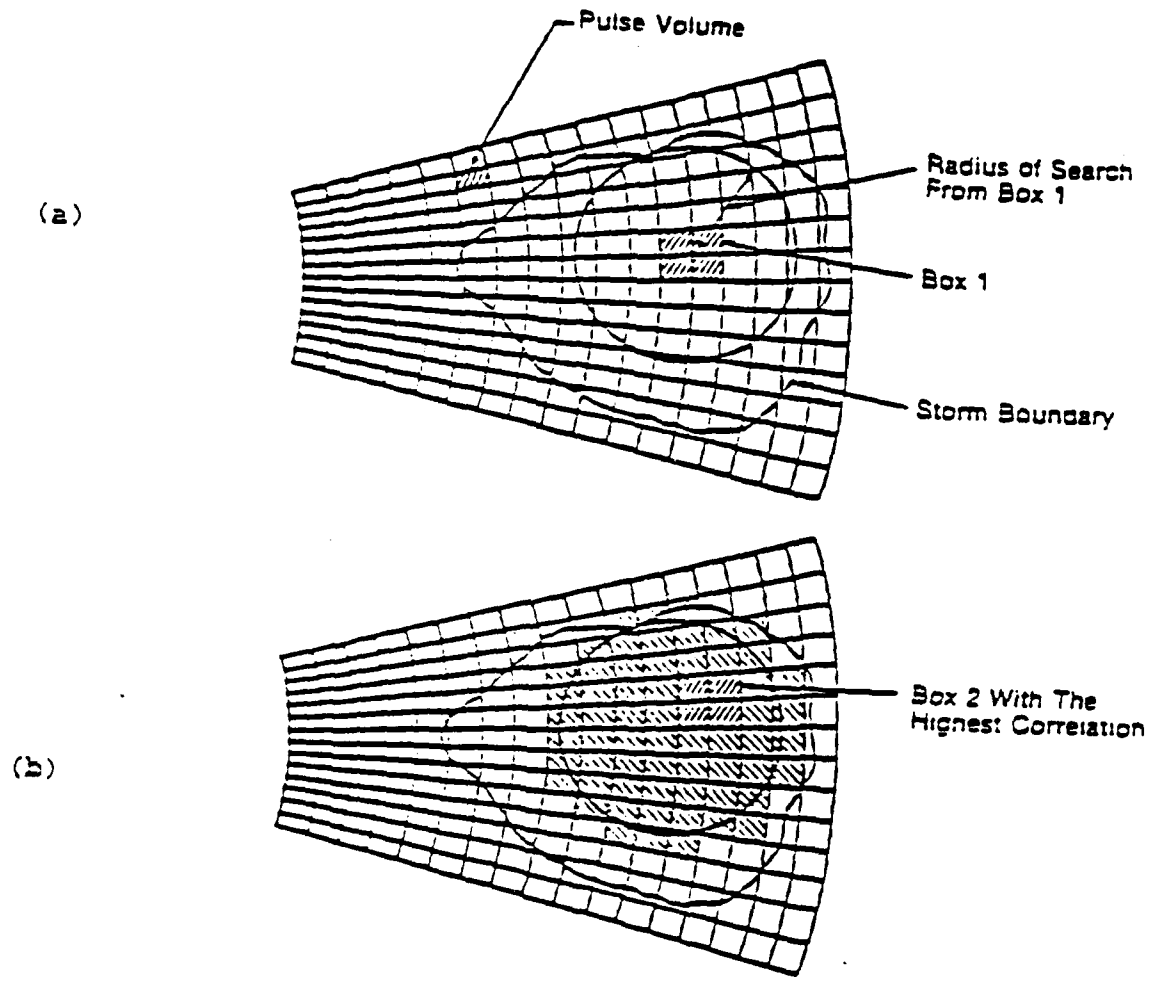

Fig. 2. TREC algorithm at (a) time 1 (b) time 2.

did not help the success of TREC. In fact, beyond 10 km the success rate decreased because the box size was so large that it could not model the small-scale features in and around the storm. Thus, for this study a 5 km box size was used.

The next important variable to the success or failure of TREC is box overlap. Again Rinehart (1979) studied this. He used box overlap when box sizes were larger than 3 km. For very large box sizes an 85% overlap was used, whereas. for box sizes on the order of 5 km a 66% overlap was used. He discovered that even with large overlap the individual boxes were reasonably successful in determining motions independent of adjacent boxes. Therefore, boxes that overlap can "see" correct motions that are different from their adjacent neighbors. Thus, in this study a 60% overlap was used, which when used in conjunction with the 5 km box size gives an effective 2 km resolution. As sampling theory states, the smallest wave that can be sampled is two times the grid distance. However, Rinehart (1979) showed that with TREC the resolution is better because each box is comprised of a number of data points and there is overlap between each box. He was able to detect wavelengths as small as one-third the box size.

The other important variable in this study is the time increment between radar scans. As with the other two variables, Rinehart (1979) evaluated the effect of the time increment on the effectiveness of TREC to produce correct vectors. He found that the correctness of vectors decreased with increasing time lags between initial and final data sets. With time increments shorter than 4.5 min, 90% or more of the vectors were correct. When the time increment was shorter than 2.5 min, 98% of the vectors were correct. Therefore, in this study a concerted effort was made to use radar volume scans that have a time increment less than 5 min.

Selection of Test Data Sets

As mentioned in Chapter I, TREC is a technique that uses data from a single radar. Therefore, to validate the results obtained from TREC a "ground" truth data set was necessary. That data set, 19 June 1980, was the subject of a recently published article (Vasiloff et al., 1986). This data set was originally taken as a dual-Doppler data set with time increments between volume scans on the order of 5 min. Therefore, the radar data from one of the radars, the Norman radar, were selected as input data for TREC. These data provided the initial testing of TREC. This testing involved the graphical output generated by TREC and the comparison of TREC generated fields with the identical fields generated by the dual-Doppler study.

A second comparison was also made, which was similar to that made using the 19 June 1980, Norman Doppler data. Because that data set was a dual-Doppler data set, the data from the second radar, Cimarron, which is located 40 km northwest of the Norman radar, were analyzed. Thus, using the Cimarron data a second comparison of the TREC derived results was made to validate the technique.

Vertical Motion Patterns

The first step in this study was the determination of the vertical motion patterns. To do this TREC processed data from two successive elevation angles, thus determining the reflectivity patterns between elevation angles. These patterns provided information about the echo structure, or tilt, of the storm. The time increment between the two elevation angles was rather small, on the order of seconds. With such a short time increment it is virtually impossible for a parcel of air to move outside an individual volume. For example, if the actual vertical motion

is 30 ms^{-1} and the time increment between scans is 20 s, the parcel will move only 600 m in that time. The distance between centers of radar beams is 1 degree or on the order of 1 km at a slant range of 50 km. Therefore, it is impossible for a parcel to move beyond the area enclosed by the elevation angles in question. Also, the vectors indicate echo structure instead of actual movement. This is because one is correlating patterns of reflectivities that are above one another. Marwitz (1978) stated there is no obvious reason why echoes could not be tracked with high-resolution, three-dimensional volume scans. This vertical pattern correlation made using TREC is precisely that kind of tracking. However, it should be emphasized that the vectors produced are not showing motions directly, but are showing the motions feeding the storm, particles falling out of the storm, and echo structure, not actual magnitudes. An example of output showing the echo structure can be seen Fig. 3. A short vector indicates a structure nearly vertical, whereas, longer vectors indicate quasi-horizontal regions. Thus, in this figure the area outlined indicates a VMP. No direction has been assigned to the vertical motion pattern at this time. It is this area that was compared with the corresponding figure in VBDR.

Horizontal Wind Field

A derivation of the horizontal wind field was the next step in this research. To do this, TREC processed data using two different volume scans at the same elevation angle. Once completed, the u and v wind components were gridded by the use of a Barnes (1973) analysis and a plot made of the resulting gridded wind field. The radar reflectivity field was then superimposed on the wind field. Fig. 4 is an example of the derived horizontal wind field. Once again graphical outputs of this kind were compared with that of VBDR.

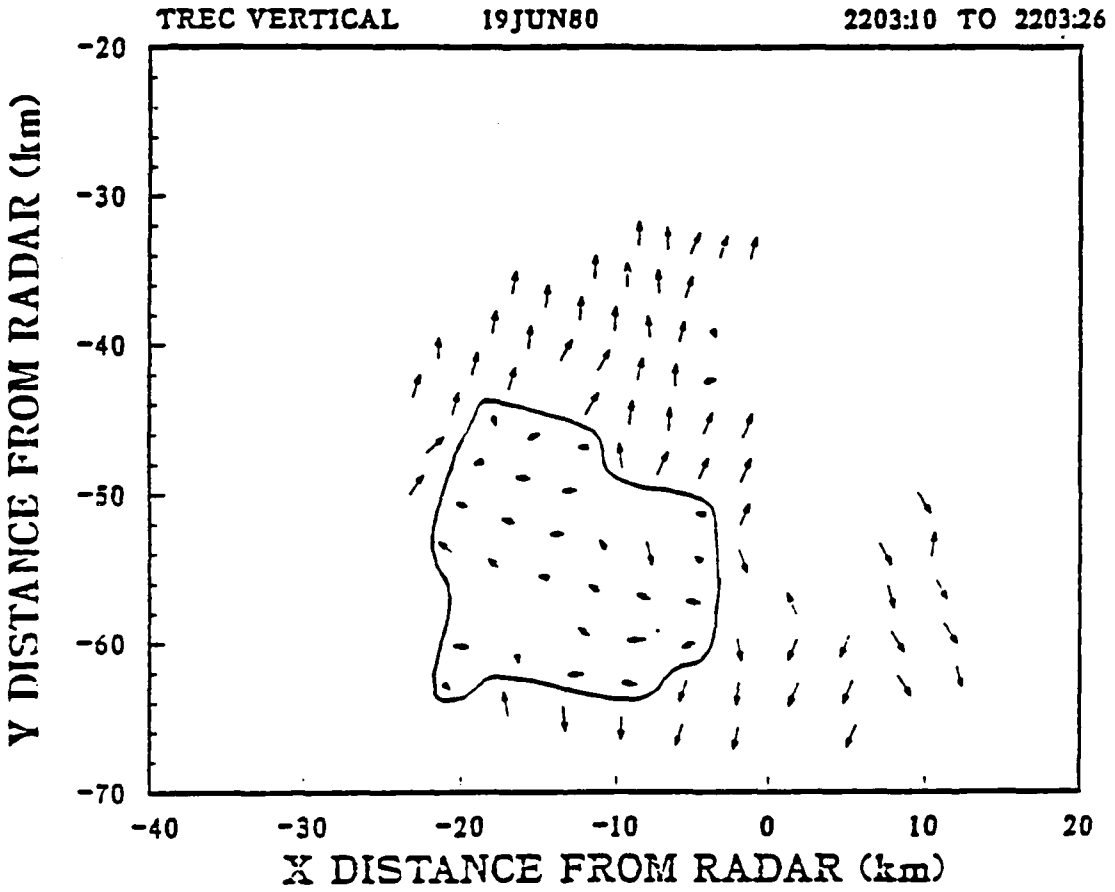

Fig. 3. Example of a TREC derived VMP.

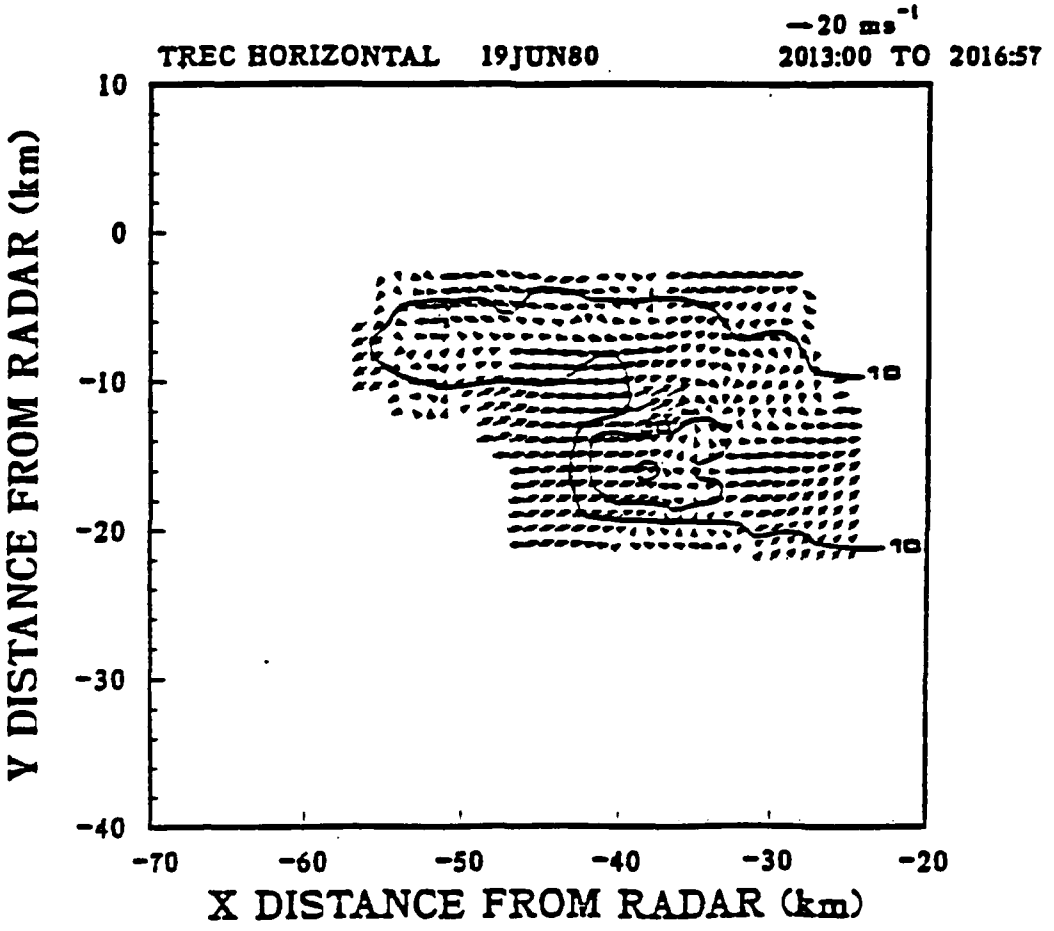

Fig. 4. Example of a TREC derived horizontal wind field.

It should be mentioned that Rinehart (1979) found a feature in the TREC wind field that was absent in the dual-Doppler wind field. Upon investigation he noticed that the dual-Doppler data contained some "suspicious" vectors. Therefore, in some cases the dual-Doppler wind field may be in error. This brings up another point addressed by Hamidi et al. (1983). They stated that the direct comparison of dual-Doppler wind fields to wind fields derived by TREC is like comparing "apples and oranges". TREC produces a wind field that is effectively a temporal and spatial average, whereas, the dual-Doppler wind field is an instantaneous, high resolution "snapshot" wind field. Both fields may be correct in terms of their relevance to different scales of atmospheric motion. Thus, the evaluation made was one of comparing the internal consistency of the vectors produced by TREC and the relation of those vectors to the known thunderstorm flow.

Vertical Motion Magnitudes

The magnitude and direction of the vertical motion patterns were calculated. The only areas in which vertical motion magnitudes were calculated were those areas wherein discernible patterns were found by the use of TREC. Only the areas reported by VBDR lent themselves to a direct comparison.

The vertical motion magnitudes were computed by using the anelastic equation of continuity (Ogura and Phillips, 1962). The computational form of this equation can be found in Appendix B. The equation was integrated upward and downward with the boundaries set to zero. The results of the upward integration were used only when the data did not extend to the storm top. Otherwise, the downward integration was used. This method of computing the vertical motions was consistent with the technique VBDR used.

Once the vertical motion was calculated a correction for the terminal fall velocity of the hydrometeors was added. The calculation of this value required three steps. First, the rainfall rate, R, inside the storm had to be determined. This was accomplished by using the Z-R relationship proposed by Jones (1956) for thunderstorms,

$$R = (\frac{Z}{486})^{.7299}, \tag{7}$$

where Z is the average reflectivity value for the area of interest. Next, the hydrometeor diameter was calculated using a formula proposed by Sekhon and Srivastava (1971),

$$D_o = \frac{A}{L}, \tag{8}$$

where A=3.67 (Atlas, 1953) and

$$L = 38R^{-0.14}. \tag{9}$$

This value for the mean diameter was then an input into the terminal fall velocity equation

$$W_t = 1690{D_o}^{0.6}, \tag{10}$$

where W_t is in cms^{-1}.

One can also calculate the hydrometeor diameter directly using a formula proposed by Sekhon and Srivastava (1971), if the rainfall rate is known,

$$D_o = .13R^{0\ 14}. \tag{11}$$

This in turn can be input into their terminal fall velocity equation (Equation 10) or one proposed by Spilhaus (1948) for thunderstorms,

$$W_t = 1.42 \times 10^3 D^{\frac{1}{2}}. \tag{12}$$

The difference between the two values for fall velocity is minimal, and either value can be used to correct the vertical motion calculation.

During the supercell stage of this storm, 2 cm hail was observed at the surface. Therefore, a separate equation was used to calculate the terminal fall velocity of the hail stones. Douglas (1964) originally determined the fall velocity using

$$W_t = 16.2D^{\frac{1}{2}}. \tag{13}$$

More recent work by Ulbrich (1977) found

$$W_t = aD_o^b, \tag{14}$$

where a is 20.52 and b has a value of 0.426. This equation is more desirable because it used Doppler radar data to derive the hail spectrum.

Once the vertical velocities were calculated and corrected they were compared with the values presented by VBDR. They stated the noise level in their calculations was on the order 5-10 ms^{-1}. Therefore, their value plus or minus this noise level was used as ground truth for the derived TREC vertical motion values.

The noise level for the vertical velocities determined by TREC was established. This determination was made in part by Rinehart (1979). He found that TREC was able to produce vectors that modeled corresponding wind vectors in the theoretically-produced field 90% of the time. Also, Bonewitz (1986) found that over 95% of the vectors generated by TREC were internally consistent. Internally consistent vectors are those vectors that are in good general agreement in magnitude and direction with the general trend of those vectors in close proximity.

Cross Sections

Once the vertical motion patterns and magnitudes were obtained, vertical cross sections through areas of interest were made. These cross sections, along with the derived horizontal wind field, provide a three-dimensional look at the severe storm environment. Figure 5 is an example of a TREC-generated cross section. When an applicable cross section was available in the VBDR paper the appropriate comparisons were conducted. Otherwise, comparisons were conducted using other known multi-Doppler studies (e.g. Brandes, 1977) and known thunderstorm flow characteristics. However, it should be noted that once again the comparisons are of the "apples and oranges" type with TREC being an average field and the dual-Doppler cross sections being an instantaneous, high resolution snapshot.

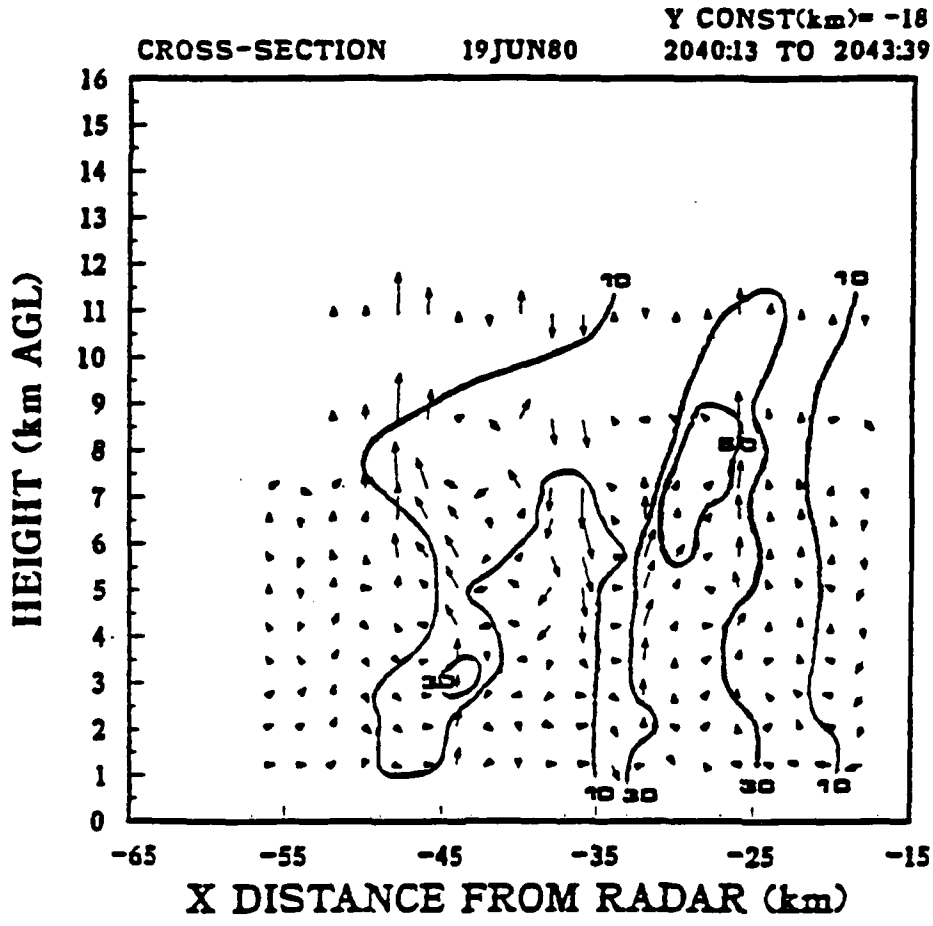

Fig. 5. Example of a TREC generated vertical cross-section.

CHAPTER III

SINGLE RADAR OBSERVATIONS

TREC Derived Radar Observations

The Lindsay, Oklahoma, storm of 19 June 1980, evolved over a $2\frac{1}{2}$ hour period. During that time the maximum radar reflectivity increased to over 60 dBZ. VBDR described the storm's evolution as occurring in three phases, the multicell phase from about 1940 to 2040 CST, the transition phase from 2040 to 2130 CST, and the supercell phase starting at 2130 CST. The dual-Doppler (DD) observations have shown updraft speeds that inceased from 10 - 20 ms^{-1} to over 60 ms^{-1}. Also, on the average, individual cells and their updrafts translated nearly with the mean wind, 255 deg at 9.2 ms^{-1}, whereas the average storm motion was 320 deg at 8 ms^{-1}. For a more complete discussion of the mesoscale environmental conditions the reader is referred to Appendix C.

Multicell Phase

As stated above the multicell phase lasted approximately an hour. During this time, the storm was comprised of individual, seemingly unattached cells. The first time that VBDR investigated was 1956 CST. However, due to data availability, the initial time for this study was 2000 CST. Also, the increment between the first two volume scans was 11 min. Therefore, as explained in Chapter II, a horizontal correlation could not be accomplished in a fashion that would give reliable results. Without the horizontal correlation, which provides the u and v wind components, a calculation of the vertical motion magnitude could not be made. Even with this

limitation, a vertical correlation was made between two adjacent elevation angles within the same volume of data. This correlation revealed the VMP for this time period (Fig. 6). The area of shorter vectors is quite evident, one major area having a southwest-northeast orientation. As shown by VBDR (Fig. 7), seven minutes earlier, the area of major vertical motion was located at (-40,-21) to (-48,-13) with minor areas centered at (-37,-11) and (-52,-13). Upon investigation, it can be seen that if TREC's major pattern was cut in half, the southern end would fit the major updraft area described by VBDR, assuming that feature were advected with the mean storm motion.

One can explain the remainder of the VMP found by TREC by referring to the radar reflectivity chart (Fig. 8). The large VMP was clearly associated with an area of reflectivities greater than 50 dBZ. The VMP centered at (-45,-3) was associated with another 50 dBZ cell. The vector-void area located in the center of the plot could now be explained. This area was one in which the reflectivities were less than 30 dBZ, thus TREC was unable to find a pattern match that met the CC criteria. The 50 dBZ cell located at (-55,-9) was not investigated. However, TREC gave an indication of a vertical motion area associated with this cell with the shorter vectors located in the western portion of Fig. 6.

To apply a direction, either up or down, to the VMP required the derivation of the horizontal wind field. During this time period it was not possible to derive the horizontal wind field that would be reliable because the time increment between scans was too large.

The first time period that lent itself to a derivation of vertical motion magnitudes began at 2011 CST. The time increment between volume scans was 4 min. The horizontal wind field derived by TREC at 6 km AGL is shown in Fig. 9. The

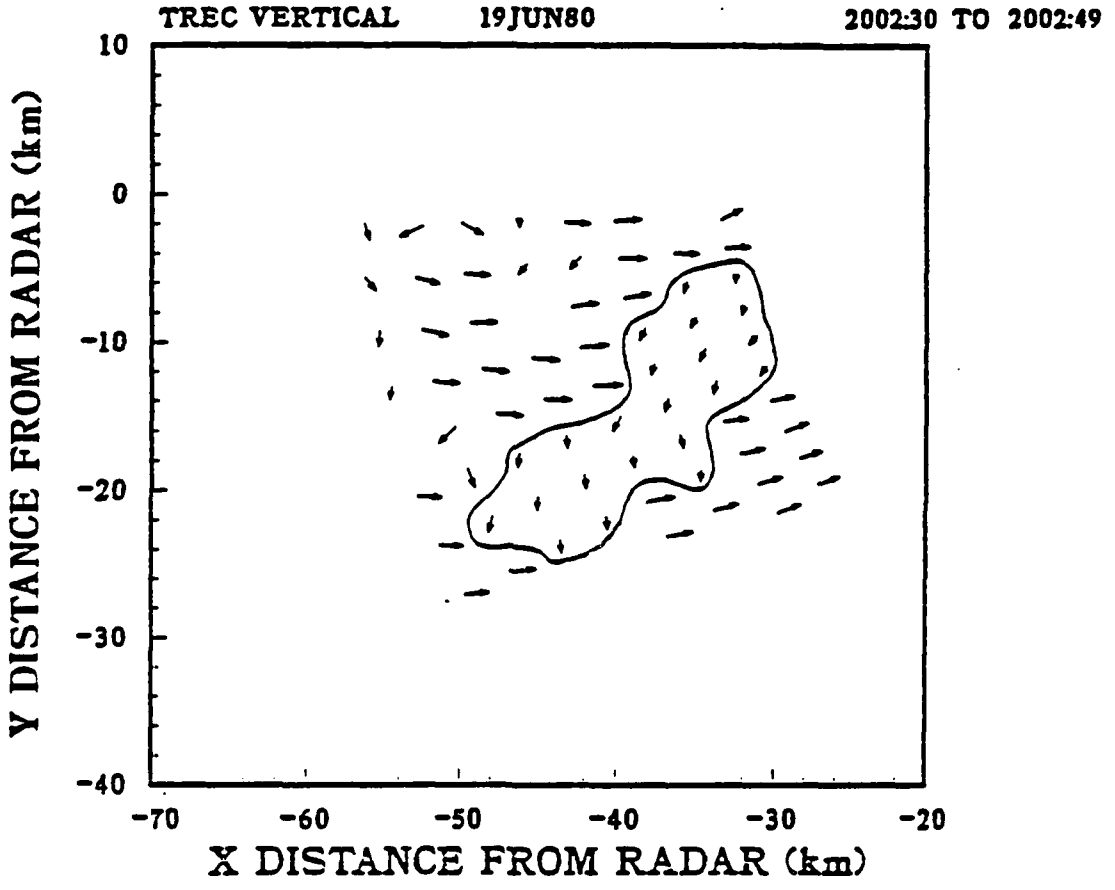

Fig. 6. Norman Doppler radar TREC derived VMP within solid line at 6 km AGL for 2002:30 to 2002:49 CST.

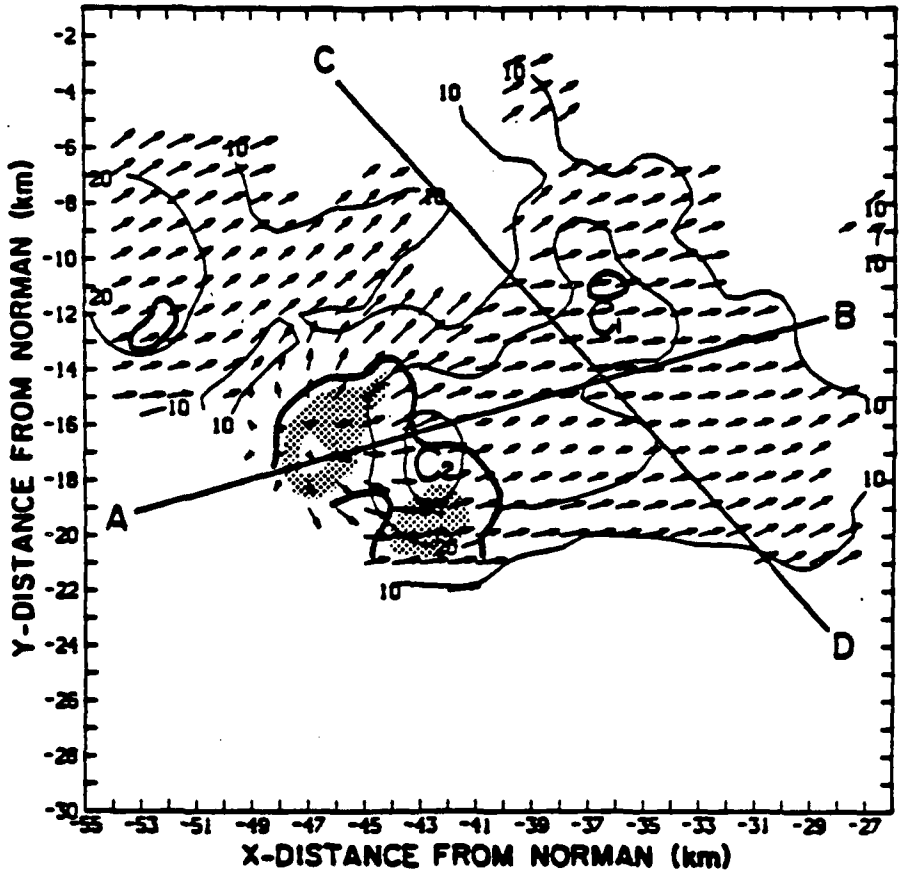

Fig. 7. Horizontal wind and reflectivity fields at 9 km AGL for 1956 CST. Heavy solid line denotes updraft greater than 5 ms^{-1} (after Vasiloff et al., 1986).

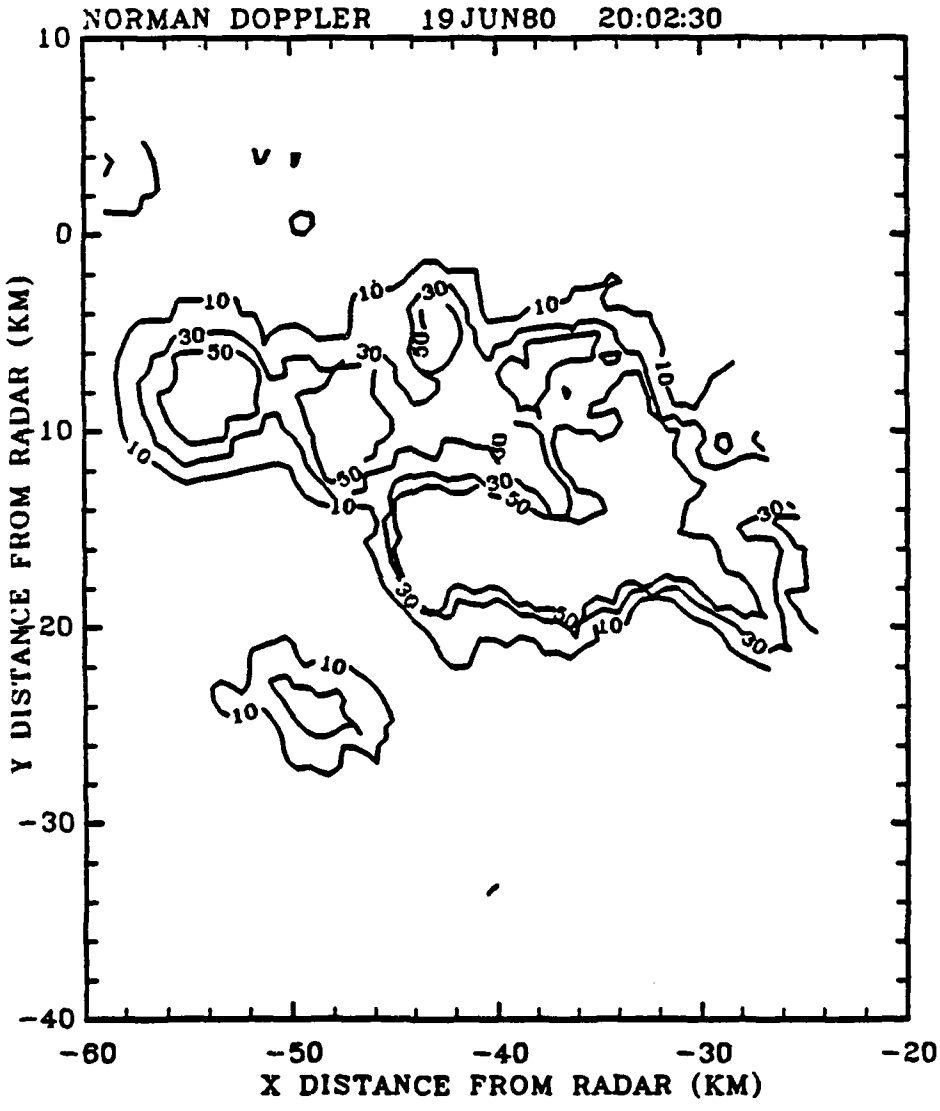

Fig. 8. Norman Doppler radar contoured reflectivity field at 6 km AGL for 2002 CST.

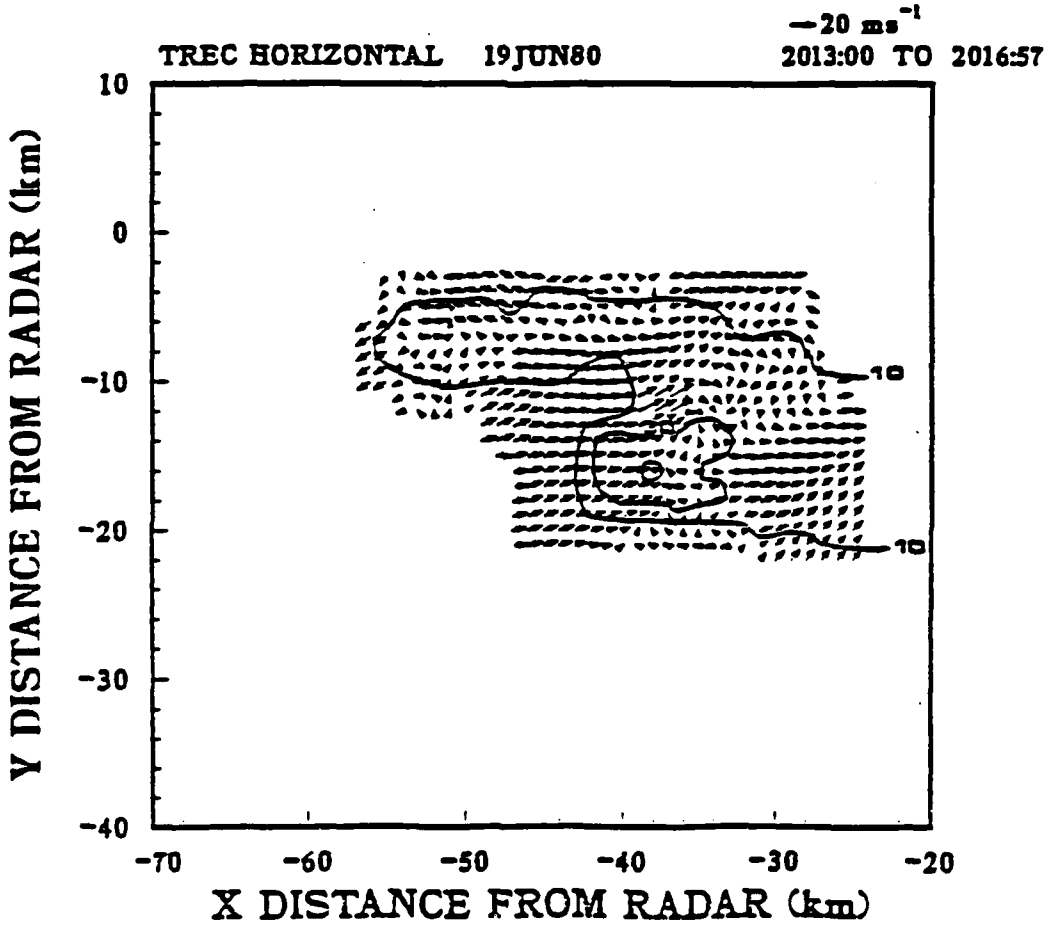

Fig. 9. Norman Doppler radar TREC derived horizontal wind and reflectivity fields at 6 km AGL for 2013:00 to 2016:57 CST.

reflectivity contours were superimposed on the figure in units of dBZ. The storm of interest was centered at (-38,-16). The corresponding reflectivity maximum was greater than 50 dBZ. The horizontal winds indicated an area of convergence near the center of the storm. There was also an area of convergence located 5 km northeast of the core. When related to the derived VMP by TREC (Fig. 10), the VMP coincided with the area of convergence and maximum reflectivity (-38,-16). This placement agrees with Lemon and Doswell's (1979) schematic three-dimensional depiction of the evolving supercell.

The magnitude of the VMP was derived next. As shown by Fig. 11 the maximum updraft was on the order of 9 ms^{-1} at 6 km AGL. VBDR reported a magnitude of approximately 15 ms^{-1}. TREC underestimated the DD value; however, when the appropriate error limits were taken into consideration, TREC's derived value was reasonable.

The divergence field indicated, except for the top and near the surface, that the storm was weakly convergent with the most convergence located near 5-6 km AGL. This coincided with the area of maximum vertical motion shown in Figs. 10 and 11. As one would expect the storm became increasingly divergent with height. A profile shown by Brandes (1984b) for the pretornadic stage of development was similar to the one derived by TREC for this time period.

It has been suggested by various authors (Rinehart, 1979; Hamidi et al., 1983; Bonewitz, 1986) that using a longer time increment for deriving the horizontal wind field would lead to contamination of that field by what is called generator level motions. Fig. 12 shows the 1 km AGL wind field for this time period, which indicates a predominantly southwesterly flow. When compared to the 6 km AGL wind field (Fig. 9), the fields do show some similarities; however, the influence of

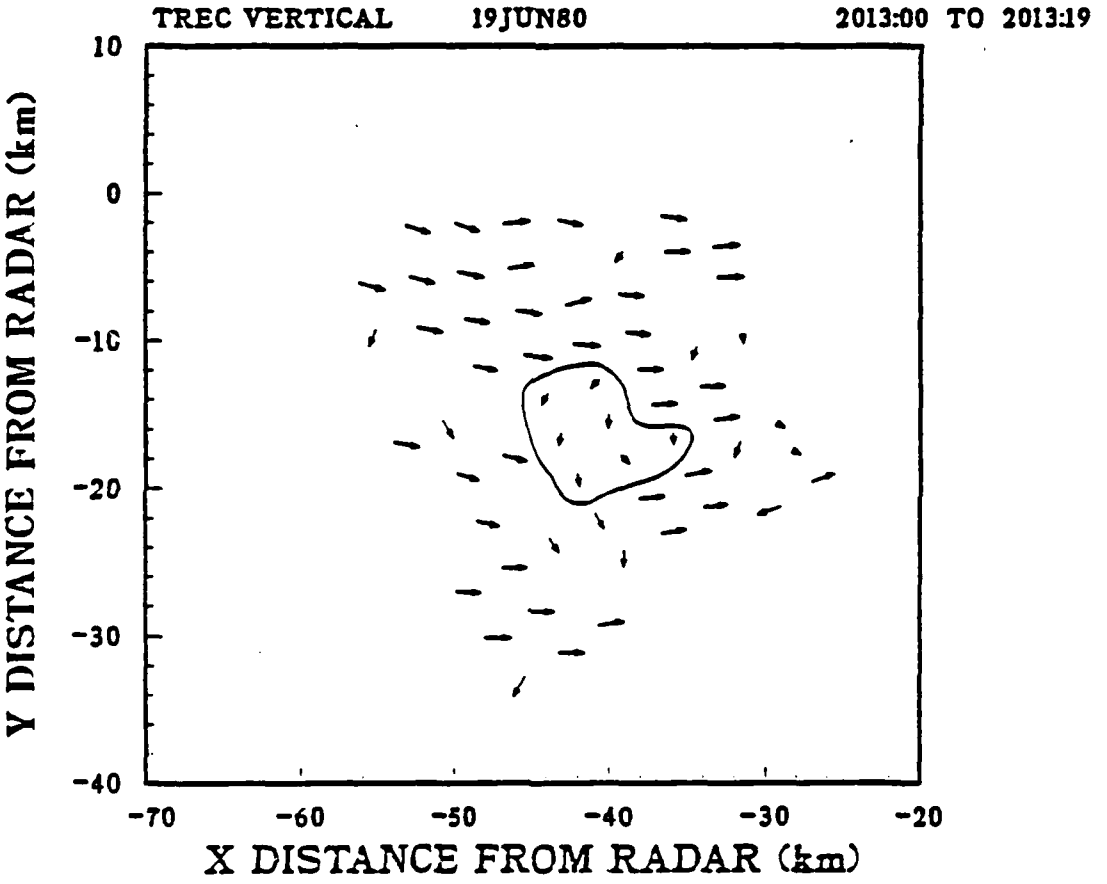

Fig. 10. As in Fig. 6, except for 2013:00 to 2013:19 CST.

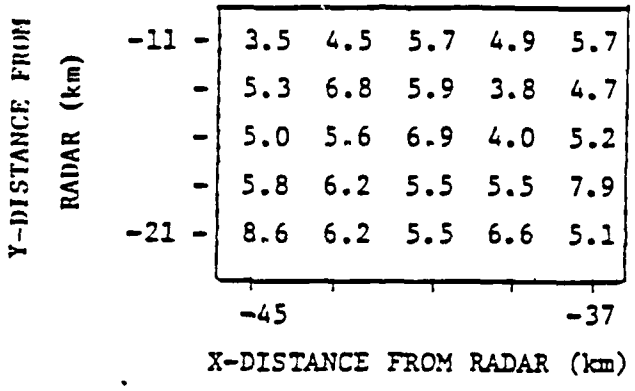

Fig. 11. Norman Doppler radar TREC derived vertical velocities at 6 km AGL for 2013:00 to 2016:57 CST.

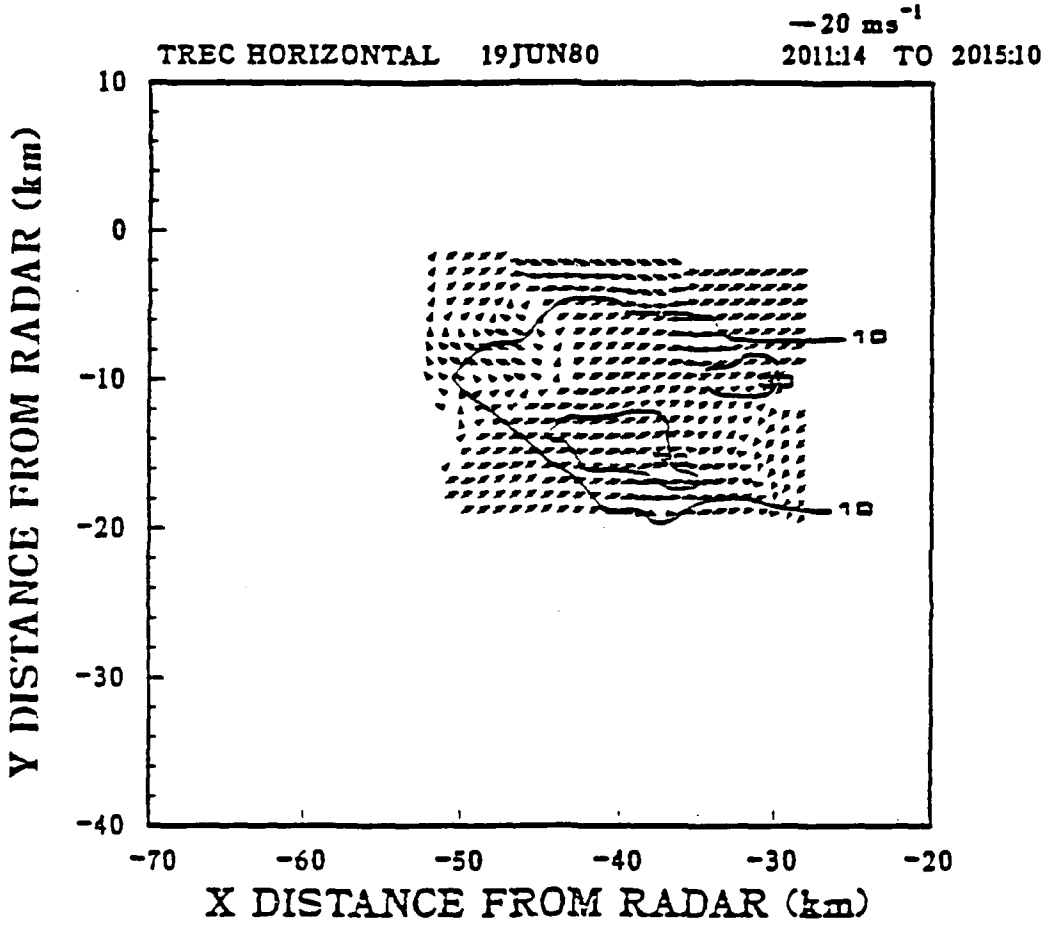

Fig. 12. Norman Doppler radar TREC derived horizontal wind and reflectivity fields at 1 km AGL for 2011:14 to 2015:10 CST.

the 50 dBZ cell at the middle-levels is not seen at the lower levels, the convergence associated with this feature going unnoticed in the lower levels.

Transition Phase

VBDR described the transition phase as the period in which a large persistent region of updraft and reflectivity formed. This period began at 2040 CST and lasted for approximately an hour. One notes for 2042 CST at 6 km AGL that a cell had developed at (-30,-17) with a reflectivity greater than 50 dBZ (Fig. 13). When comparing the TREC derived wind field to the DD derived wind field (Fig. 14), it is seen in that area that both wind fields indicated a southerly flow converging with a westerly flow at (-25,-20). TREC did, however, show an area of cyclonic wind flow at (-28,-21) which did not appear in the DD field. Upon examination, this feature was associated with an individual cell of reflectivity greater than 40 dBZ (not contoured). Therefore, apparently TREC modeled the wind flow correctly.

In the western area of the field, centered at (-43,-15), the TREC and DD fields did not agree. The apparent disagreement between the two techniques could be linked to the difference in a time-averaged field (TREC) and the instantaneous velocities (DD). The TREC field in that region had a realistic pattern of cyclonically rotating winds associated with the higher reflectivities.

Using the data from the CIM radar to estimate the 6 km AGL wind field yielded similar results (Fig. 15). The corresponding area of converging winds (3,-50) agreed with the NOR radar when the fields were overlaid. Because of orientation of the radars, the only direct comparison that could be made was for the cell of interest. For that area, the flow field generated by TREC for the NOR radar agreed with that of the CIM radar, thus indicating radar orientation did not have an affect on

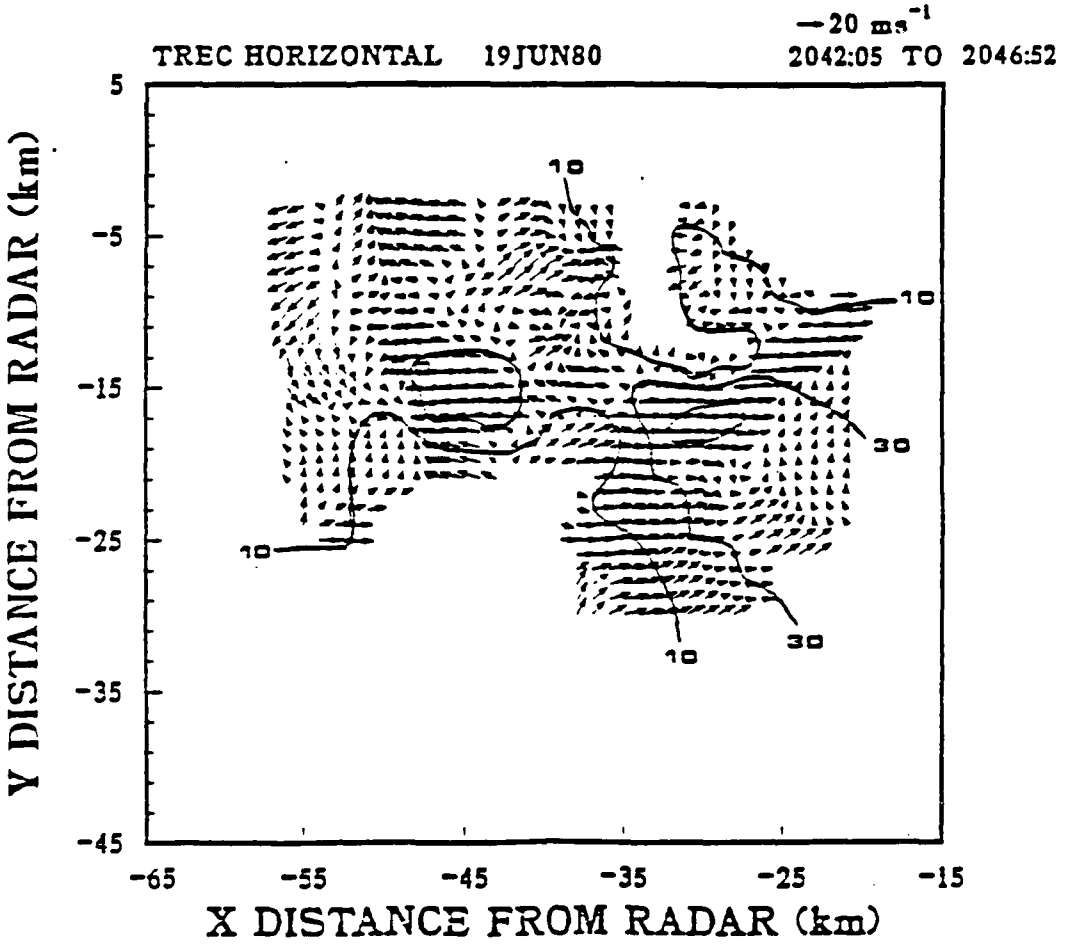

Fig. 13. As in Fig. 9, except for 2042:05 to 2046:52 CST.

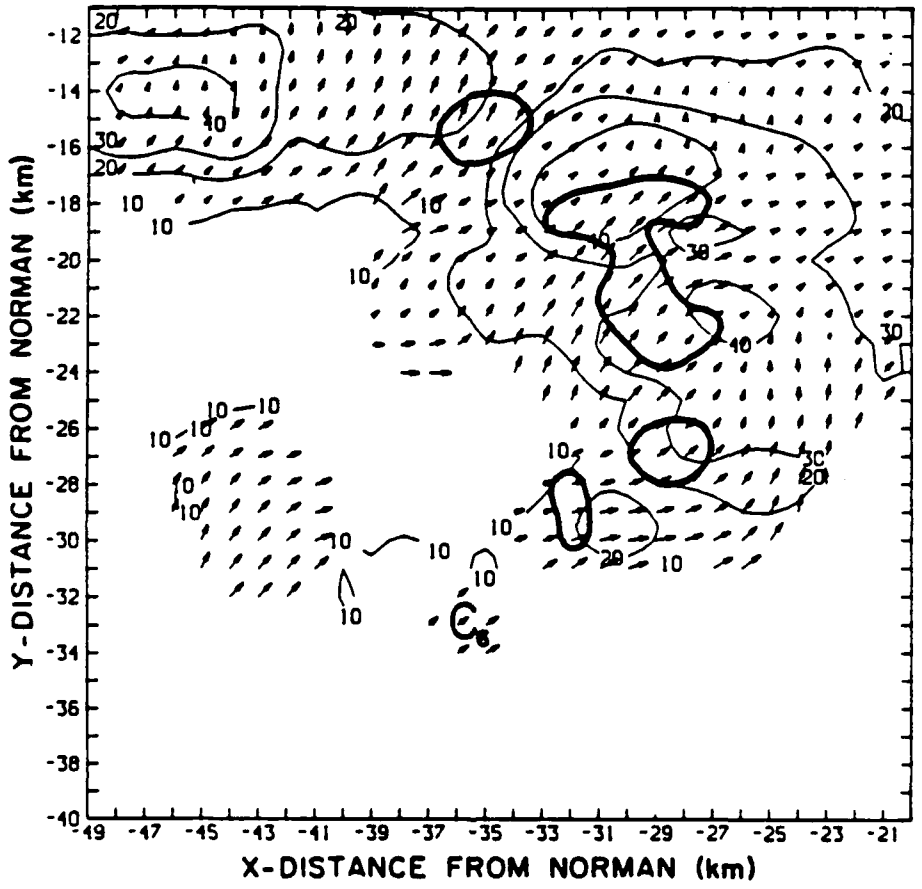

Fig. 14. As in Fig. 2, except at 6 km AGL for 2042 CST.

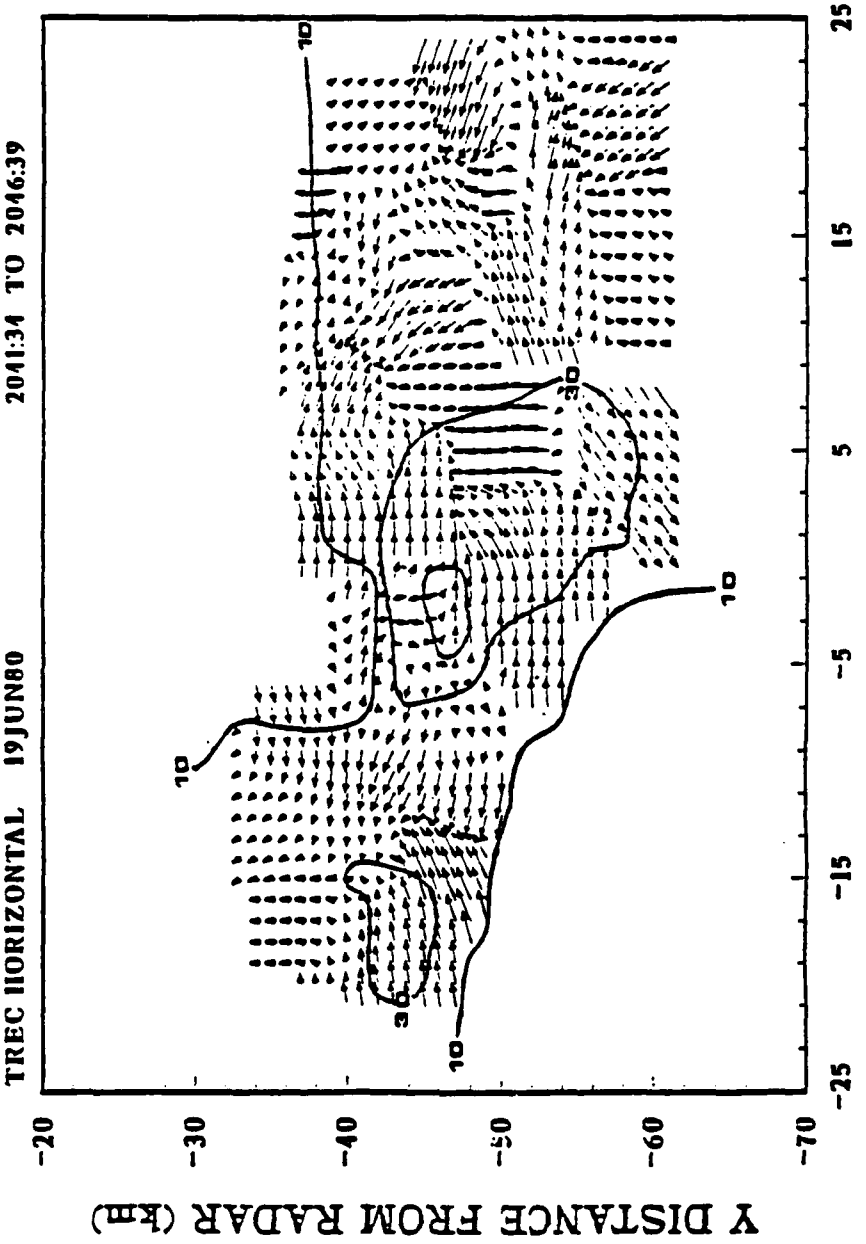

Fig. 15. Cimarron Doppler radar derived horizontal wind and reflectivity fields at 6 km AGL for 2041:34 to 2046:39 CST.

the TREC-derived wind field.

The field of low-level, 1 km, winds for CIM (Fig. 16) showed southerly winds under the westerly winds shown in Fig. 15 at the point (-3,-50). East of this area the low level winds became more westerly while above, the winds had become southerly (9,-50). Once again, as with the earlier time, each level tended to exhibit an independent wind flow.

Using TREC to generate the VMP was the next step. In Fig. 17 the VMP at 6 km AGL as derived from the NOR radar is shown. TREC identified the major area of vertical motion that VBDR identified (see Fig. 14). TREC did combine the main vertical motion area with the one located just south of it. It should be noted, however, that the pattern was resolved, even to the point of the same shape. The VMP derived using the CIM data is shown in Fig. 18. It is apparent that the area of vertical motion derived by the CIM data was not the same shape as that derived by either VBDR or the NOR data. However, the pattern was located in the same region as that recorded by VBDR and the TREC NOR results. Also, the derived magnitudes of the vertical motion field (Fig. 19) were in agreement. In fact, VBDR indicated a maximum magnitude of 10 ms^{-1}, and both orientations, NOR and CIM, showed total agreement with the DD finding.

It has been suggested by Rinehart (1979) that a way of deducing the direction of the wind flow in the VMP, either up or down, could be obtained by comparing the direction of vectors produced in finding the VMP to the vectors produced when deriving the horizontal wind field using TREC. If the vectors are pointing in the same direction then the pattern is indicating upward motion, whereas, if the vectors are pointing in the opposite direction then the pattern is showing predominantly downward motion. This type of comparison produced inconclusive results in this

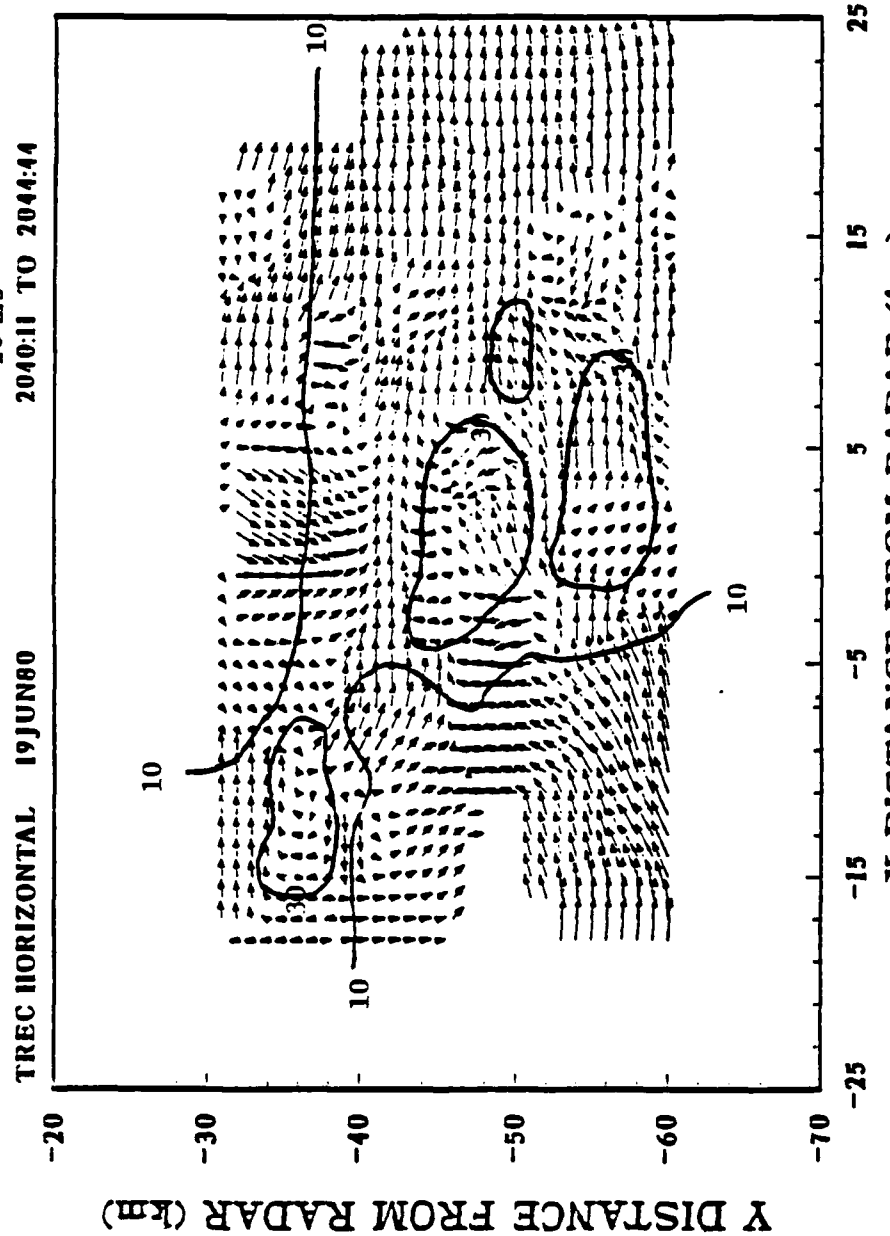

Fig. 16. Cimarron Doppler radar derived horizontal wind and reflectivity fields at 1 km AGL for 2040:11 to 2044:44 CST.

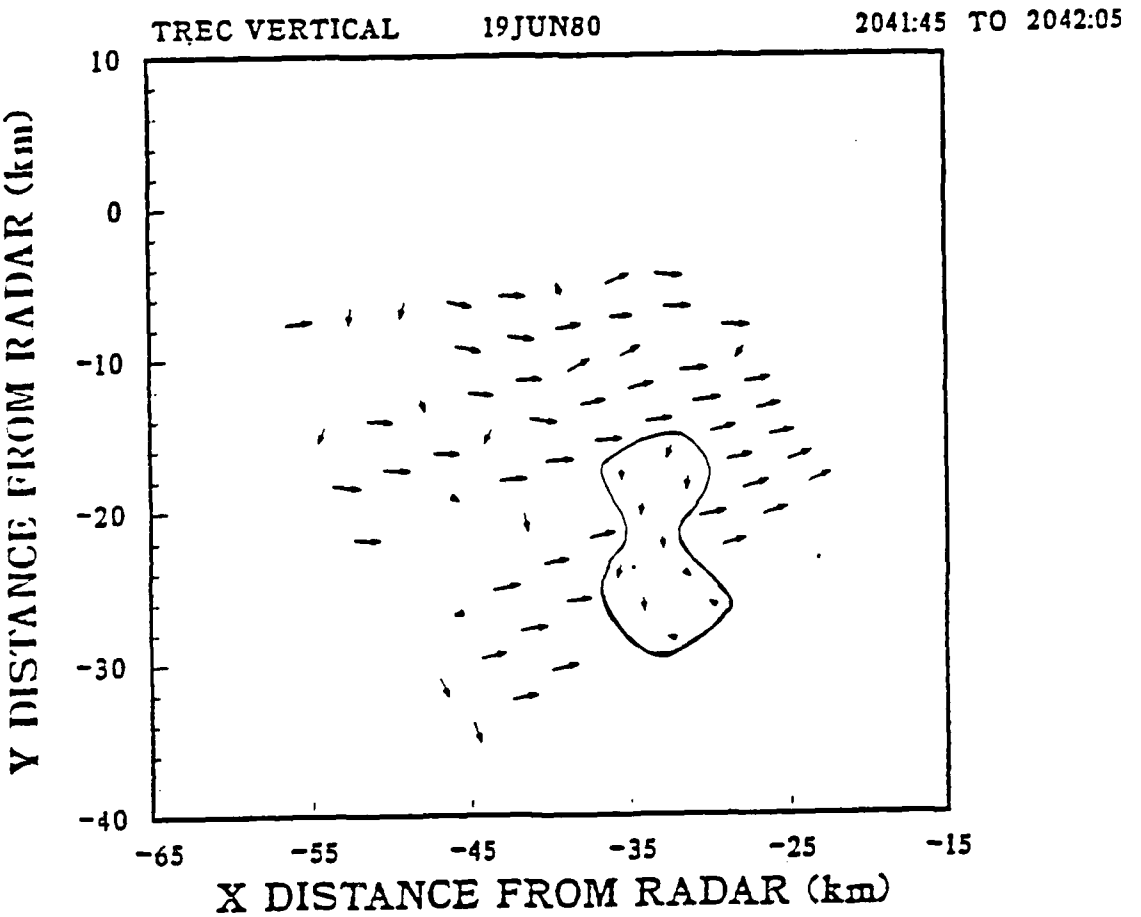

Fig. 17. As in Fig. 6, except for 2041:45 to 2042:05 CST.

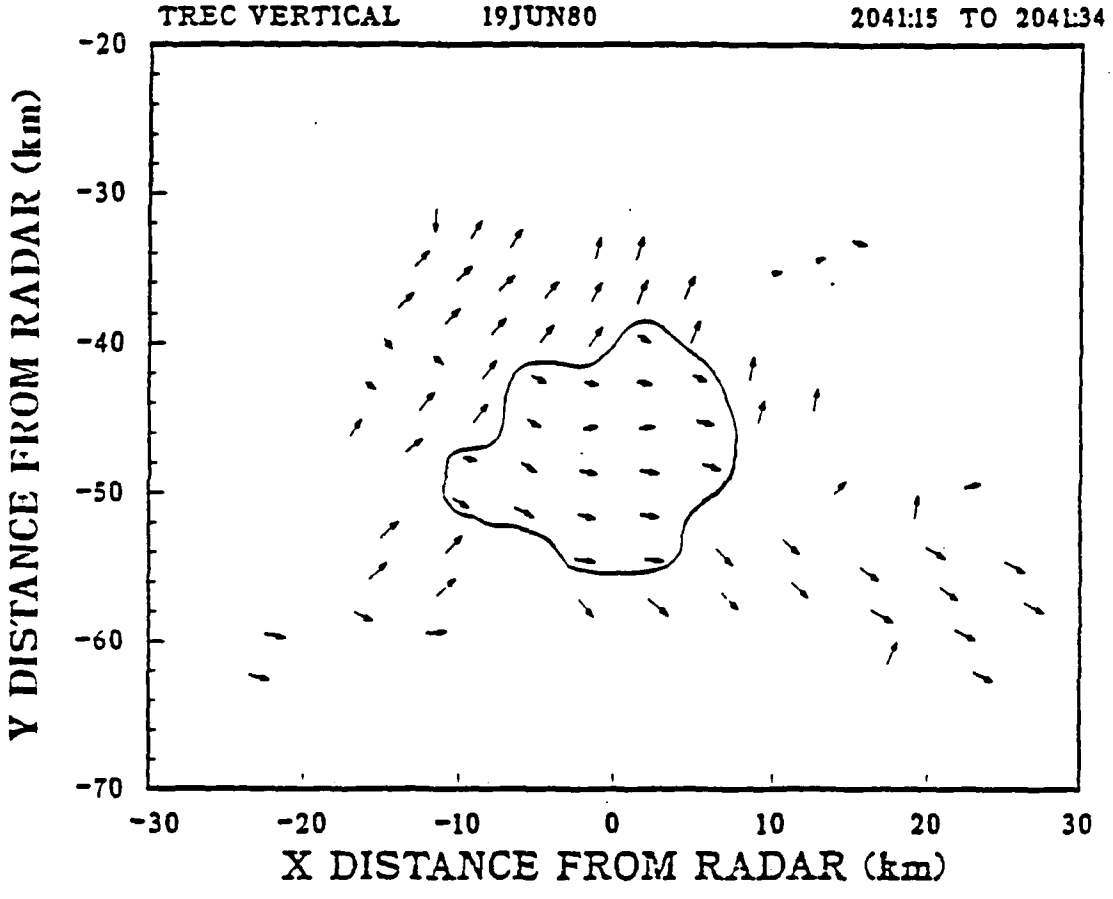

Fig. 18. Cimarron Doppler radar derived VMP within the solid line at 6 km AGL for 2041:15 to 2041:34 CST.

(a)

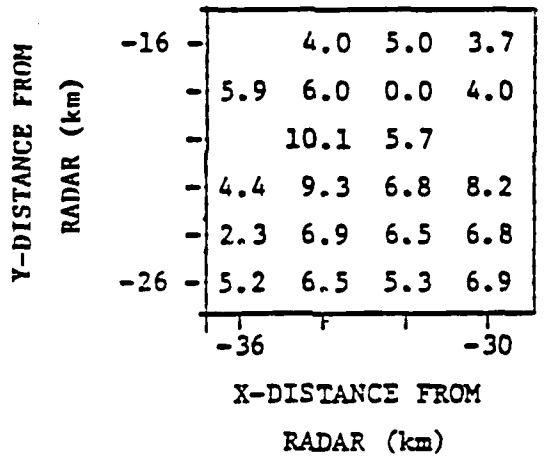

(b)

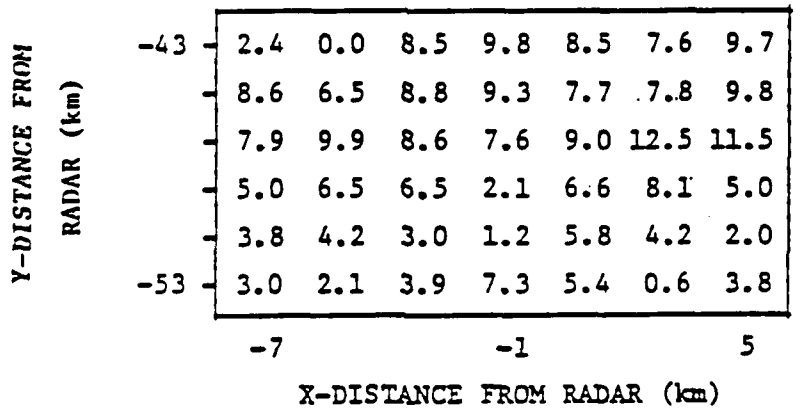

Fig. 19. As in Fig. 11, except (a) for 2042:05 to 2046:52 CST; (b) Cimarron for 2041:45 to 2046:05 CST.

study. The NOR data showed vectors that were mostly orthoganal in the northern quadrant. In the southern area, however, the comparison did lead to the conclusion that the area was dominated by upward motion. However, when using the CIM results one would conclude just the opposite. Therefore, two conclusions could be made. The first is that the original suggestion by Rinehart is not absolutely correct for the entire pattern. Secondly, radar orientation does seem to have an effect. The CIM data gave a completely different and incorrect result.

A cross-section was constructed through the center of the storm (Fig. 20). The reflectivities were superimposed on the graph. Vectors that lay in regions of weak reflectivities should be viewed with caution (Bonewitz, 1986). The region of the main updraft was quite evident (x = -31 to -27). Also, in the lower levels the air flow indicated that entrainment was taking place. A middle- to upper-level downdraft was seen on the western edge of the storm. This was not reported by VBDR and was not analyzed by TREC because it was found to be located in a weak reflectivity region. However, this feature was most likely a return air flow from the thunderstorm to the east.

At 2052 CST the vertical motion area and magnitude at 6 km AGL, as shown by VBDR, had increased (Fig. 21). The maximum updrafted was 30 ms^{-1} and was associated with a relatively weak reflectivity maximum of 36 dBZ.

As indicated in Chapter II the data were gathered by NSSL in sector format, which means only the area of interest was scanned by the radar. This type of data gathering format can cause major difficulties for TREC. When the phenomena of interest are located near the edge of the sector, TREC cannot completely resolve those phenomena. The specification of box size and search radius cause resolution problems at the edge of a sector and, depending on these values, the first reliable

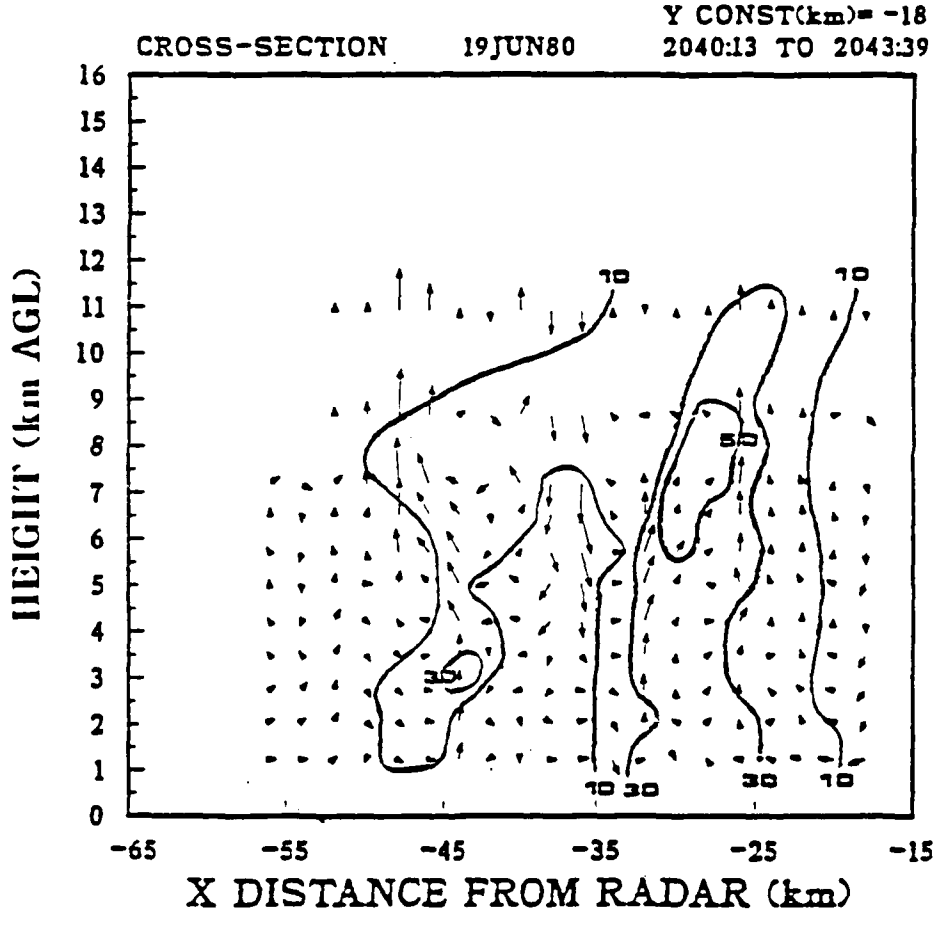

Fig. 20. Norman Doppler radar vertical cross-section and reflectivity field at y=-18 km for 2040:13 to 2043:39 CST.

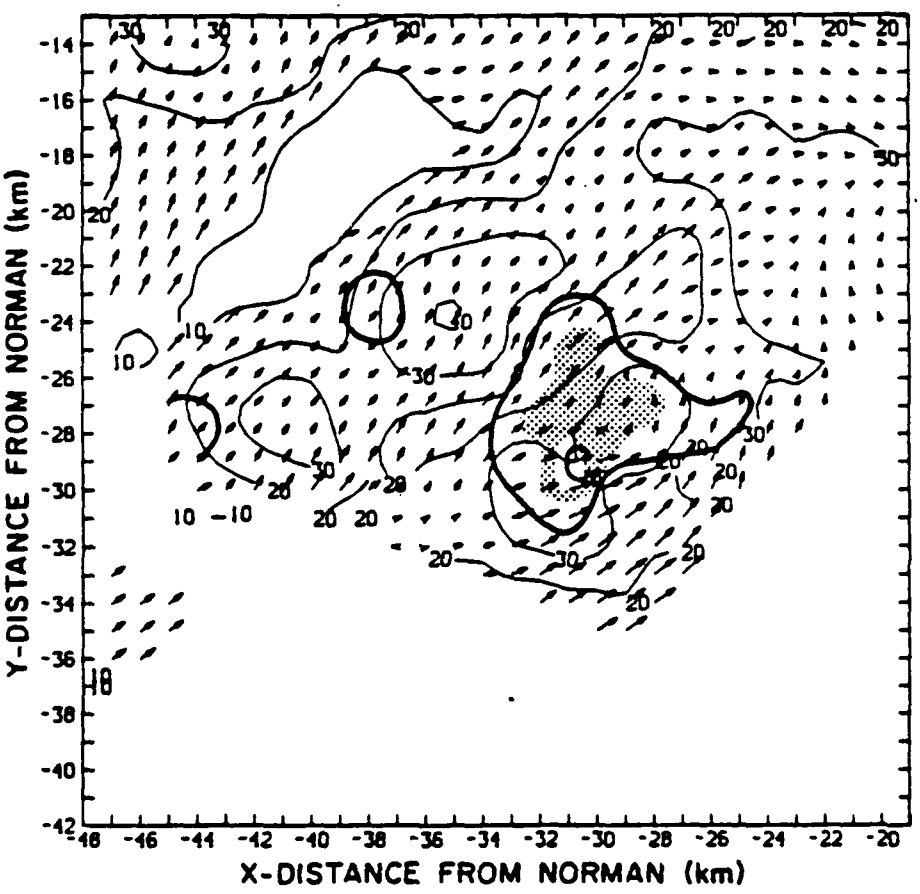

Fig. 21. As in Fig. 7, except at 6 km AGL for 2052 CST.

vector produced by TREC can be located up to 5 km from the edge of the sector.

It can be seen in Fig. 21 that the major updraft area was located near the edge of the sector and in Fig. 22 TREC was unable to resolve the pattern. By using the CIM data this problem was solved. In Fig. 23 the complete VMP was resolved. It does extend a few kilometers farther north and east than reported by VBDR, but TREC has identified the major updraft.

The 6 km AGL horizontal wind field for CIM is shown in Fig. 24. In the western region, (-3,-57), the wind field agreed with the DD wind field, however, TREC did show an area of converging winds (-1,-55) that did not appear in the DD field. This area was located in the center of the VMP and was obviously contributing to the updraft. Even though this pattern was not found in the DD field, it was a reasonable feature. Rinehart (1979) stated that both fields, TREC and the DD, may be correct, the difference between them resulting from the difference in a time averaged field, TREC, and a high resolution, instantaneous field, the DD field. The western portion of Fig. 24 did agree with the DD results. In that region both fields had predominantly southwesterly winds varying between 5-15 ms^{-1}. For the most part the eastern region of Fig. 24 did not lend itself to direct comparison because the DD field did not extend that far eastward.

The 1 km AGL horizontal wind field is shown in Fig. 25. Both low and middle-level wind fields (Figs. 24-25) indicated convergence centered at (5,-55), however, the low-level field indicated predominantly west to southwest flow. The convergent feature found in the middle-level field was a dominant feature with all vectors within a 5 km radius of the center of the directed into it. Thus, the two wind fields were not the same, which indicated that there was no influence of generator level flow as suggested by other researchers.

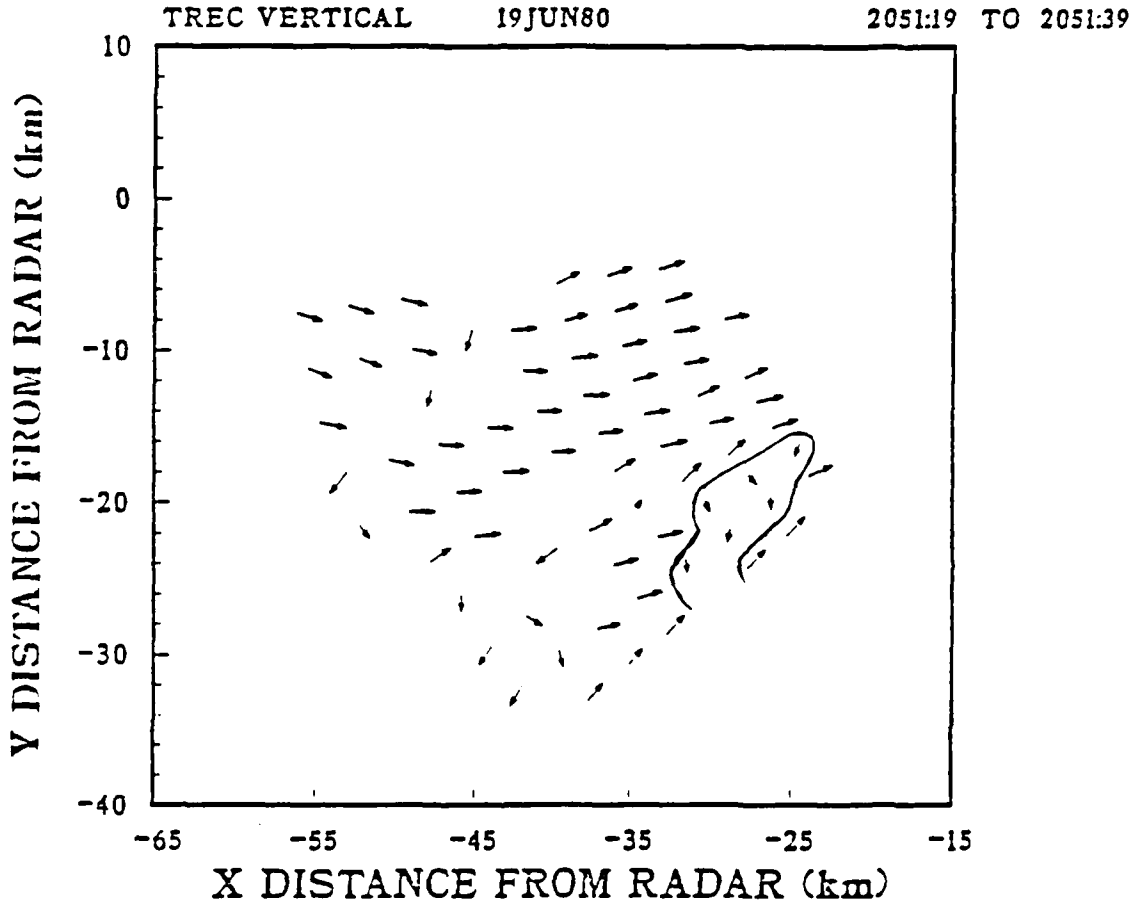

Fig. 22. As in Fig. 6, except for 2051:19 to 2051:39 CST.

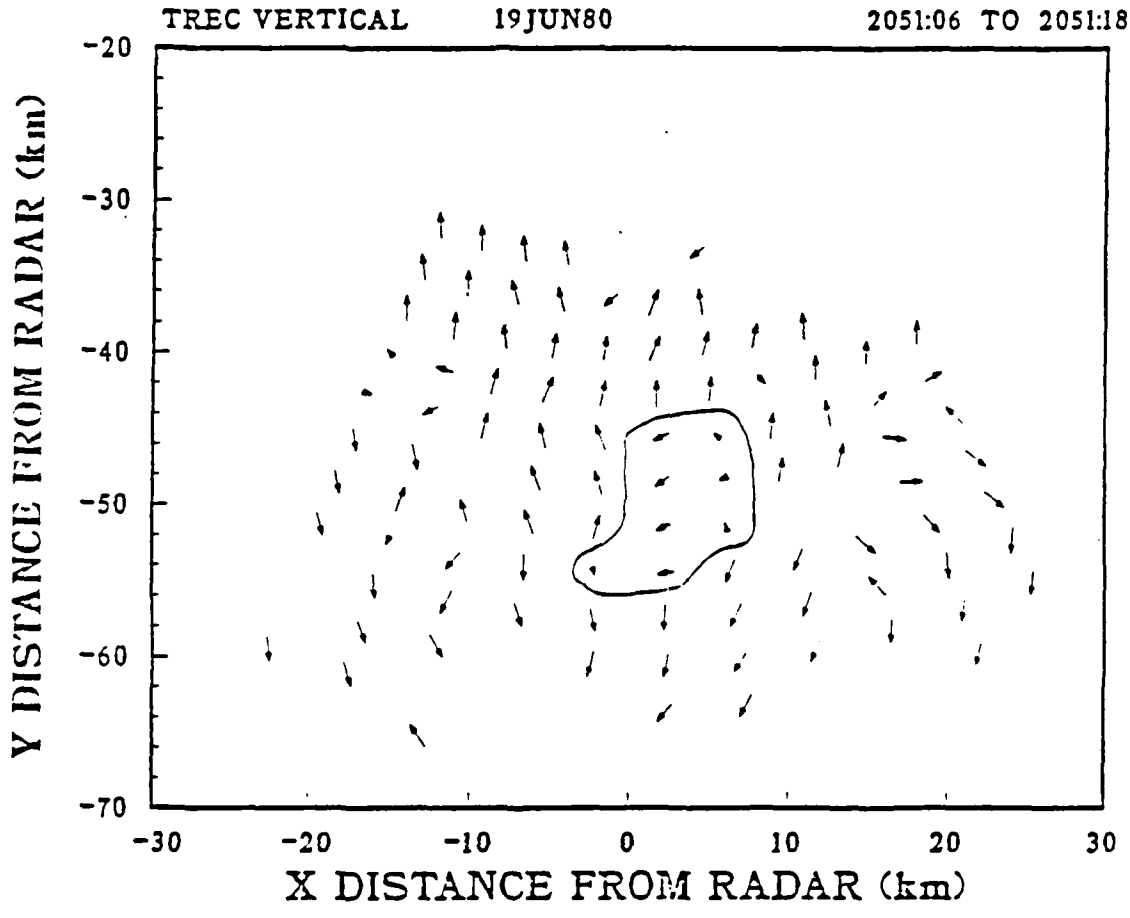

Fig. 23. As in Fig. 18, except for 2051:06 to 2051:18 CST.

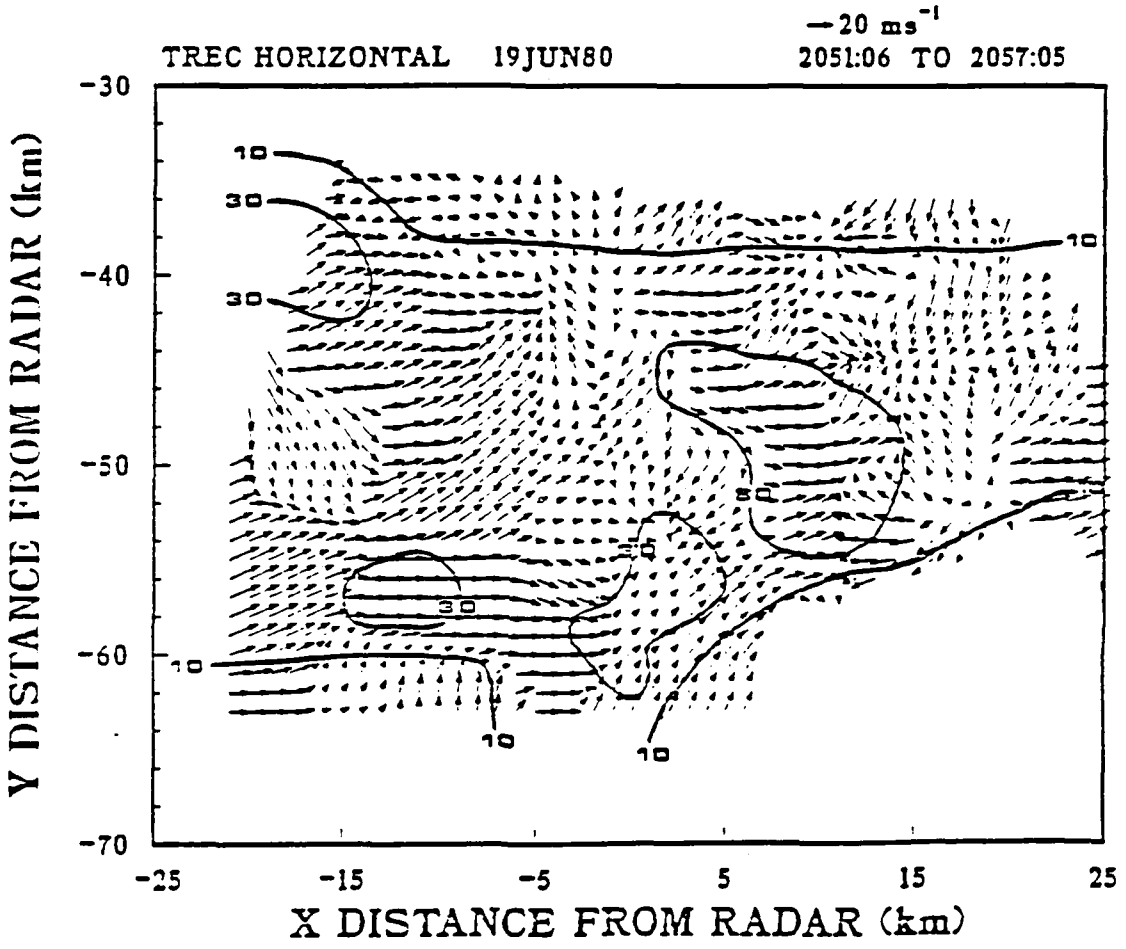

Fig. 24. As in Fig. 15, except for 2051:06 to 2057:05 CST.

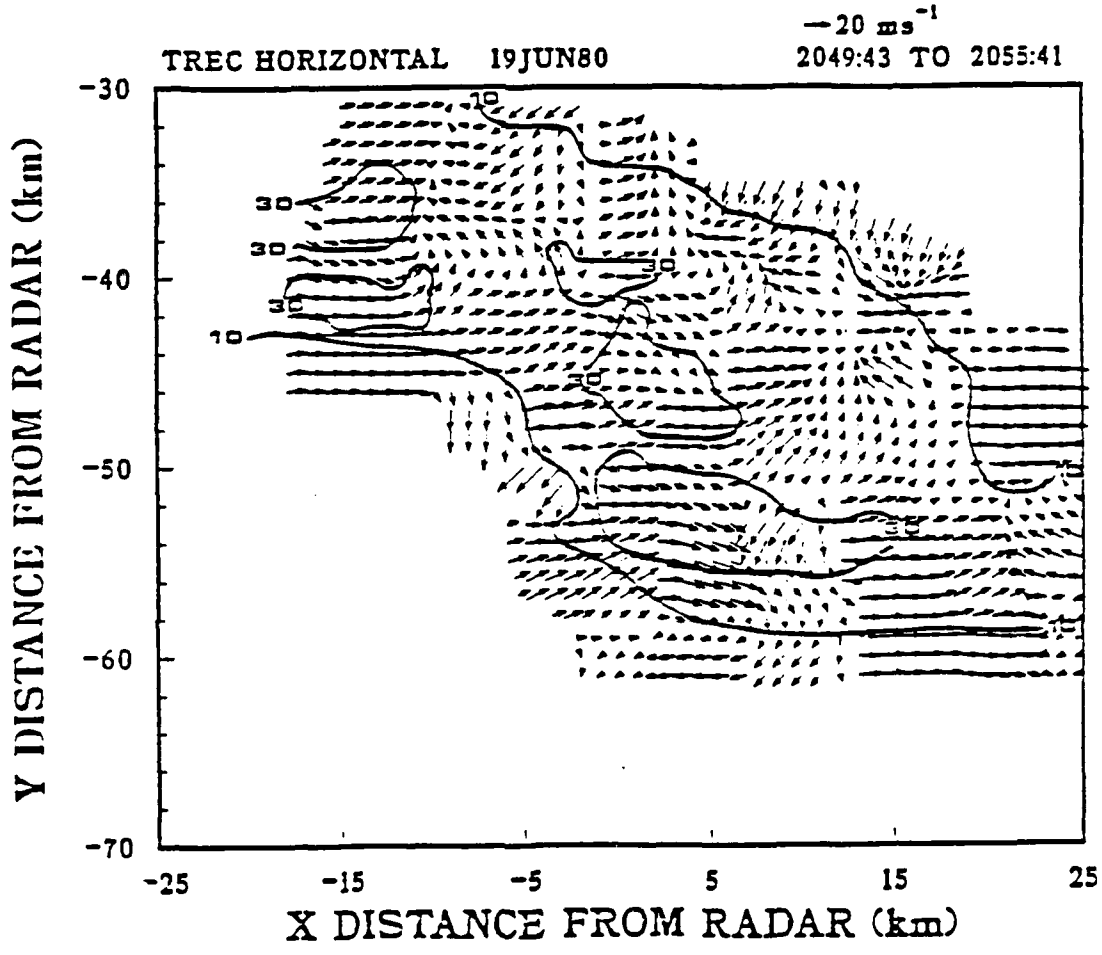

Fig. 25. As in Fig. 16, except for 2049:43 to 2055:41 CST.

The calculation of the vertical motion magnitudes was performed after the horizontal wind field was found. VBDR reported a maximum updraft of 30 ms^{-1}. Using TREC the maximum updraft was found to be 18 ms^{-1}. When considering the error limits supplied by VBDR for the DD field and by Rinehart for the TREC field, TREC does show agreement with the DD results. It is apparent,however, that TREC did underestimate the vertical velocities. This underestimation could be attributed to two factors. First, the maximum reflectivity in the VMP area was 36 dBZ. For TREC to operate effectively one needs a very distinct pattern with sharp reflectivity gradients together with a strong flow field. These two requirements were not exceptional at this time. Second, the time increment was too long. The desirable time increment, as indicated in Chapter II, should be less than 5 min. In this case it was 6 min. The longer time lag allowed greater averaging of the field. Therefore, the calculated vertical velocities reflected a velocity averaged over a longer time. However, even with this obvious shortfall an important conclusion can be drawn from this time period. TREC did indicate that a more intense updraft had formed in the same region that was reported by the DD analysis.

Twenty min later the storm complex took the appearance of a uniform echo mass instead of a series of individual cells. As VBDR indicated, the area enclosed by the 40 dBZ contour increased from 27 km^2 to more than 125 km^2 in only 30 min. Beginning with the 2116 CST period the storm took on more supercell characteristics. In fact, within 15 min, 2116 to 2131 CST, a hook echo formed. Upon comparison of the two derived wind fields and the TREC VMP field at 6 km AGL (Figs. 26-28) one sees a surprising amount of similarity.

In Fig. 27 the TREC VMP has the same shape that was reported by VBDR (Fig. 26) for the major updraft region. TREC did give an indication of this area

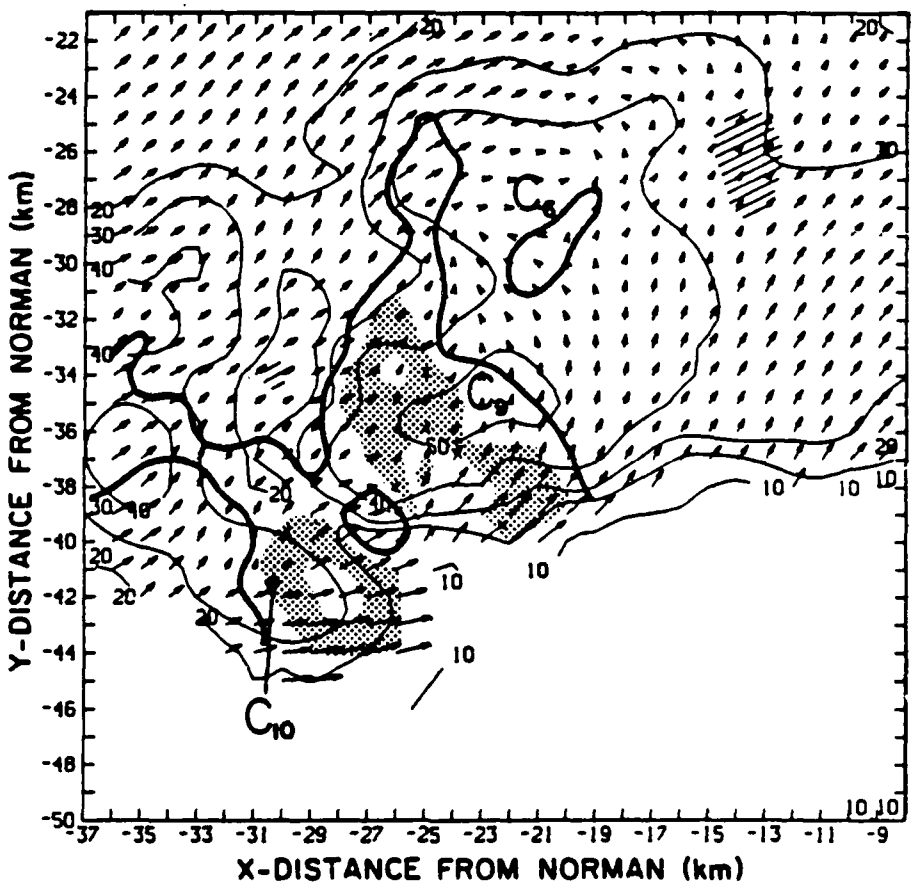

Fig. 26. As in Fig. 7, except at 6 km AGL for 2116 CST.

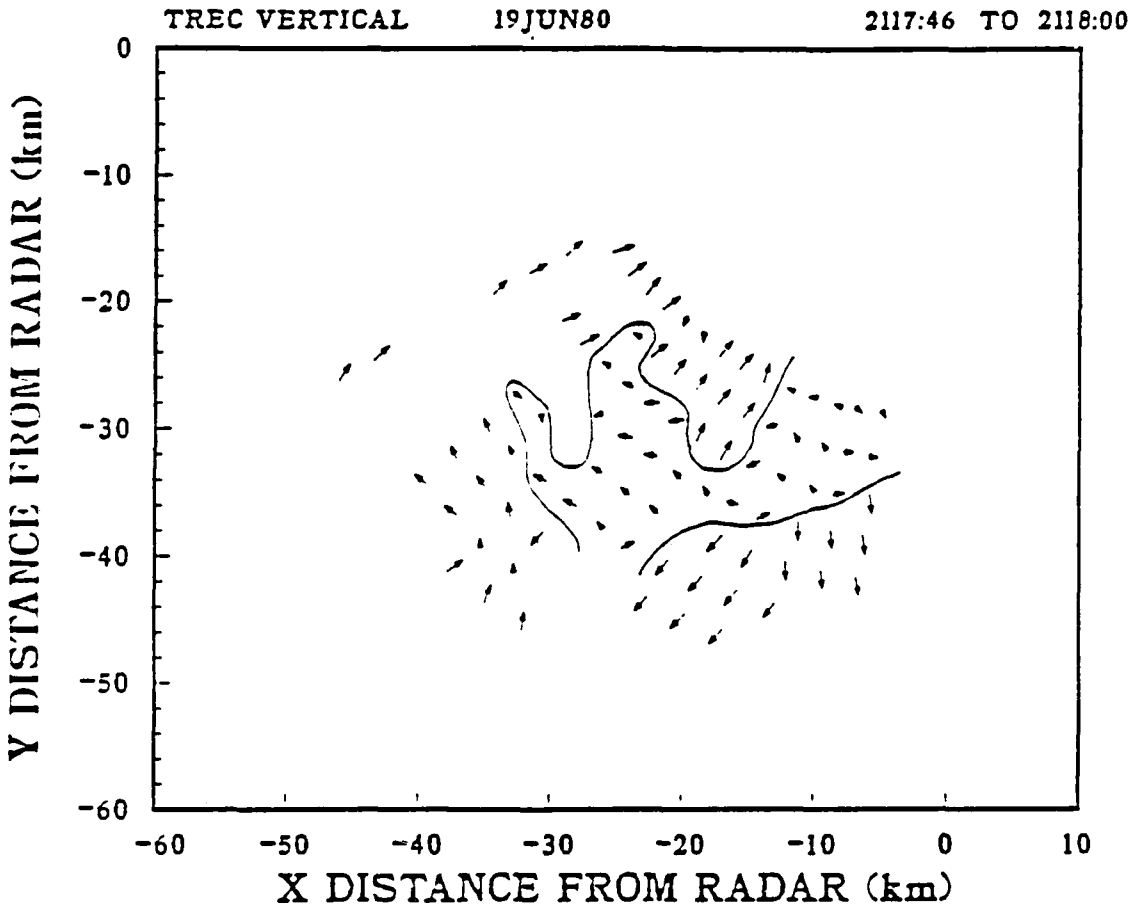

Fig. 27. As in Fig. 6, except for 2117:46 to 2118:00 CST.

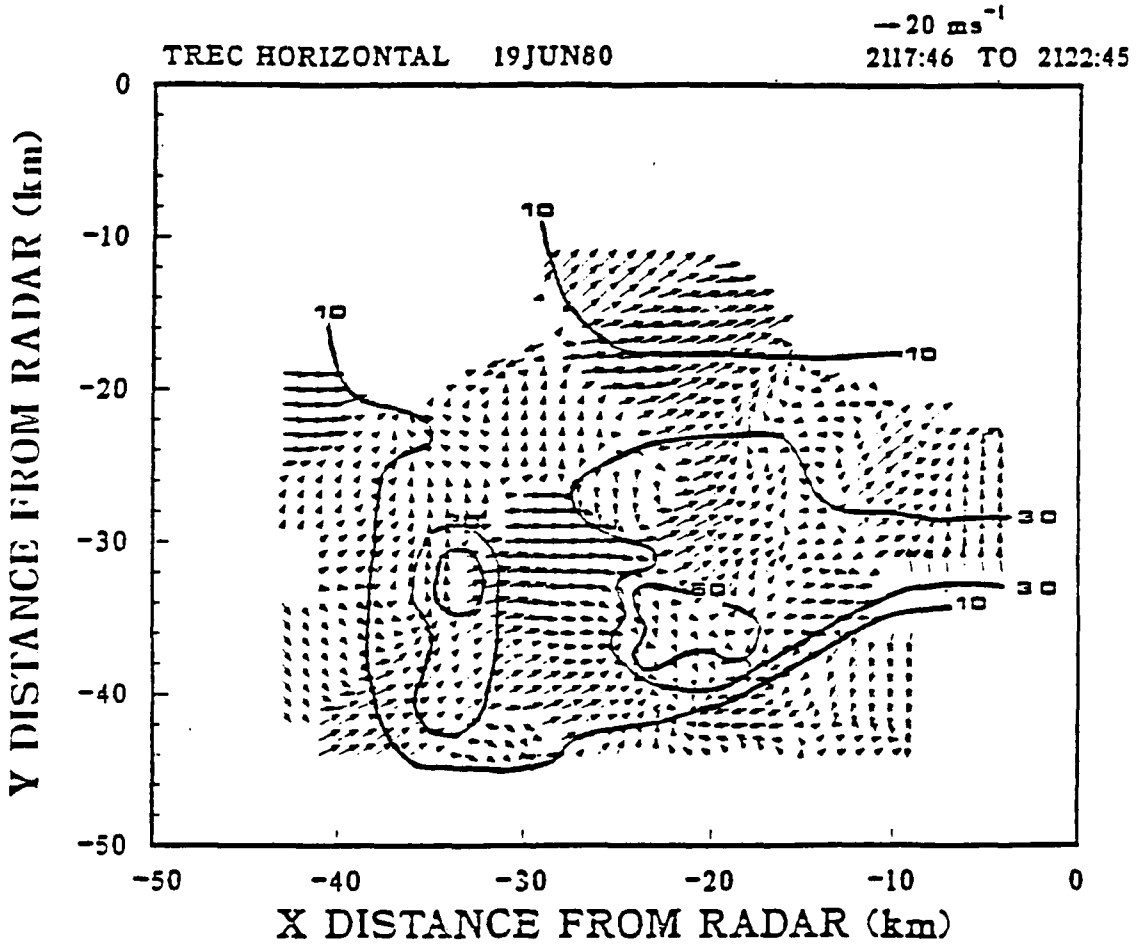

Fig. 28. As in Fig. 9, except for 2117:46 to 2122:45 CST.

extending farther eastward. This extension coincided with the expanding 40 dBZ area. The vertical velocities in this region were less than 5 ms^{-1}. VBDR also reported a downdraft centered at (-13,-26). In that region TREC showed a very weak downdraft of 0.5 ms^{-1}.

The two 6 km AGL horizontal wind fields were also in agreement (Figs. 26 and 28). Both derived fields indicated southwesterly flow in the western section. There was some disagreement between the wind fields in the eastern quadrant. Both showed a general southerly flow; however, at (-15,-26) TREC's field was somewhat erratic. This feature was related to the somewhat uniform reflectivity field in that area. When the uniqueness of the reflectivity field was lost, the ability of TREC to discern the proper pattern, thus wind direction, was lost. This reinforced the need for a strong meteorological phenomena to be present over the entire observation area to make TREC completely effective.

Both TREC and the DD fields showed several convergent patterns located at (-17,-24), (-21,-29), and (-26,-37). TREC indicated an area of convergence at (-21,-39) that did not appear in the DD field. This feature was in the vicinity of a forming hook echo and an updraft of 35 ms^{-1} .

The TREC derived vertical velocities at 6 km AGL are shown in Fig. 29. The values within the VMP indicated a weak downdraft associated with the 50 dBZ cell centered at (-20,-37). TREC produced speeds of greater than 10 ms^{-1} in the north where the DD indicated values between 5-10 ms^{-1}. The regions of maximum velocities agreed with both indicating a maximum of 35 ms^{-1} at (-21,-39). TREC also showed an area of 16 ms^{-1} in the western area of the VMP. This feature was lacking in magnitude in the DD analysis . However, it did seem to be a realistic feature being associated with a 50 dBZ cell.

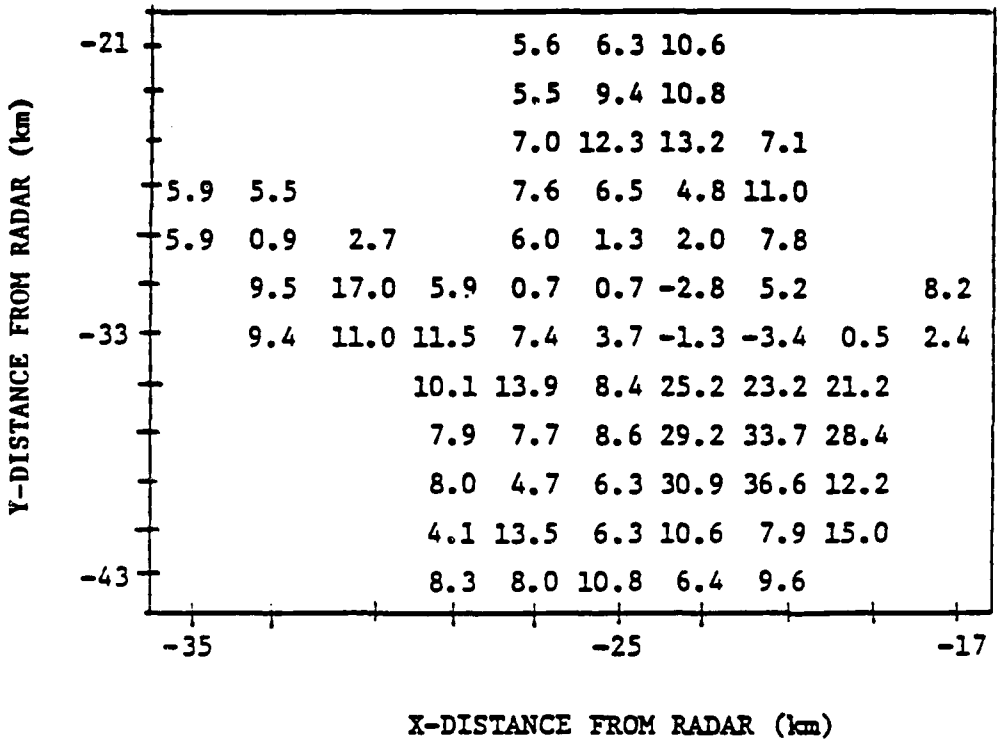

Fig. 29. As in Fig. 11, except for 2117:46 to 2122:45 CST.

Within 5 min the VMP at 6 km AGL had increased to over 300 km^2 (Fig. 30). The general movement of the VMP had been southeasterly, which coincided with the movement of the major reflectivity pattern. Also, the southwestern edge of this pattern was the site wherein the hook echo became visible within ten min. When compared with the reflectivity field (Fig. 31) at that level, an area of greater than 50 dBZ was centered within the VMP. There was an area of convergence coinciding with the location of the forming hook echo (-26,-41). The horizontal wind field within the VMP exhibited a definite cyclonic rotation. This rotation pattern would be expected in this situation. The rotation resulted in a stronger convergence (Brandes, 1981) which reinforced the developing updrafts.

The horizontal wind field for 1 km AGL is shown in Fig. 32. The western portion of the field had air flowing from the southwest. In the region where the hook echo was forming, the air flow abruptly turned anti-cyclonically and became northerly. The region of northerly winds was much broader than at 6 km. Other than this feature the two fields had little in common, thus at this stage of development little influence of the generator level was seen.

Upon computation of the vertical motion magnitudes at 6 km AGL, the updraft in the region of the developing hook echo was on the order of 35 ms^{-1} (Fig. 33). At (-11,-35) the horizontal winds indicated a weak divergent pattern and subsequent magnitudes in this area dropped to 3 ms^{-1}. With this one exception the vertical velocities were all on the order of 5 ms^{-1} or greater with the strongest values found in the vicinity of the developing hook echo.

A cross-section was taken through the developing hook echo (Fig. 34). In the lower levels around the developing hook echo (x = -23) one notes an echo overhang with air flowing inward, turning abruptly, and flowing upward with a greater vertical

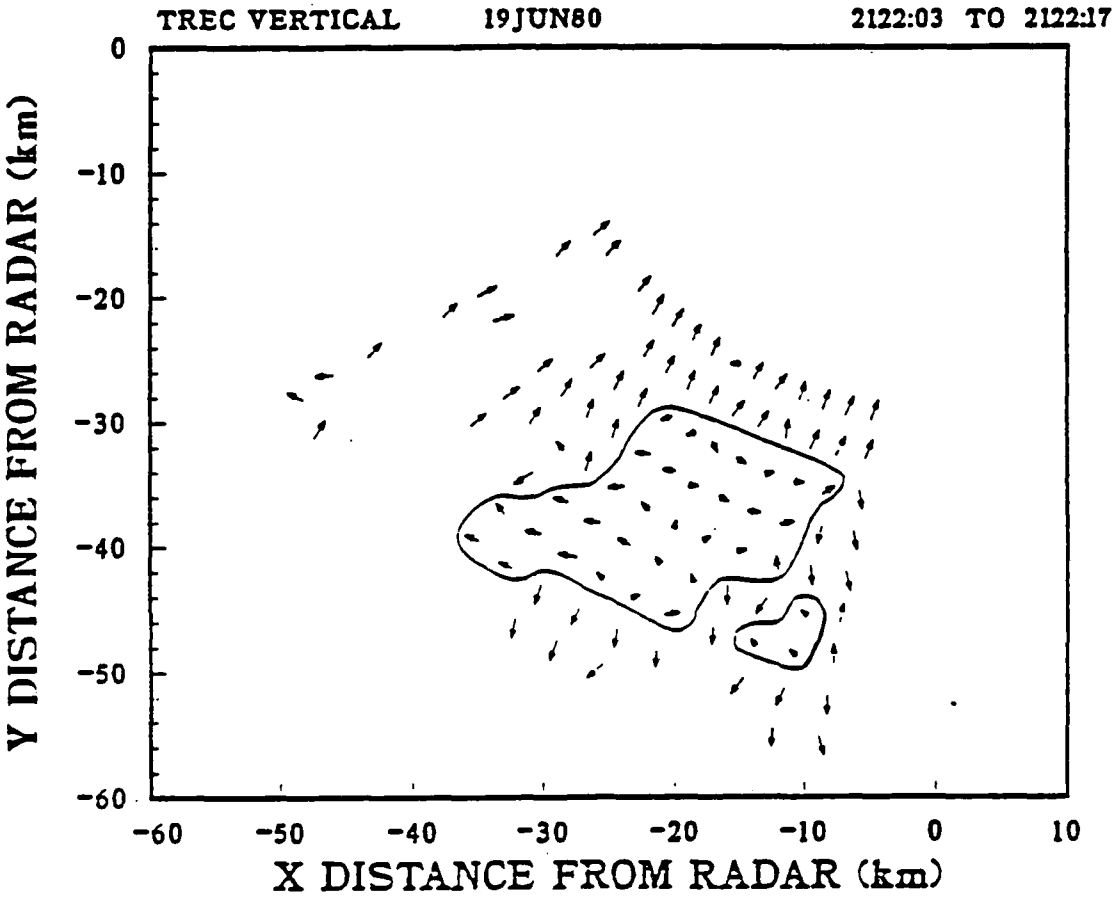

Fig. 30. As in Fig. 6, except for 2122:03 to 2122:17 CST.

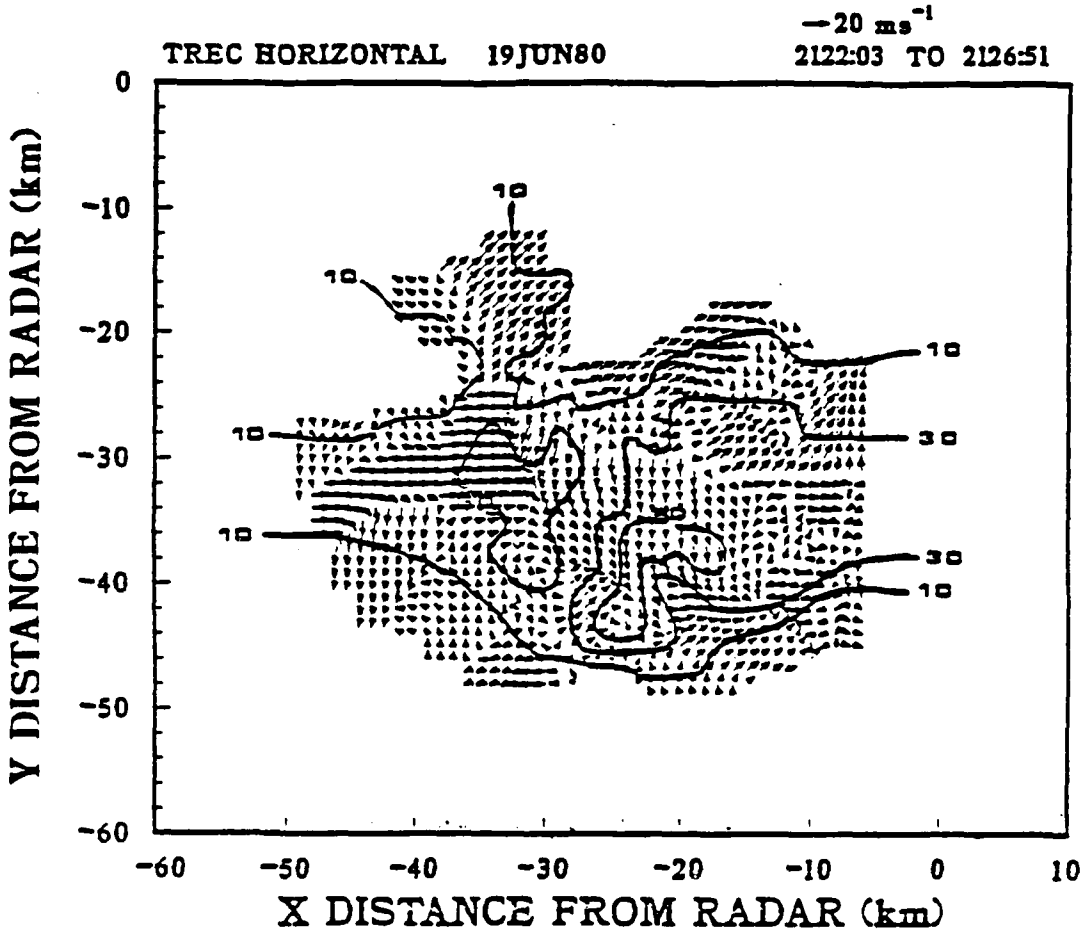

Fig. 31. As in Fig. 9, except for 2122:03 to 2126:51 CST.

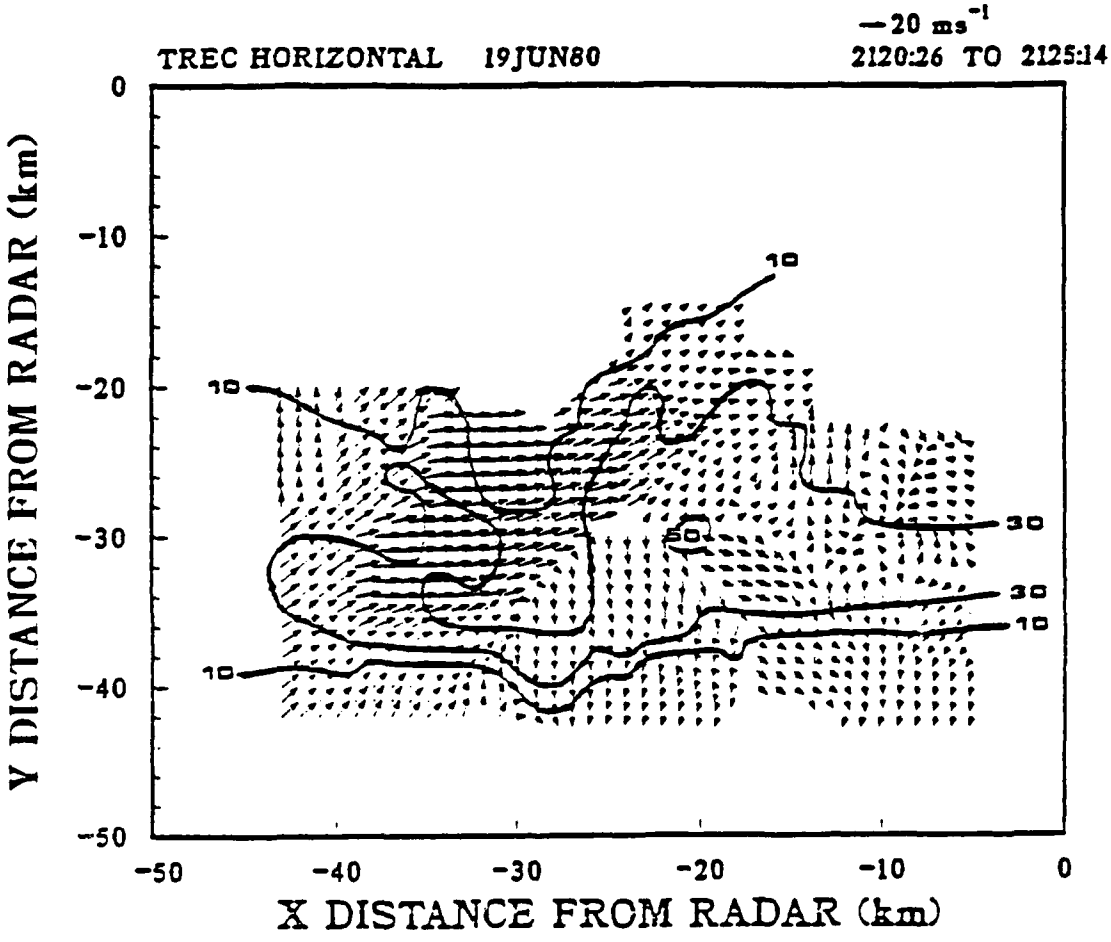

Fig. 32. As in Fig. 12, except for 2120:26 to 2125:14 CST.

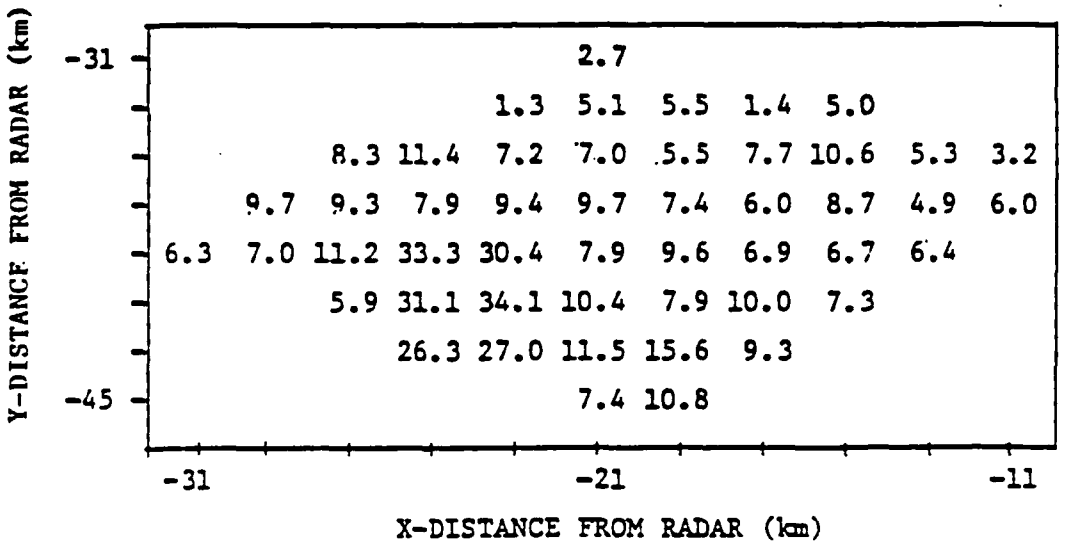

Fig. 33. As in Fig. 11, except for 2122:03 to 2126:51 CST.

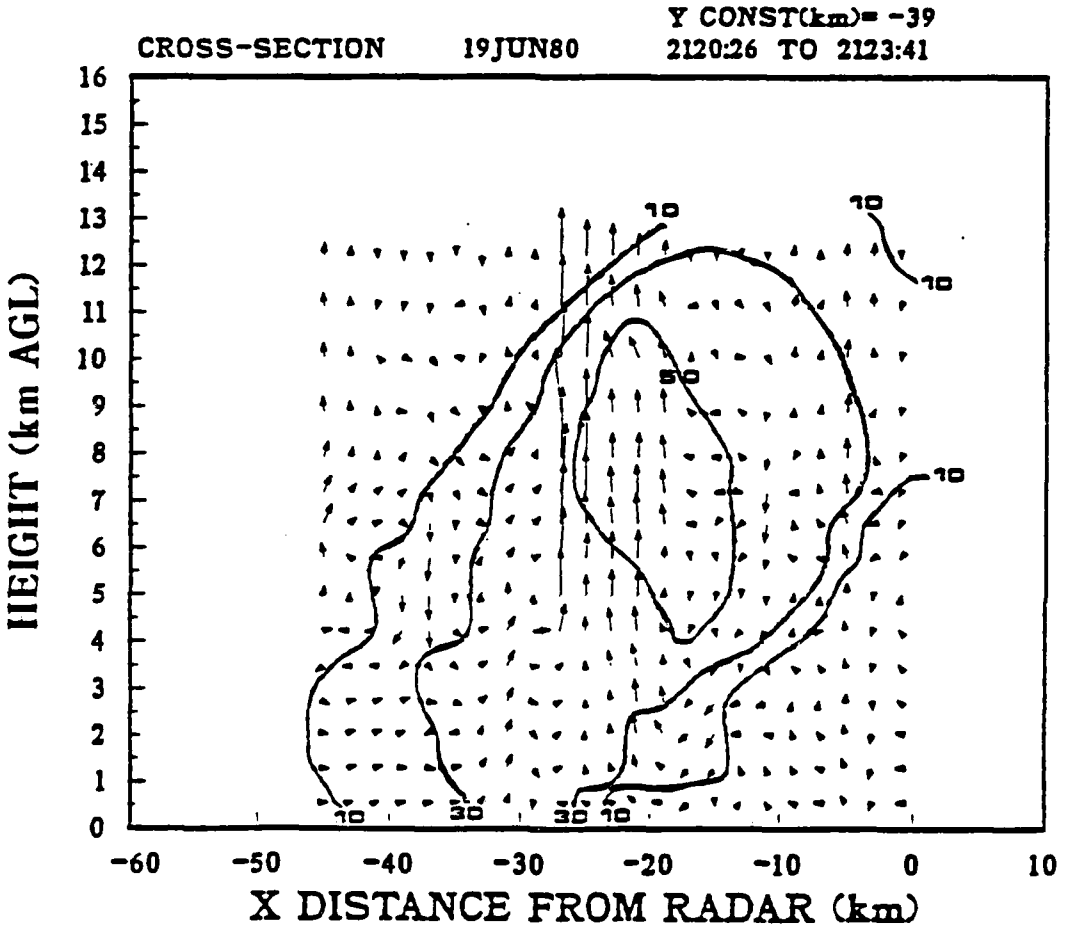

Fig. 34. As in Fig. 20, except at y=-39 km for 2120:26 to 2123:41 CST.

velocity. Air was being entrained into the main storm complex from both sides of the storm. The maximum updraft was located on the western edge of the 50 dBZ cell. Air was exiting the storm top and returning on either side.

The CIM data for this time revealed that the VMP at 6 km AGL had a shape similar to that shown by VBDR for 2116 CST (Fig. 35). The pattern had moved southeastward, but still coincided with the region of maximum reflectivity. The TREC derived horizontal wind fields (not shown) indicated westerly winds of 10 ms^{-1} throughout this area, which was somewhat in disagreement with VBDR, who reported southwesterlies. Also, an area of convergence was located in the eastern region of the 50 dBZ contour, which coincided with an area of vertical motion greater than 10 ms^{-1}. It was in this region that the hook echo formed. Another area of convergence was found in the northern portion of the derived VMP. This area was soon to be engulfed in the 50 dBZ contour and have a vertical velocity in excess of 30 ms^{-1}. Just east of the main VMP, TREC indicated an area of downward motion. This area was most probably associated with precipitation. The TREC calculated vertical motions are shown in Fig. 36. The larger values centered at (3,-60) were related to the developing hook echo. Once again the values were usually larger than 5 ms^{-1}, were in agreement with the DD values, and indicated a wider area of moderate to strong updrafts developing.

Supercell Phase

The supercell phase was chacterized by an increase in updraft speeds, reflectivity, and areal coverage of the storm. The Lindsay storm continued to propagate southeastward with DD values of the aforementioned variables exceeding 60 ms^{-1}, 60 dBZ, and 250 km^2, respectively.

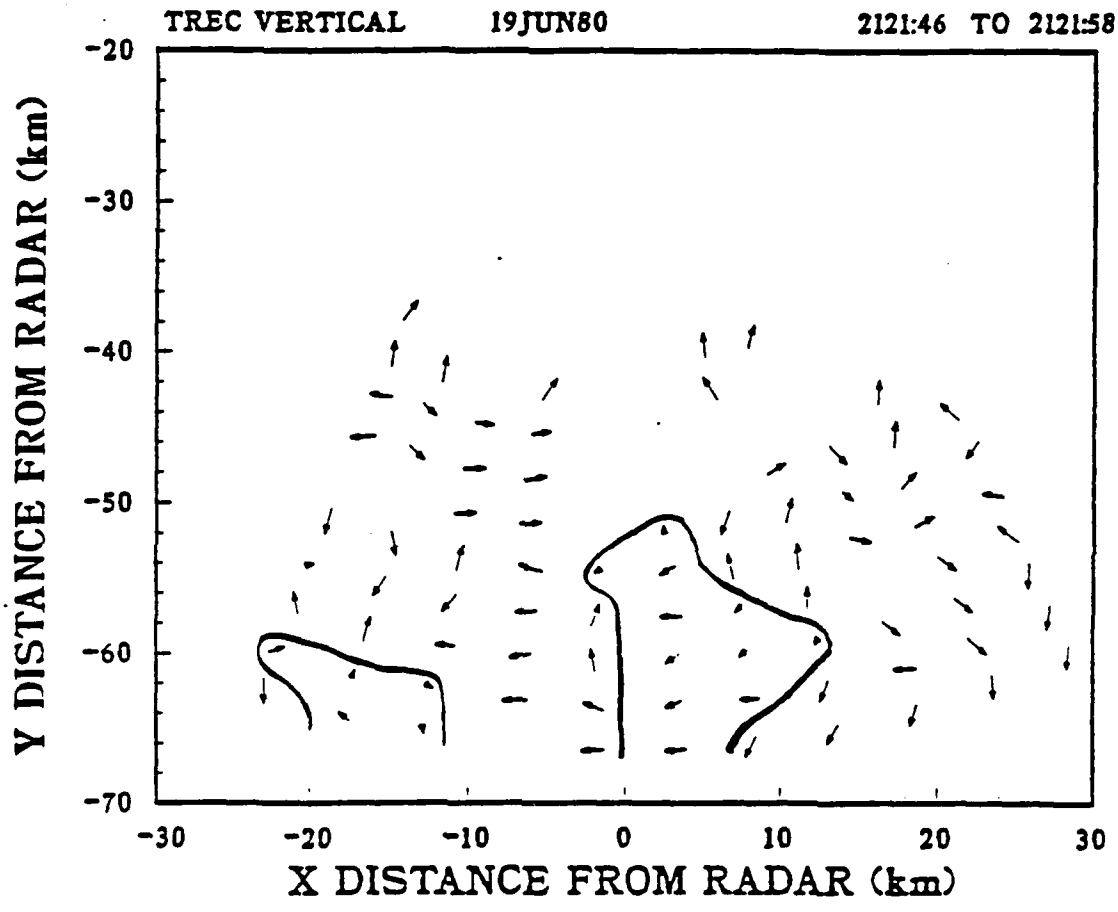

Fig. 35. As in Fig. 18, except for 2121:46 to 2121:58 CST.

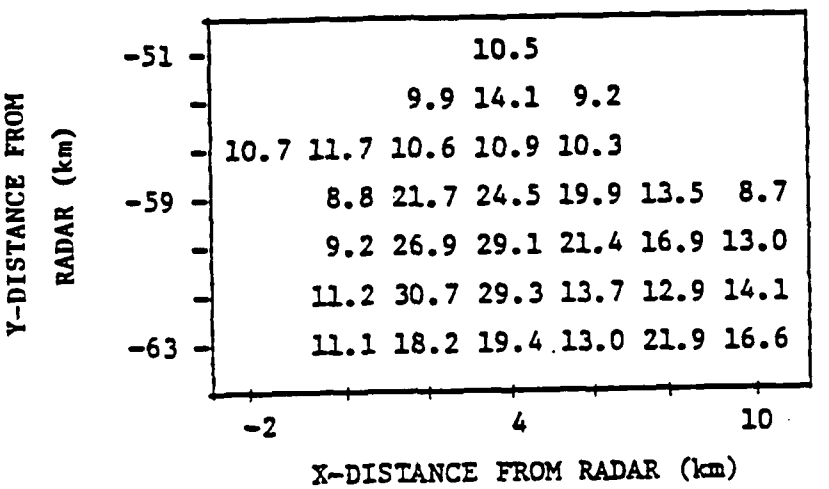

Fig. 36. As in Fig. 11, except Cimarron for 2116:35 to 2121:46 CST.

Doppler data available for this phase began at 2150 CST with three complete volumes extending to 2205 CST. There was a 5 min time increment between the volumes. After 2205 CST the data were gathered sporadically and often had a time increment of 7 - 10 min, making these data unusable in this study.

At 2152 the VMP at 6 km AGL is shown in Fig. 37. Within the last 30 min the area of vertical motion had doubled in size (see Fig. 35) in conjunction with the development of the mesocyclone. The 12 km AGL VMP (Fig. 38) encompassed the same region as the 6 km VMP. The western areas appeared to be truncated due to the radar sector scanning.

The derived horizontal wind field at 6 km AGL is shown in Fig. 39. The general flow pattern was from the northwest. This flow agreed with the 50 kPa and the skew-T diagram winds shown in Appendix C. The TREC field indicated an overall cyclonic pattern, which was be expected for a supercell storm. Also, a very definite cyclonic circulation had developed *southeast of the major cell*. This could be in response to the cell and the accompanying mesocyclone propagating southeast.

The 12 km AGL derived wind field is shown in Fig. 40. Once again the major core of cyclonic circulation located at (-8,-50) could be seen. Within 5 min this area became what VBDR described as a core of a fully developed supercell thunderstorm with reflectivities on the order of 60 dBZ and vertical velocities greater than 40 ms^{-1}.

A comparison of these TREC derived wind fields at each level clearly indicated a distinct flow field at these two levels. In fact, there was clearly a directional shear between them. This shear was not as evident in the lower levels. The low-levels (not shown) indicated a predominant north to northwest flow in the western regions, which agree with the middle-levels. It is obvious there was similarity between the

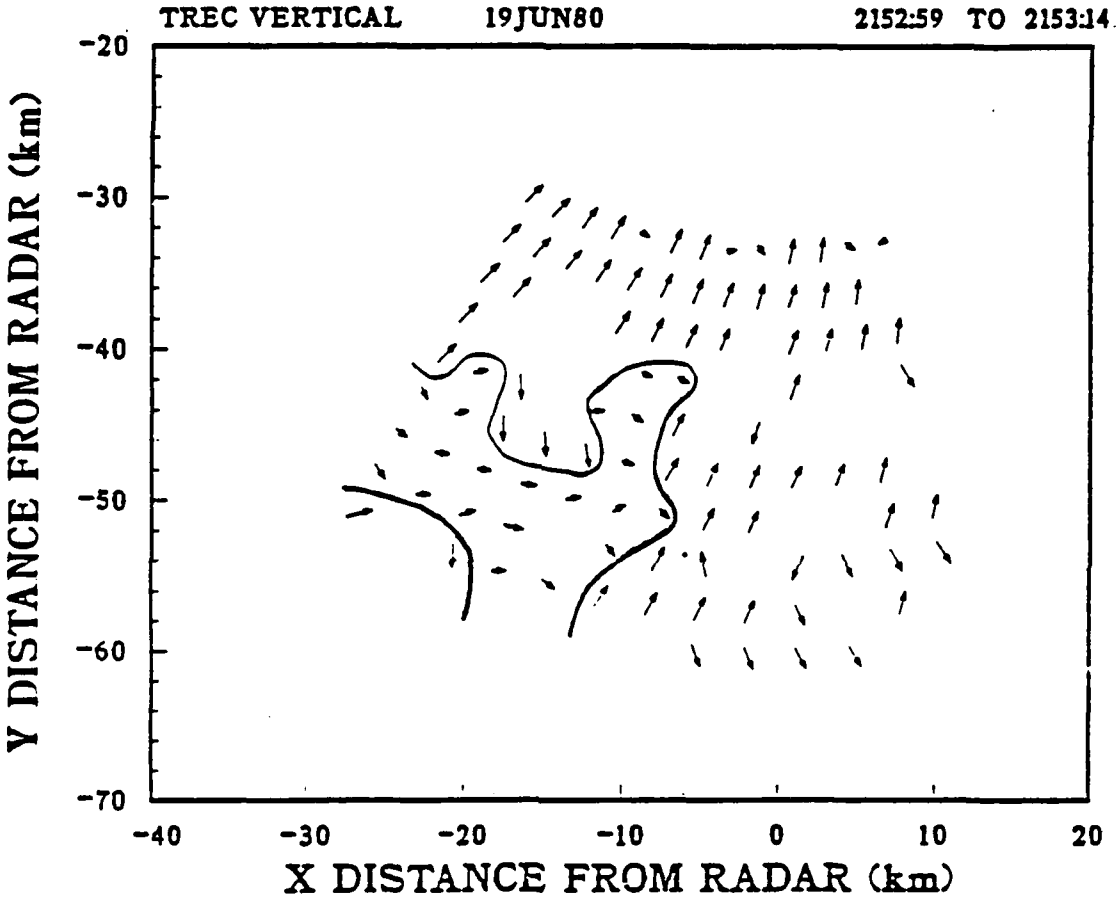

Fig. 37. As in Fig. 6, except for 2152:59 to 2153:14 CST.

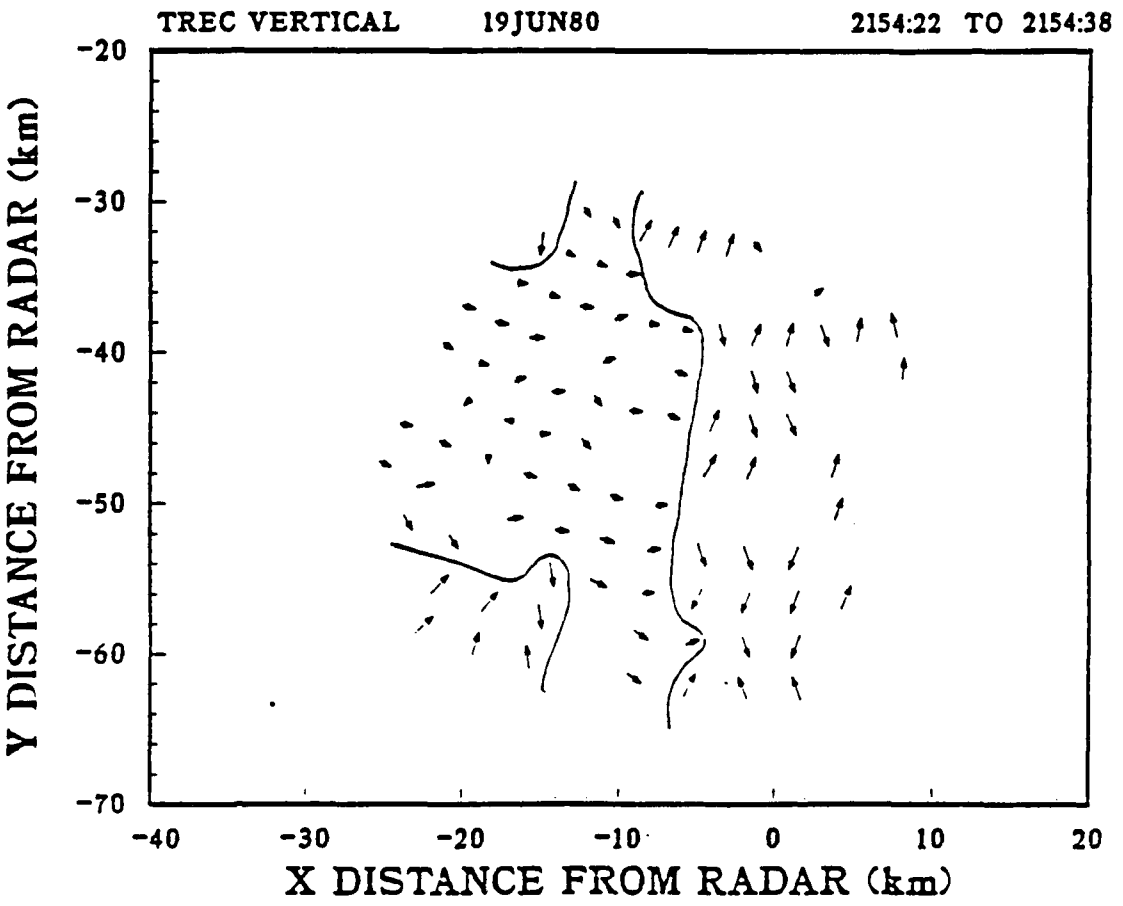

Fig. 38. As in Fig. 6, except at 12 km AGL for 2154:22 to 2154:38 CST.

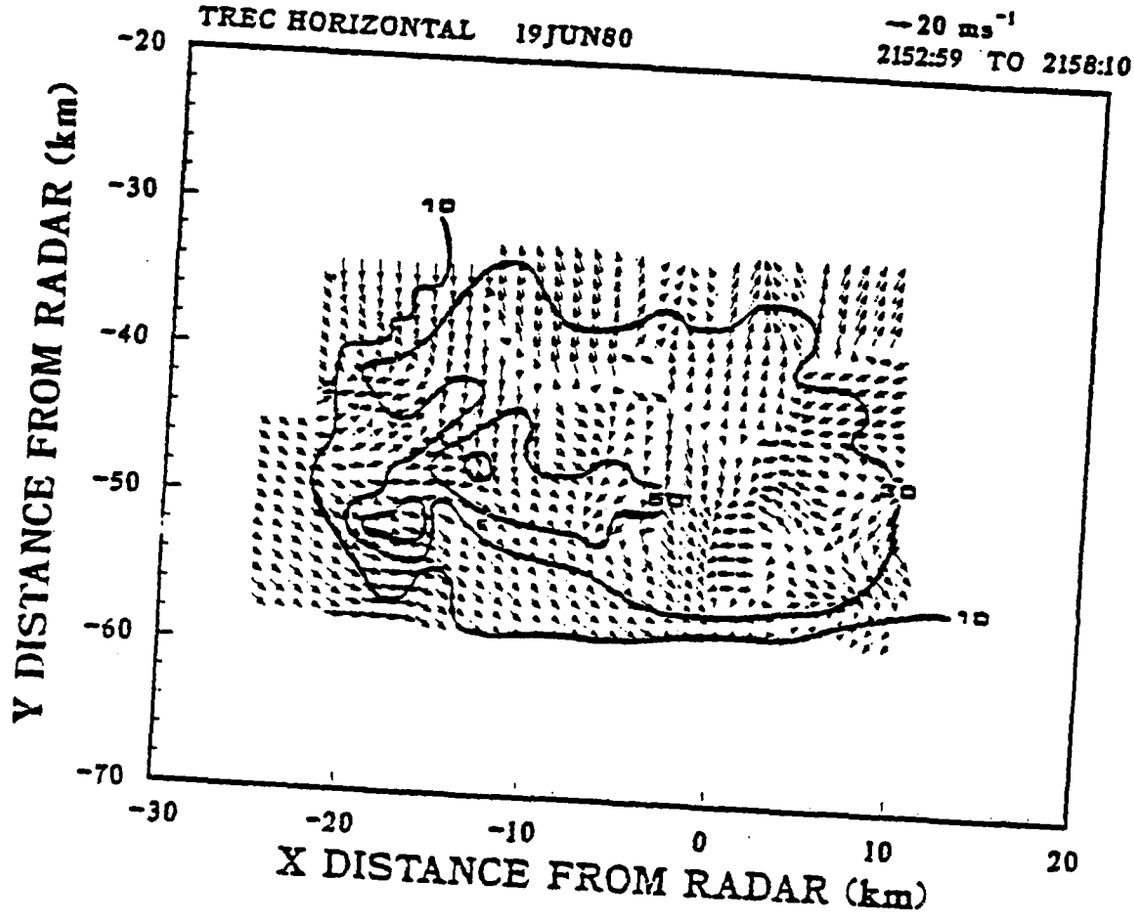

Fig. 39. As in Fig. 9, except for 2152:59 to 2158:10 CST.

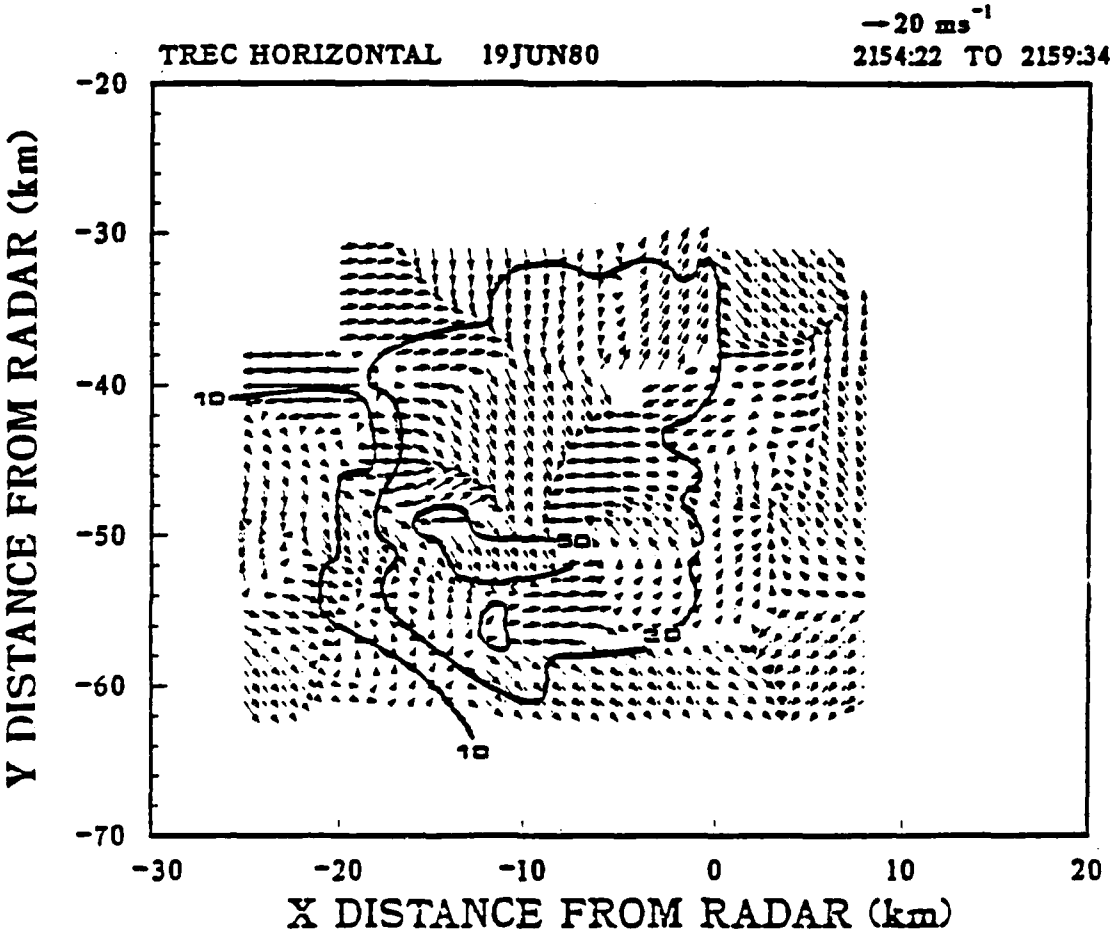

Fig. 40. As in Fig. 9, except at 12 km AGL for 2154:22 to 2159:34 CST.

fields, which gave the first good indication of the generator-level motions influencing the flow below. Thus, as a storm develops into a supercell storm, the possibility of generator-level motions contaminating the surrounding wind fields is apparently greater.

The derived vertical velocities are shown in Fig. 41 for 6 km AGL. For the VMP area (see Fig. 37) the vertical velocities indicated the presence of a strong updraft on the order of those calculated by VBDR. The hook echo was the area in which the highest vertical velocities were found. Even though the magnitudes were slightly different from those calculated by VBDR, there was a striking similarity between the single- and multiple-Doppler analyses.

A vertical cross-section was constructed through the main storm complex (Fig. 42). It was evident that throughout the storm there was upward motion. Also, toward the storm top the 50 dBZ area narrowed and the motion indicated air flowing out of the storm and possibly yielding the area of downward flow at y = -39 km. In the lower levels at y = -59 km, where the hook echo was forming, the air flow was converging and indicated a definite upward flow.

Ten min later, the VMP at 6 km AGL (Fig. 43) indicated that the majority of the field was experiencing vertical motion. This pattern was identical to the DD region of vertical velocity (Fig. 44) in size and extent. The upper-level VMP was somewhat different from the DD pattern (Figs. 45-46), with TREC displaying some areas of horizontal rather than vertical patterns centered at (-3,-53). Also, TREC indicated that the VMP extended farther eastward. This was in response to the slope of the reflectivity field with the thunderstorm tilting eastward.

The TREC derived horizontal wind field at 6 km AGL is shown in Fig. 47. It only slightly resembled the DD field. However, TREC was reacting to the

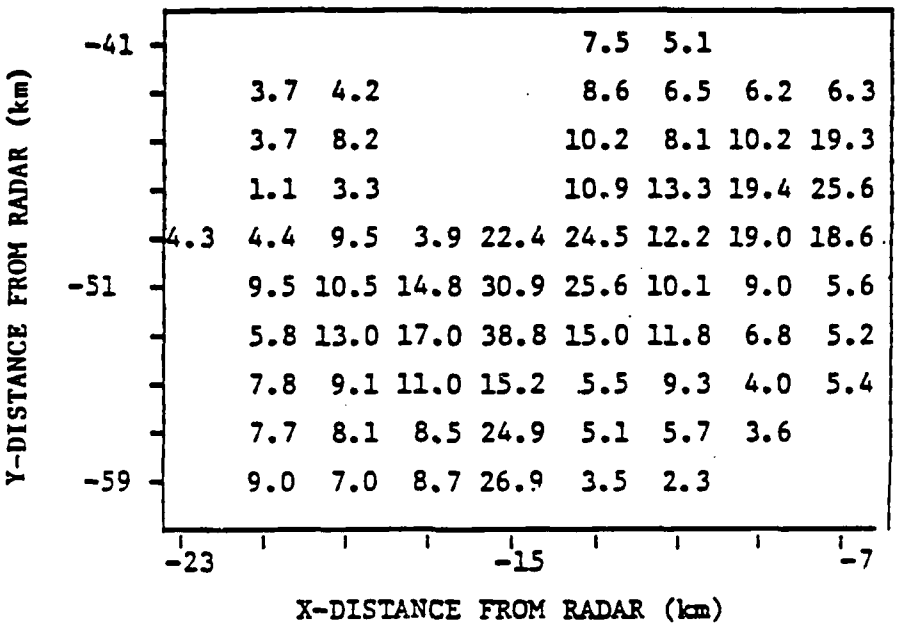

Fig. 41. As in Fig. 11, except for 2152:59 to 2158:10 CST.

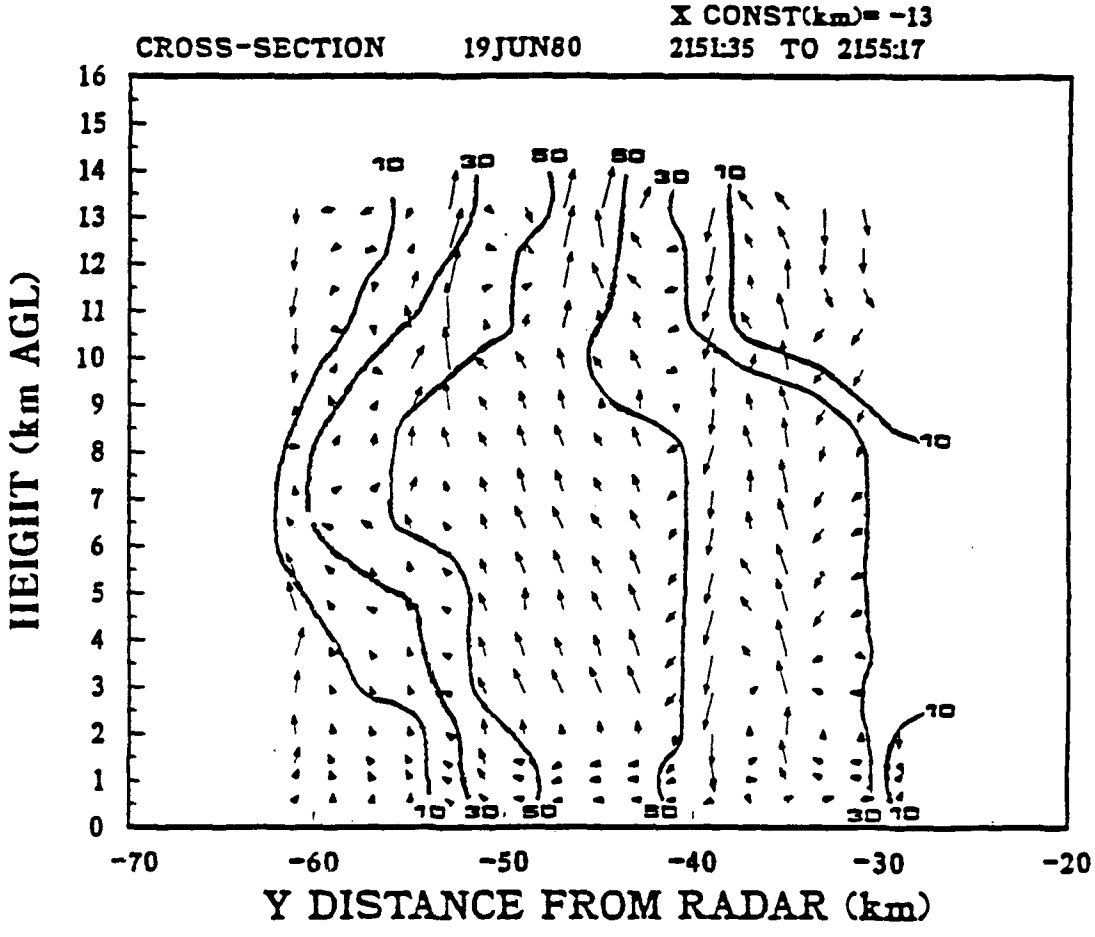

Fig. 42. As in Fig. 20, except at x=-13 km for 2151:35 to 2155:17 CST.

AD-A196 405 ON DERIVING THE THREE-DIMENSIONAL KINEMATIC STRUCTURE OF CONVECTIVE STORM..(U) AIR FORCE INST OF TECH WRIGHT-PATTERSON AFB OH R M COX MAY 88 2/2

UNCLASSIFIED AFIT/CI/NR-88-30 F/G 17/9 NL

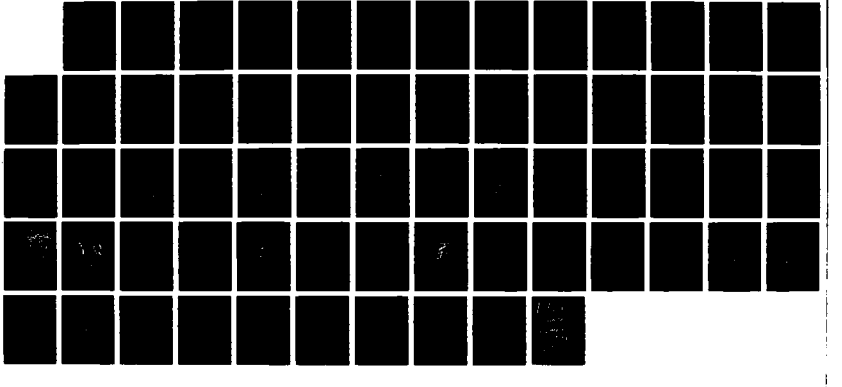

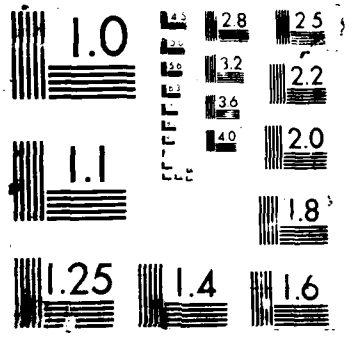
1.0
1.1
1.25
1.4
1.6
1.8
2.0
2.2
2.5
2.8
3.2
3.6
4.0

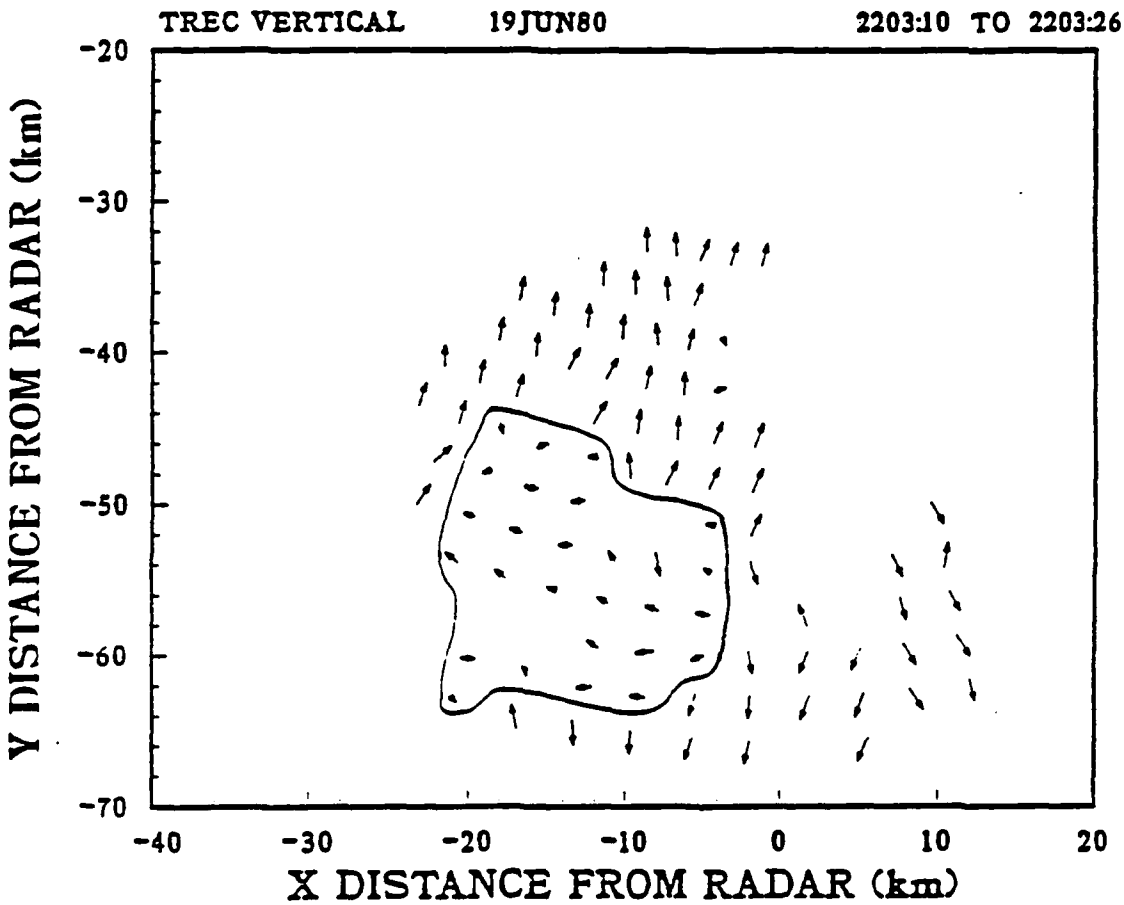

Fig. 43. As in Fig. 6, except for 2203:10 to 2203:26 CST.

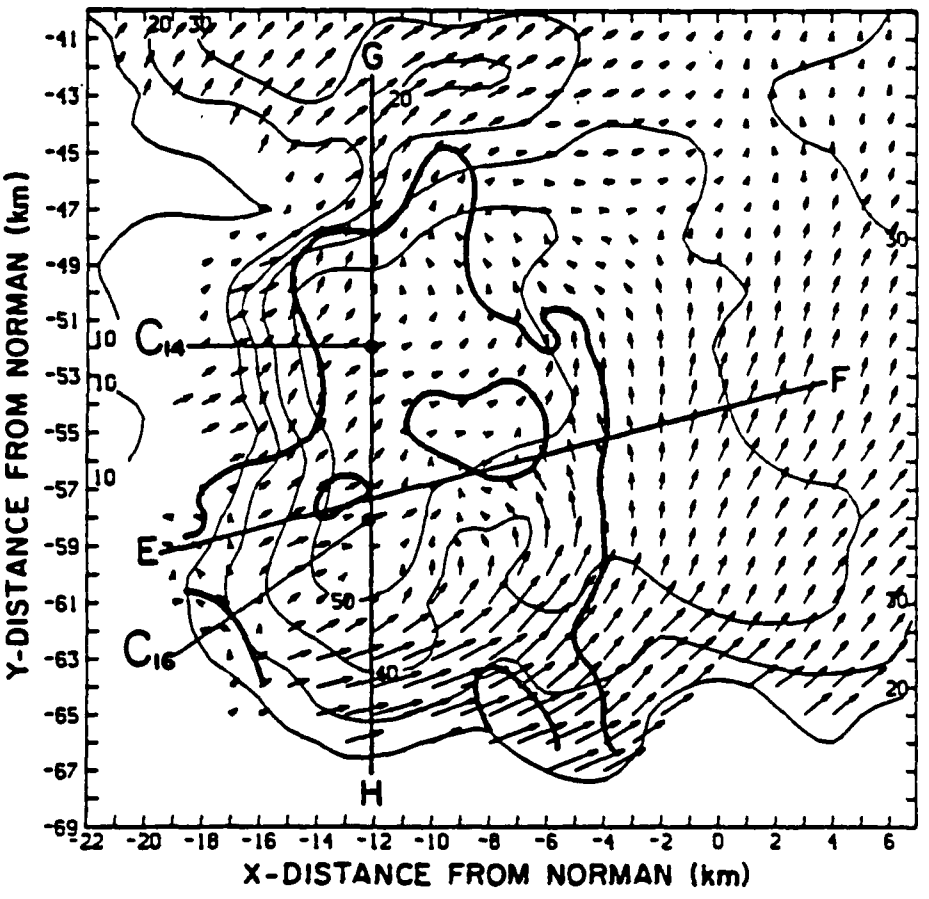

Fig. 44. As in Fig. 7, except at 6 km AGL for 2203 CST.

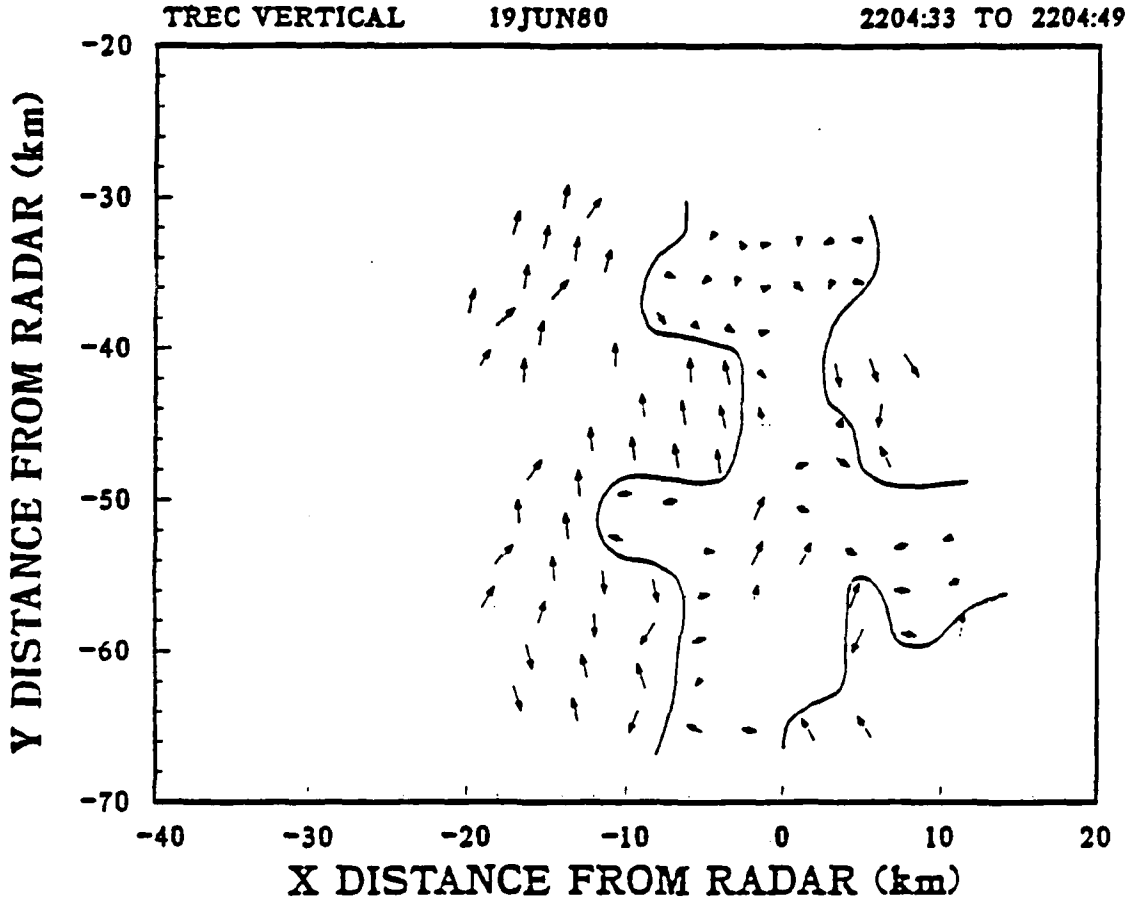

Fig. 45. As in Fig. 6, except at 12 km AGL for 2204:33 to 2204:49 CST.

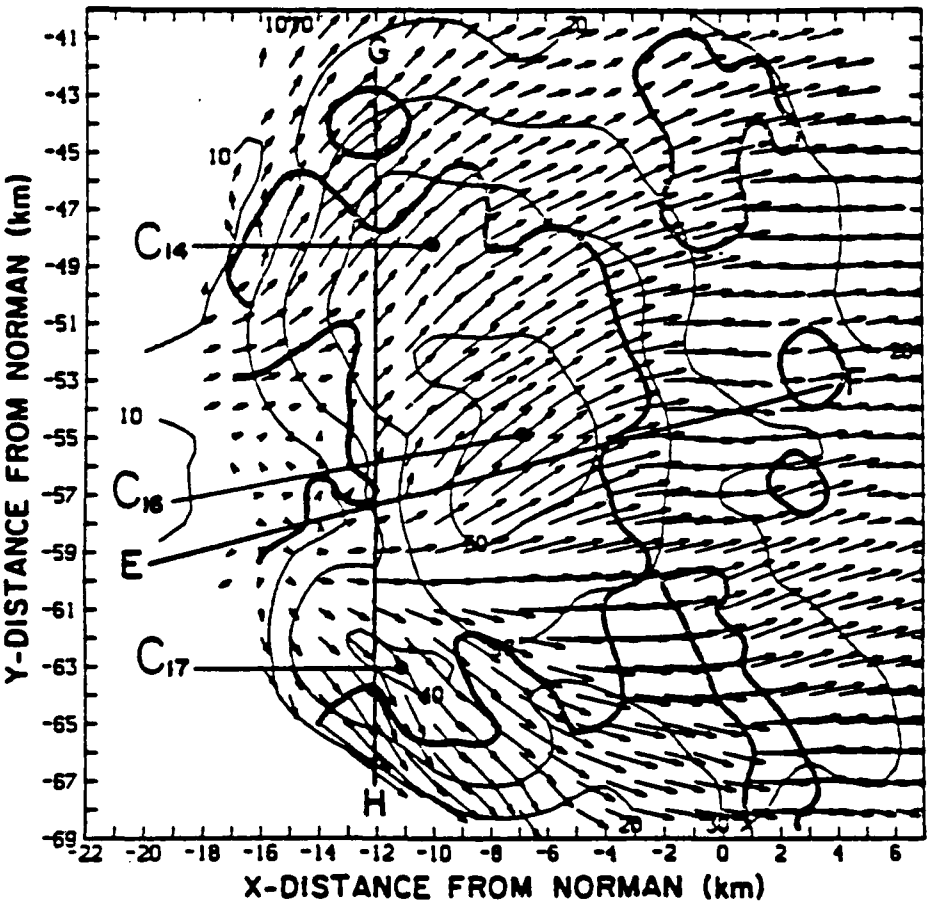

Fig. 46. As in Fig. 7, except at 12 km AGL for 2203 CST.

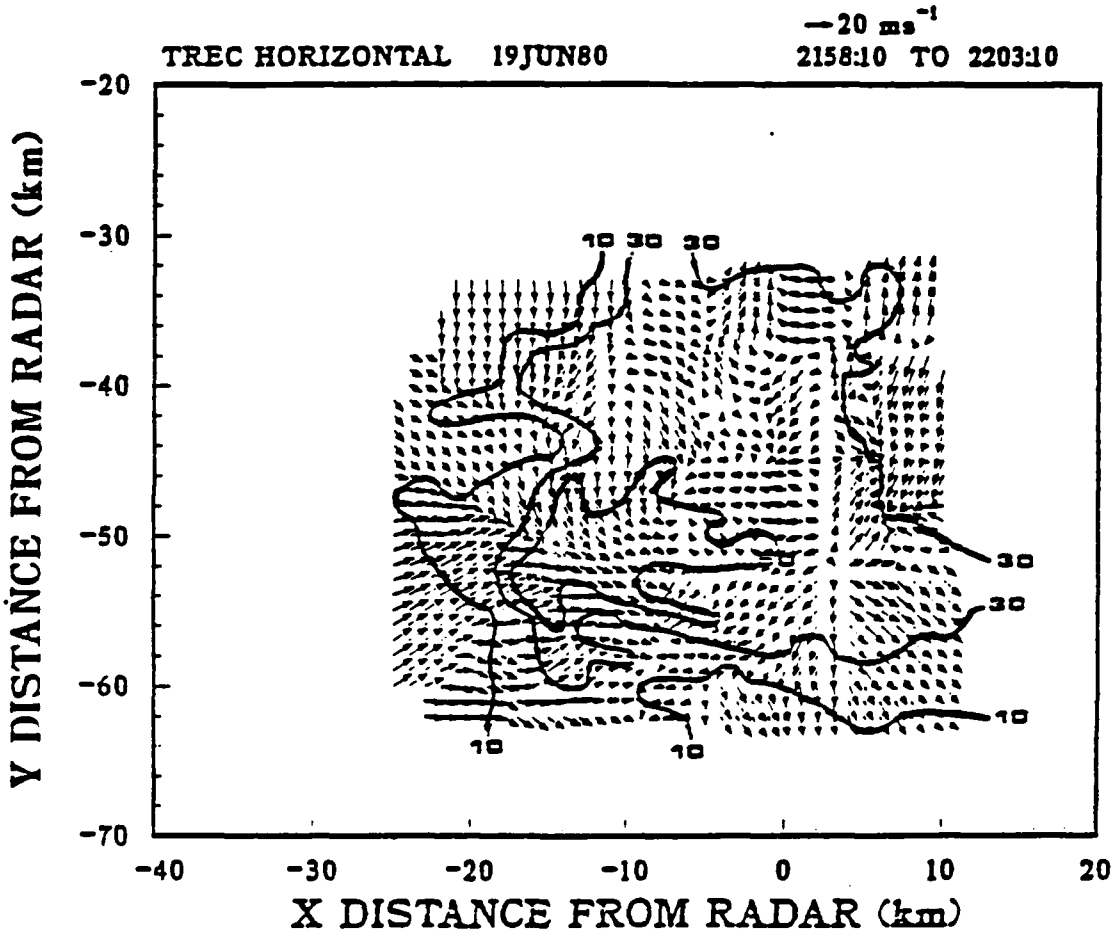

Fig. 47. As in Fig. 9, except for 2158:10 to 2203:10 CST.

influence of the mesocyclone and indicating an area of convergence centered at (-8,-58), which coincided with the DD center of cyclonic circulation associated with the mesocyclone. TREC also showed an area of cyclonic rotation centered at (-8,-50). As VBDR indicated this was the leading edge of a persistent updraft zone. A divergent area was located at (-7,-52) and within 5 min VBDR reported a weak downdraft forming here with a magnitude of 5 ms^{-1}. This feature was seen in the TREC derived vertical motion magnitudes (Fig. 48). A weak downdraft had formed in that region. Also, the areas of strong updrafts were quite evident. These coincided with the location of the mesocyclone and the areas of convergence indicated in Fig 47.

The 12 km AGL TREC derived wind field is shown in Fig. 49. Once again there was not much agreement between the DD field and TREC. TREC indicated some west to southwest flow; however, TREC was influenced by a few preferred regions of activity, (-15,-49), (-5,-51), (-9,-57), and (-11,-47). All of these areas indicated convergent flow and VBDR reported these areas as having updrafts greater than 30 ms^{-1}.

A vertical cross-section was constructed north to south through the hook echo (Fig. 50). Convergence due to the hook echo was seen at x = -60 km. As the air rose through the storm there was an indication of increasing vertical motion with a maximum at 5 km. One should note the weak echo region in that location and the echo overhang. Also, there was another indication of the weak echo region with the less than 30 dBZ contour located at 4 to 5 km. Another interesting feature was the downward pattern associated with the decaying 50 dBZ cell located at x = -40 km. All levels indicated a downward pattern that produced an apparent gust front extending to x = -30 km. Thus, this cross-section verified the upward motion in

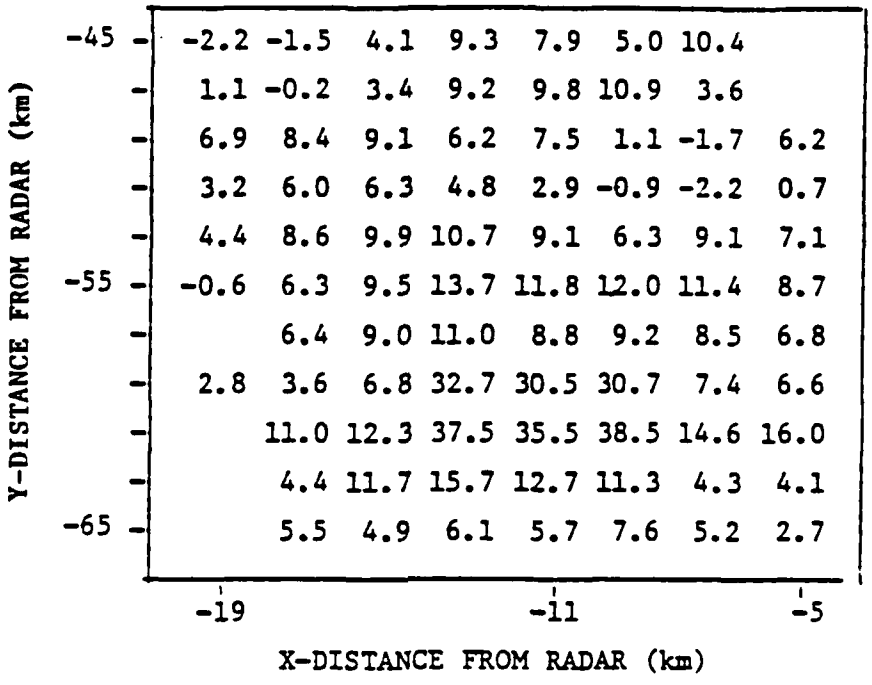

Fig. 48. As in Fig. 11, except for 2158:10 to 2203:10 CST.

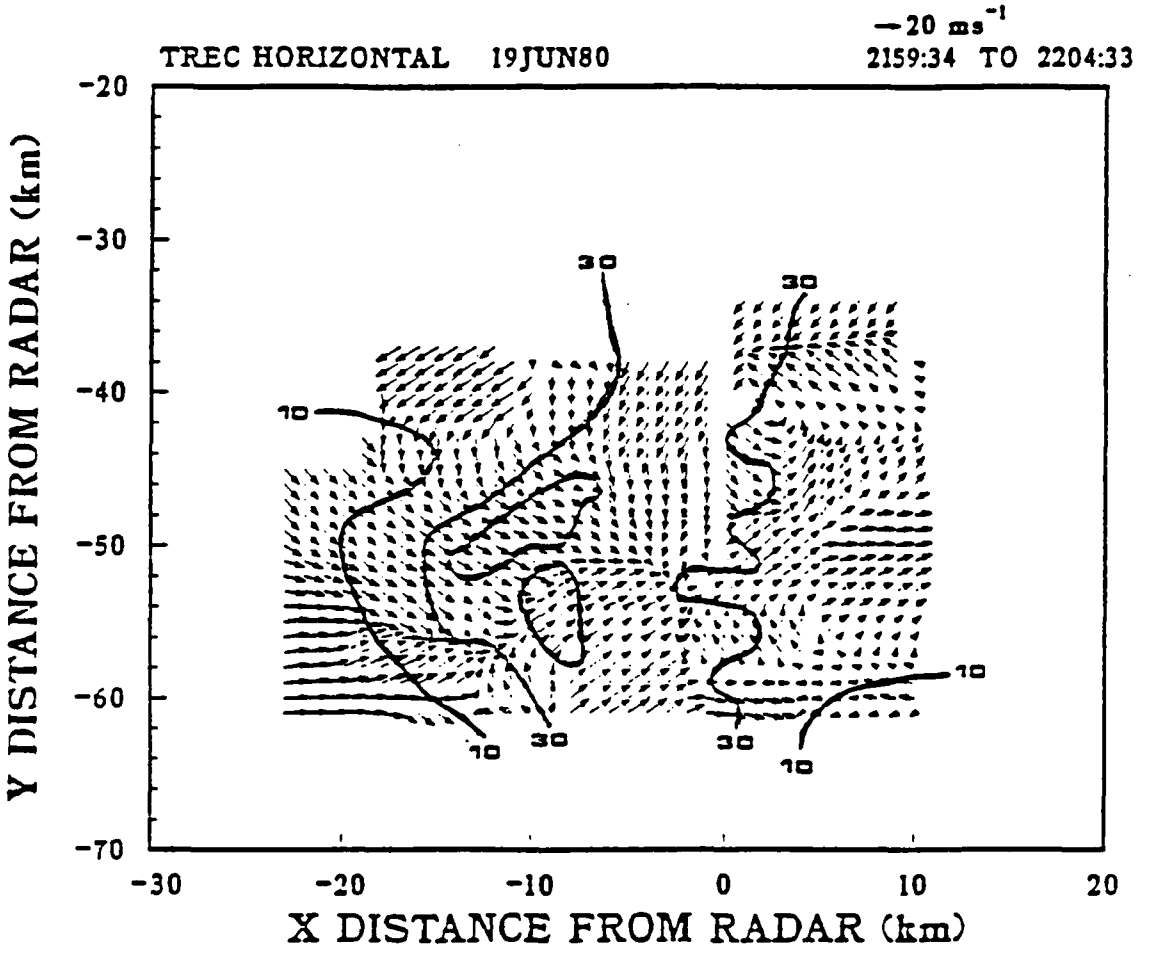

Fig. 49. As in Fig. 9, except at 12 km AGL for 2159:34 to 2204:33 CST.

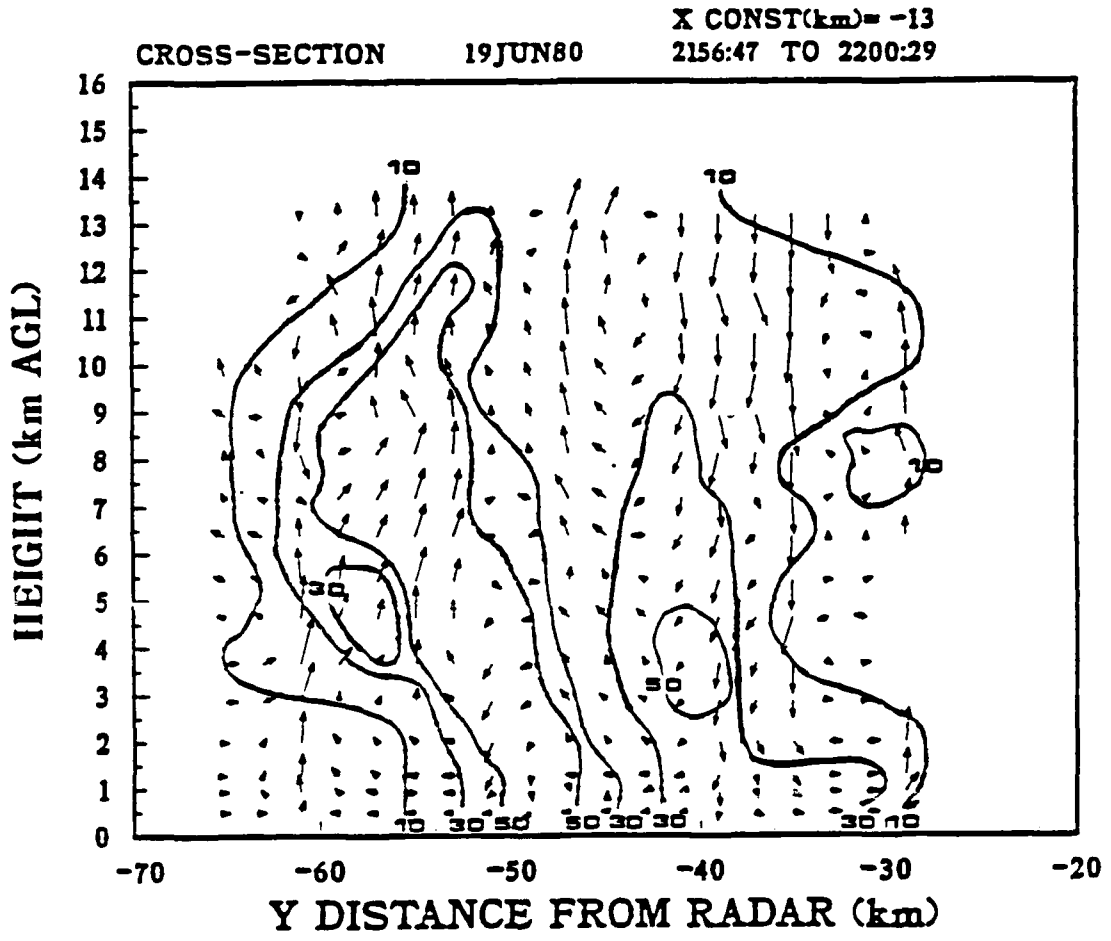

Fig. 50. As in Fig. 20, except at x=-13 km for 2156:47 to 2200:29 CST.

the vicinity of the hook echo and revealed a developing gust front associated with a decaying cell.

The change in vertical motion for the entire storm is shown in a time series format in Fig. 51. The solid line indicates the values VBDR found in his DD study, whereas, the dashed lines are the TREC derived values. As one can see TREC mirrored the multiple-Doppler analysis through the multicell and transition stages of development. During the supercell stage TREC underestimated the vertical velocities, however, TREC indicated an increase in magnitude and exhibited the same pattern of increase/decrease in velocities that VBDR found. Thus, there is a remarkable resemblance between the two analysis techniques.

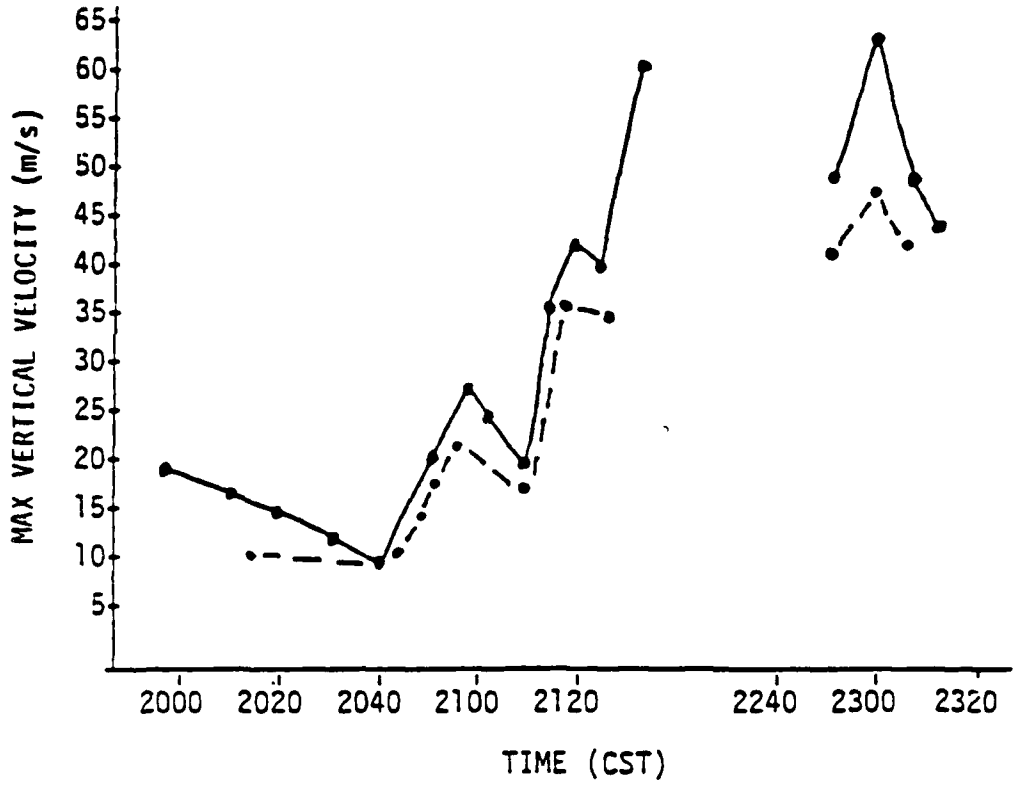

Fig. 51. Comparison of dual-Doppler derived vertical velocities (solid lines) to TREC derived vertical velocities (dashed lines).

CHAPTER IV

CONCLUSIONS AND RECOMMENDATIONS

Conclusions

The objectives of this research were to determine the feasibility of deriving vertical velocity patterns, the magnitudes of those patterns, and the three-dimensional wind field in severe convective storms using data from a single radar and a technique called TREC. The research was divided into three components. First, the VMP was derived by using TREC within a single volume scan. Next, TREC was used to derive the horizontal wind field. The u and v wind components so obtained were used in the final step, the derivation of the vertical motion magnitudes within the derived VMP.

Vertical Motion Patterns

During the multicell stage of the storm, those VMP shown by VBDR were identified. Other times and elevation angles were investigated and the VMP identified were associated with thunderstorm activity in regions described by Lemon and Doswell (1979) and Brandes (1981) as areas of developing updrafts for the evolving supercell storm.

The transition stage of the storm was the most advantageous stage for analyzing results from the CIM radar along with the results from the NOR radar. The VMP derived from each radar agreed in location and size. There were some minor differences in the shape of given patterns. At 2115 CST the VMP extended farther eastward than that shown by VBDR. This extention was in response to a 40 dBZ cell and had vertical velocities less than 5 ms^{-1}. Time periods not shown by VBDR

were investigated also. The areas with a VMP were easily identified. These patterns had their origins in previous time periods and could be advected to the next time period as discussed by VBDR.

At 2052 CST a limitation of the TREC technique was identified. The main updraft pattern identified by VBDR was located at the very edge of the given radar sector. The present inplementation of TREC required at a minimum a 2 km region along the edges of the sector to properly perform the correlation analysis. Thus, using the NOR data the total VMP could not be resolved; however, using the CIM data the VMP was completely resolved.

All corresponding VMP increased in size due to the formation of a mesocyclone during the supercell stage. The middle-level VMP was in total agreement with VBDR, whereas, the upper-level patterns disagreed somewhat. TREC indicated a pattern extending farther eastward than indicated by the dual-Doppler analysis. Upon investigation it was seen that the storm tilted eastward and TREC was showing the slope of the echo pattern.

TREC-Derived Winds

The multicell stage of the storm found no effects of the generator level winds. In fact, each level of the storm, low, middle, and high, had a very distinct flow pattern associated with the nature and severity of the storm at that level. During this stage no direct comparisons between the dual-Doppler wind field and the TREC derived wind field were made because the initial radar scans used by VBDR had time increments greater than 7 min, thus making them unusable for this study. However, the results were compared with known qualities of severe storms at this stage of development and TREC effectively modeled the horizontal wind field.

During the transition stage of the storm full comparisons between VBDR, the NOR TREC results, and the CIM TREC results were made. At 2042 CST all three agreed except for one minor area. The NOR TREC results indicated a cyclonic circulation that was not seen in the dual-Doppler field. Upon investigation it was seen that this circulation was associated with a developing 40 dBZ thunderstorm and thus was a realistic flow feature. The probable reason why the feature was overlooked in the dual-Doppler results was that the dual-Doppler field is a high resolution, instantaneous snapshot of the wind field, whereas, TREC is a time-averaged wind field. It should be noted that both fields were correct in this situation. TREC was just modeling the wind field with a longer time step. Therefore, TREC was able to "see" the devlopment of this cell, whereas, the dual-Doppler "snapshot" was taken before a definite circulation had developed.

At 2052 CST an area of convergence was found in the TREC field that VBDR did not identify. This area of convergence was associated with an area of upward motion and once again the time-averaged field was able to show the prevailing nature of the developing storm.

Toward the end of the transition period, 2115 and henceforth, the horizontal wind fields agreed with those presented by VBDR except for some minor differences. Those differences were that TREC indicated a more cyclonic circulation and more areas of convergence. These are due in part to a developing mesocyclone and the convergence that occurred in the individual thunderstorms. These areas of convergence were located in regions that were experiencing greater upward motion.

Upon investigation and comparison with the model proposed by Lemon and Doswell (1979) the effects of generator-level contamination on the wind field appeared to be minor to non-existent. The individual levels of the storm were

apparently acting independent of one another, although this did change during the supercell stage.

It was found that at the supercell stage of the storm, the derived low-level winds resembled the derived middle-level wind field. Thus, as the storm had increased in intensity, the transfer of momentum had become faster, more apparent, and had begun to influence the ability of TREC to model the low-level wind fields within the storm. This was the first indication that the generator-level winds were affecting the entire field and the derived wind fields did not follow the model suggested by Lemon and Doswell (1979).

The middle-level wind field derived by TREC did not agree totally with the dual-Doppler analysis. However, TREC did indicate an overall cyclonic circulation and did show convergent areas in regions where VBDR found higher vertical velocities. TREC was also able to show an area of smaller scale circulation in the vicinity of the reported hook echo. In that region a convergent pattern was indicated.

TREC-Derived Vertical Velocity Magnitudes

By using the u and v wind components obtained from the second phase of this investigation the third phase was accomplished, the derivation of vertical motion magnitudes for the VMP found in the first phase. During the multicell stage and transition stage of the storm TREC was able to correctly model the trend of vertical velocities within acceptable error limits; however, when the storm became a supercell, TREC underestimated the magnitude of the vertical velocities. This underestimation can be explained. The time-averaged nature of TREC smoothed the field sufficiently to omit the instantaneous rises in vertical motion, but not

the general increase in storm severity due to a higher average vertical motion as the storm increased in severity. This can be understood by making an analogy to real-time weather observations. When a wind observation is taken, the value reported is an average wind for a given amount of time. In the remarks section of the observation a report of the peak wind observed is shown. That is what has occurred here and accounts for the difference between the TREC and dual-Doppler analysis. Even though the magnitudes are different there is still a remarkable similarity between the velocity values and overall pattern of the two techniques.

When TREC was proposed as a method to deduce vertical velocities, it was hypothesized that the direction, either up or down, of the vertical motion could be found by comparing the direction of the vectors produced when deriving the VMP to those of the TREC-derived horizontal wind field for that level. This research found that method to be doubtful. Only about half the time did that comparison render the correct direction for the vertical velocity.

To complete the three-dimensional view of the storm environment with TREC, vertical cross-sections were constructed. These graphs confirmed regions of updrafts and gave an indication of air inflow into the storm. During the multicell stage of the storm, the cross-section indicated a region of return air flow between two cells. For the transition period, when cells were merging into one large storm, air was shown to be entering the storm complex at various levels, then turning and becoming a part of the major updraft. Finally at the supercell time, the echo overhang and the bounded weak echo region (BWER) were shown as having air entering from the boundary layer, flowing through the BWER, and becoming a part of the major updraft. Also, a collapsing cell was observed with downward motion throughout until the boundary layer and an apparent gust front began to form.

Summary

To summarize the major findings:

1) All areas of vertical motion found by VBDR were found using the technique called TREC.

2) By using a time increment between radar volume scans of less than 5 min, the horizontal wind fields derived by TREC for the multicell and transition periods of the storm agreed with those reported by VBDR except for some minor differences. The supercell stage did not agree with VBDR, but did have an overall cyclonic circulation, which was to be expected for a mesocyclone environment.

3) The effects of a generator-level motion on the horizontal wind fields for the low, middle, and high levels were not seen during the multicell and transition periods. During the supercell stage it was evident.

4) The TREC-derived vertical velocities within a VMP were qualitatively similar to those published by VBDR.

5) Vertical cross-sections indicated regions of updrafts, air entrainment, updrafts extending through BWER, and an apparent gust front.

Recommendations

Based on this research effort, the next logical step would be to investigate TREC's ability to accurately compute vorticity values. That effort would conclude the initial testing of the TREC algorithm. From that point, as data sets become available, a statistical analysis of the variations of the storm's kinematic parameters derived using TREC versus those derived using a multiple-Doppler analysis should be made. This would provide, especially for the supercell stage of the storm, the needed information to accurately determine these parameters using a single radar.

Finally, the use of the TREC algorithm is by no means a "stand-alone" technique. Its integration with a system of other algorithms, like that proposed for the NEXRAD system, will provide a complete three-dimensional picture of the severe storm from development to decay. Using TREC in concert with other algorithms such as the divergence, hail, mesocyclone, and TVS algorithms will enable the forecaster to have all the possible information available to make the necessary decisions as whether a storm will become severe and the extent of that severity.

REFERENCES

Armijo, L., 1969: A theory for the determination of wind and precipitation velocities with Doppler radars. *J. Atmos. Sci.*, **26**, 570-573.

Atlas, D., 1953: Optical extinction by rainfall. *J. Meteor.*, **10**, 486-488.

——, 1963: Radar analysis of severe storms. *Meteor. Monogr.*, No. 38, 177-220.

Barnes, S. L., 1964: A technique for maximizing details in numerical weather analysis. *J. Appl. Meteor*, **3**, 396-409.

——, 1973: *Mesoscale objective map analysis using weighted time series observations.* NOAA Tech. Memo. ERL NSSL-62, 60 pp.

——, 1976: Severe local storms: Concepts and understanding. *Bull. Amer. Meteor. Soc.*, **57**, 412-419.

——, 1980: Report on a meeting to establish a common Doppler radar data exchange format. *Bull. Amer. Meteor. Soc.*, **61**, 1401-1404.

Battan, L. J., 1973: *Radar Observations of the Atmosphere.* Univ. of Chicago Press Chicago, IL, 324 pp.

Beebe, R. G., and F. C. Bates, 1955: A mechanism for assisting in the release of convective instability. *Mon. Wea. Rev.*, **83**, 1-10.

Bensinger, R., 1986: *Personal communication.*

Bjerkaas, C. L., and D. E. Forsyth, 1980: Operational test of the three-dimensional echo tracking program. *Preprints 19th Conf. on Radar Metoer.*, Miami Beach, Amer. Meteor. Soc., 244-247.

Bluestein, H. B., and C. R. Parks, 1983: A synoptic and photographic climatology of low-precipitation severe thunderstorms in the southern plains. *Mon. Wea. Rev.*, **111**, 2034-2046.

Bonesteele, R. G., and Y. J. Lin, 1978: A study of updraft-downdraft interaction based on perturbation pressure and single-Doppler radar data. *Mon. Wea. Rev.*, **106**, 62-69.

Bonewitz, J. D., 1986: *Surface wind fields in the vicinity of meso-convective storms as derived from radar observations: Non-tornadic storms.* Ph.D. Dissertation, Texas A&M University, College Station, TX, 171 pp.

Brandes, E. A., 1977: Flow in severe thunderstorms observed by dual-Doppler radar. *Mon. Wea. Rev.*, **105**, 113-120.

——, 1978: Mesocyclone evolution and tornadogenesis: Some observations. *Mon. Wea. Rev.*, **106**, 996-1011.

——, 1981: Finestructure of the Del City-Edmond tornadic meso-circulation. *Mon. Wea. Rev.*, **109**, 635-647.

——, 1984a: Relationships between radar-derived thermodynamic variables and tornadogenesis. *Mon. Wea. Rev.*, **112**, 1033-1052.

——, 1984b: Vertical vorticity generation and mesocyclone sustenance in tornadic thunderstorms: The observational evidence. *Mon. Wea. Rev.*, **112**, 2253-2269.

——, 1986: Personal communication..

Browning, K. A., 1964: Airflow and precipitation trajectories within severe local storms which travel to the right of the winds. *J. Atmos. Sci.*, **21**, 634-639.

——, and W. C. Ludlam, 1962: Air flow in convective storms. *Quart. J. Roy. Meteor. Soc.*, **88**, 117-135.

Bumgarner, B., 1987: Personal communication..

Burgess, D. W., J. D. Bonewitz, and D. R. Devore, 1978: Joint Doppler operational project: Results year 1. *Preprints, 18th Conf. on Radar Meteor.*, Atlanta, Amer. Meteor. Soc., 442-448.

Chisholm, A. J., 1973: Alberta hailstorms. Part I: Radar case studies and airflow models. *Meteor. Monogr.*, No. 36, 1-36.

Crawford, K. C., and R. A. Brown, 1972: Doppler velocity measurements in an approaching squall line. *Preprints, 15th Radar Meteor. Conf.*, Champaign-Urbana, Amer. Meteor. Soc., 27-34.

Djurić, D., and M. S. Damiani, 1980: On the formation of the low-level jet over Texas. *Mon. Wea. Rev.*, **108**, 1854-1865.

Doswell, C. A., 1982: *The Operational Meteorology of Convective Weather Volume I: Operational Mesoanalysis.* NOAA Tech. Memo. NWS NSSFC-5, 164 pp.

Douglas, R. H., 1964: Hail size distribution. *Preprints, 11th Conf. on Radar Meteor.*, Boston, Amer. Meteor. Soc., 146-149.

Doviak, R. J., and D. S. Zrnić, 1984: *Doppler Radar and Weather Observations.* Academic Press, New York, NY, 458 pp.

Fawbush, E. J., and R. C. Miller, 1954: The types of air masses in which North American tornadoes form. *Bull. Amer. Meteor. Soc.*, **35**, 154-165.

Goff, R. C., 1976: Vertical structure of thunderstorm outflows. *Mon. Wea. Rev*, **104**, 1429-1440.

Groginsky, H. L., 1972: Pulse pair estimation of Doppler spectrum parameters. *Preprints, 15th Radar Meteor. Conf.*, Champaign-Urbana, Amer. Meteor. Soc., 233-236.

Gunn, R., and G. Kinzer, 1949: Terminal velocity of fall for water droplets in stagnant air. *J. Meteor.*, **6**, 243-248.

Haltiner, G. L., and R. T. Williams, 1980: *Numerical Prediction and Dynamic Meteorology.* John Wiley and Sons, New York, NY, 477 pp.

Hamidi, S., R. E. Rinehart, and J. D. Tuttle, 1983: Test of a transverse-wind algorithm for NEXRAD in real-time. *Preprints, 21st Conf on Radar Meteor.*, Edmonton, Amer. Meteor. Soc., 409-412.

Hennington, L. D., and D. W. Burgess, 1981: Automatic recognition of mesocyclones from single-Doppler radar data. *Preprints, 20th Conf. Radar Meteor.*,, Boston, Amer. Meteor. Soc., 704-706.

Heymsfield, G., 1981: Evolution of downdrafts and rotation in an Illinois thunderstorm. *Mon. Wea. Rev.*, **109**, 1969-1988.

Hogue, R., and I. Zawadzki, 1986: Vertical velocity within radar echo regions derived from single-Doppler measurements. *Preprints, Joint Sessions 23rd Conf. on Radar Meteor. and Conf. on Cloud Physics*,, Snowmass, CO, Amer. Meteor. Soc., JP128-131.

Holton, J. R., 1979: *An Introduction to Dynamic Meteorology.* Academic Press, New York, NY, 391 pp.

Jones, D. M. A., 1956: *Rainfall drop-size distribution and radar reflectivity.* Res. Rept. No. 6, Urbana Meteor. Lab., Illinois State Water Survey, 50 pp.

Kessler, E, 1969: On the distribution and continuity of water substance in atmospheric circulation. *Meteor. Mono.*, 10, 84 pp..

Klemp, J. B., and R. B. Wilhelmson, 1978: Simulation of right- and left-moving storms produced through storm splitting. *J. Atmos. Sci.*, **35**, 1097-1110.

Klingle, D. L., D. R. Smith, and M. M. Wolfson, 1987: Gust front characteristics as detected by Doppler radar. *Mon. Wea. Rev.*, **115**, 905-918.

Leary, C. A., and R. A. Houze, 1979: The structure and evolution of convection in a tropical cloud cluster. *J. Atmos. Sci.*, **36**, 437-457.

Lemon, L. R., and C. A. Doswell III, 1979: Severe thunderstorm evolution and mesocyclone structure as related to tornadogenesis. *Mon. Wea. Rev.*, **107**, 1184-1197.

Lhermitte, R. M., 1964: Doppler radar as a severe storm sensor. *Bull. Amer. Meteor. Soc.*, **45**, 587-596.

——, and D. Atlas, 1961: Precipitation motion by pulse Doppler. *Proc. Ninth Weather Radar Conf.*, Boston, Amer. Meteor. Soc., 218-223.

Ludlam, F. H., 1963: Severe local storms: A review. *Meteor. Monogr.*, No. 27, Amer. Meteor. Soc., 1-30.

Maddox, R. A., and C. A. Doswell III, 1982: An examination of jet stream configuration, 500 mb vorticity patterns, and low-level thermal advection

patterns during extended periods of intense convection. *Mon. Wea. Rev.*, **110**, 184-197.

Marwitz, J. D., 1978: Vertical streaks in radar scans from convective storms. *Preprints 18th Conf. on Radar Meteor.*, Atlanta, Amer. Meteor. Soc., 260-265.

Miller, R. C., 1972: *Notes on Analysis and Severe-Storm Forecasting Procedures of the Air Force Global Weather Central.* AWS Tech. Rep. 200 (Rev.), Air Weather Service, Scott AFB, Il, 190 pp.

Moncrieff, M. W., and J. S. A. Green, 1972: The propogation and transfer properties of steady convective overturning in shear. *Quart. J. Roy. Meteor. Soc.*, **98**, 336-352.

NEXRAD JSPO Staff, 1983: *NEXRAD Res. and Dev. Plan.* NEXRAD Report, Silver Spring, MD, 48 pp.

——, 1984: *Next Generation Weather Radar Algorithm Report.* NEXRAD Report R400A-AR202, Silver Spring, MD, 284 pp.

Ogura, Y, and N. A. Phillips, 1962: Scale analysis of deep and shallow convection in the atmosphere. *J. Atmos. Sci.*, **19**, 173-179.

Peace, R. L., Jr., R. A. Brown, and H. G. Camnitz, 1969: Horizontal motion field observations with a single pulse Doppler radar. *J. Atmos. Sci.*, **26**, 1096-1103.

Pruppacher,H. R., and J. D. Klett, 1980: *Microphysics of Clouds and Precipitation.* Reidel Publishing, Boston, MA, 714 pp.

Ray, P. S., C. L. Ziegler, and W. Bumgarner, 1980: Single- and multiple-Doppler radar observations of tornadic storms. *Mon. Wea. Rev.*, **108**, 1607-1625.

Rhea, J. O., 1966: A study of thunderstorm formation along dry lines. *J. Appl. Meteor.*, **5**, 59-63.

Rinehart, R. E., 1979: *Internal storm motions from a single non-Doppler weather radar.* NCAR Tech. Note NCVAR/TN-146+STR, Boulder, CO, 262 pp.

——, and E. T. Garvey, 1978: Three-dimensional storm detection by conventional weather radar. *Nature*, **273**, 287-289.

Sekhon, R. S., and R. C. Srivastava, 1971: Doppler radar observations of drop-size distributions in a thunderstorm *J. Atmos. Sci.*, **28**, *983-994.*

Smythe, G. R., and F. I. Harris, 1984: *Sub-cloud layer motions from radar data using correlation techniques.* AFGL Tech. Rept. AFGL-TR-84-0272, Hanscom AFB, MA, 24 pp.

Spilhaus, A. F., 1948: Drop size intensity and radar echo of rain. *J. Meteor.*, **5**, 161-164.

Stricherz, J., 1987: Personal communication..

Uccellini, L. W., and D. R. Johnson, 1979: The coupling of upper and lower tropospheric jet streaks and implications for the development of severe convective storms. *Mon. Wea. Rev.*, **107**, 682-703.

Ulbrich, C. W., 1977: Doppler radar relationships for hail at vertical incidence. *J. Appl. Meteor.*, **16**, 1349-1359.

Vasiloff, S., and E. A. Brandes, 1984: An investigation of the transition from multicell to supercell storms. *Preprints, 22nd Conf. Radar Meteor.*, Zurich, Amer. Meteor. Soc., 77-82.

——, ——, R. P. Davies-Jones, and P. S. Ray, 1986: An investigation of the transition from multistorm to supercell storms. *J. Climate Appl. Meteor.*, **25**, 1022-1036.

Waldteufel, P., and H. Corbin, 1979: On the analysis of single-Doppler radar data. *J. Appl. Meteor.*, **18**, 532-542.

Weisman, M. L., and J. B. Klemp, 1982: The dependence of numerically simulated convective storms on vertical wind shear and buoyancy. *Mon. Wea. Rev.*, **110**, 504-520.

——, and ——, 1984: The structure and classification of numerically simulated convective storms in directionally varying wind shears. *Mon. Wea. Rev.*, **112**, 2479-2498.

Wilk, K., 1986: Personal communication.

Wood, V. T., E. A. Brandes, and R. A. Brown, 1986: Computation of vorticity and vertical velocity from single Doppler radar measurements in severe thunderstorms. *Preprints, Joint Session 23rd Conf. on Radar Meteor. and Cloud Physics*,, Snowmass, CO, Amer. Meteor. Soc., JP115-118.

APPENDIX A

ACRONYMS AND ABBREVIATIONS

AWS	Air Weather Service
BWER	Bounded Weak Echo Region
CAPE	Convective Available Potential Energy
CST	Central Standard Time
DD	Dual-Doppler
DISKW	Disk Write Program
DISSPLA	Display Integrated Software System and Plotting Lang
FAA	Federal Aviation Administration
JSPO	Joint System Program Office
kPa	kilo-Pascals
LI	Lifted Index
LLJ	Low Level Jet
NEXRAD	Next Generation Weather Radar
NSSL	National Severe Storms Laboratory
NWS	National Weather Service
PPP	Pulse-Pair Processor
PRF	Pulse Repetition Frequency
TREC	Tracking Radar Echoes by Correlation
TTS	Total Totals Index
TVS	Tornado Vortex Signature
UF	Universal Format
ULJ	Upper Level Jet
VAD	Velocity Azimuth Display
VERTMT	Vertical Motion Program
VMP	Vertical Motion Pattern
VVP	Velocity Volume Processing
WER	Weak Echo Region
WPLOTG	Wind Plot Horizontal Gridded Data Program
WPLOTV	Wind Plot Vertical Program

APPENDIX B

THE ANELASTIC EQUATION OF CONTINUITY

The purpose of this appendix is to provide the reader with the derivation of the computational form of the anelastic equation of continuity. For the theoretical discussion of this equation the reader is referred to Ogura and Phillips (1962).

The anelastic equation of continuity presented by Ogura and Phillips (1962) is

$$\frac{\partial w}{\partial z} = -(\frac{\partial u}{\partial x} + \frac{\partial v}{\partial y}) + Kw, \tag{B.1}$$

where K is defined as the negative logarithmic rate of change of density with height. This value is approximated from an appropriate sounding (Kessler, 1969).

Integrating the above equation with respect to height, z,

$$\int_{z_0}^{z_1} \frac{\partial w}{\partial z} dz = -\int_{z_0}^{z_1} (\frac{\partial u}{\partial x} + \frac{\partial v}{\partial y}) dz + K \int_{z_0}^{z_1} w dz, \tag{B.2}$$

gives

$$w_1 - w_0 = -(\overline{\frac{\partial u}{\partial x} + \frac{\partial v}{\partial y}})\Delta z + K\bar{w}\Delta z, \tag{B.3}$$

where

$$\bar{w} = \frac{w_1 + w_0}{2}. \tag{B.4}$$

The divergence term is an average divergence for that layer. Solve for w_1.

$$w_1 = -(\overline{\frac{\partial u}{\partial x} + \frac{\partial v}{\partial y}})\Delta z + \frac{Kw_1\Delta z + Kw_0\Delta z}{2} + w_0, \tag{B.5}$$

Rearrange (B.5) to obtain

$$w_1(1 - \frac{K\Delta z}{2}) = -(\overline{\frac{\partial u}{\partial x} + \frac{\partial v}{\partial y}})\Delta z + w_0(\frac{K\Delta z}{2} + 1). \tag{B.6}$$

Algebraic manipulation renders the final computational form

$$w_1 = -\frac{(\overline{\frac{\partial u}{\partial x} + \frac{\partial v}{\partial y}})\Delta z}{(1 - \frac{K\Delta z}{2})} + \frac{w_0(\frac{K\Delta z}{2} + 1)}{(1 - \frac{K\Delta z}{2})}. \tag{B.7}$$

APPENDIX C

MESOSCALE ENVIRONMENTAL CONDITIONS

Introduction

The purpose of this appendix is to provide a general discussion of the meteorological conditions present during the time the radar data were gathered on 19 June 1980. As mentioned in previous chapters these data were chosen because both NSSL Doppler radars were operating at the time, which permitted dual-Doppler verification for the results of this research.

The approach is to discuss the environmental conditions from a general meteorological standpoint. Therefore, the 1800 CST 50 kPa and 85 kPa charts will be discussed first. Next, the 1800 CST sounding is shown. Finally, selected surface analyses, NWS radar summaries, and radar reflectivity from the Norman Doppler will be presented.

The 50 kPa Chart

At the 50 kPa level (Fig. 52) the most striking feature was the temperature gradient that extended from the Texas panhandle to central Oklahoma. The gradient was on the order of 1 deg C per 100 km. Cold air advection coupled with the converging flow in the same region was one of the mechanisms responsible for the severe weather that occurred. One also notes an area of confluent flow in northeast Texas, which was associated with a jet maximum. The location and strength of this maximum was in ageement with Miller (1972) who presented a pattern for typical summertime severe weather.

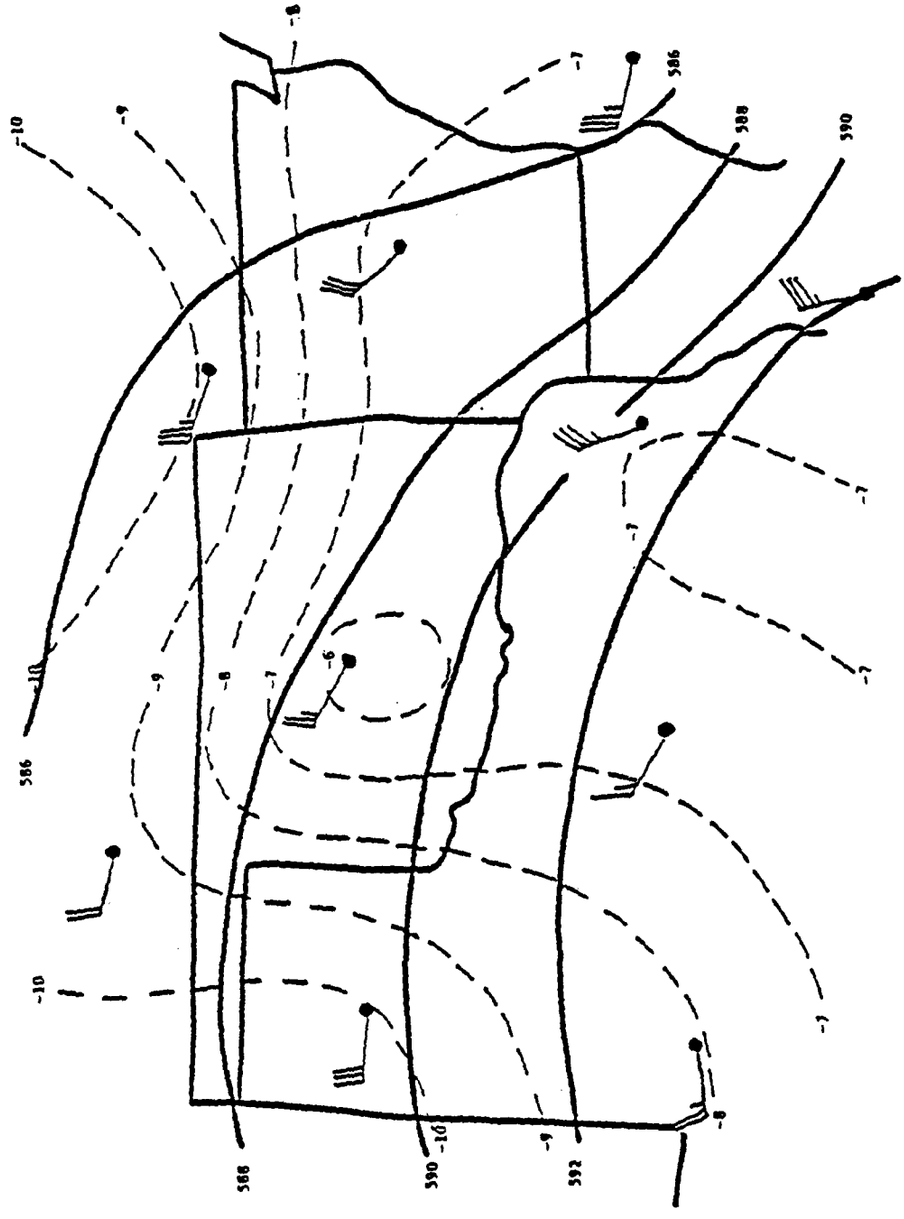

Fig. 52. 50 kPa chart with temperatures (dashed lines) in deg C and heights (solid lines) in gpm.

The 85 kPa Chart

The frontal position was easily located at 85 kPa (Fig. 53) with the center of low pressure located near the border of Texas and New Mexico. A cold front extended from the center of low pressure back through New Mexico and a stationary front was positioned through south central Oklahoma. Also, a trough of low pressure developed in central west Texas. This was associated with a dry line at the surface. There was a weak low level (LLJ) over central Texas that extended into central Oklahoma. Upon investigation (analyzing the sounding which will be discussed later) it was found that just above this level the winds in central Oklahoma doubled. As Djurić and Damiani (1980) indicated the LLJ is a very important mechanism for supplying water vapor and latent heat for middle-latitude storms. Even though the LLJ and upper level (ULJ) were weaker than normally observed in spring-time, their orientation was such that conditions were favorable for the development of severe weather just north of the Red river in Oklahoma (Beebe and Bates, 1955; Miller, 1972; Uccellini and Johnson, 1979; Maddox and Doswell, 1982).

The LLJ beneath the exit region of the ULJ provided favorable conditions for the development of severe convective storms within the exit region of the ULJ. The LLJ transported moisture and sensible heat northward in the lower troposphere, while the ULJ transported cooler drier air eastward in the middle-levels. The effect of this interaction was to generate convective instability from the surface to the 50 kPa level, lower the level of free convection, and raise the equilibrium level. All these coupled together were conducive to the formation of deep convection.

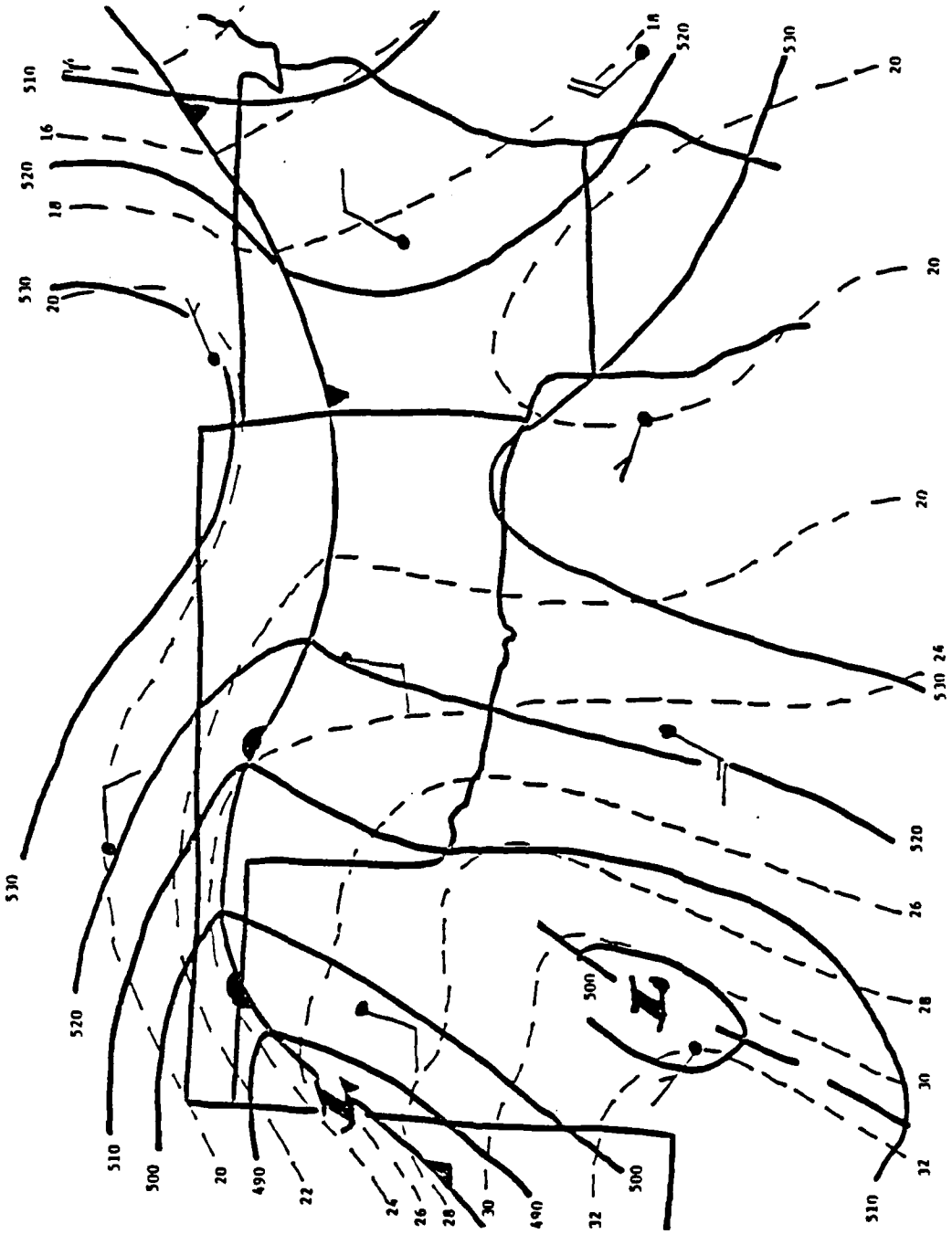

Fig. 53. As in Fig. 52, except for 85 kPa level.

The Skew-T, log P Diagram

As Doswell (1982) indicated, nothing can or should replace an examination of the individual sounding. Figure 54 is the 1800 CST sounding for Oklahoma City.

Upon examination the winds are seen to veer with height. This is the normal condition in the supercell case. The low-level winds had a southerly maxima at about 76 kPa, whereas, the upper-level winds had a westerly maxima centered at 30 kPa. A dry surface layer was noted with a moister middle layer capped by a dry stable layer. This sounding resembled one discussed by Fawbush and Miller (1954) and Bluestein and Parks (1983). The lifted index (LI) and total totals index (TTS) were calculated for this sounding. These measures of the stability of the air mass over central Oklahoma revealed that the air was potentially unstable with a LI of -5 and a TTS of 50.

Another method of determining the thermodynamic instability of the air or buoyant energy available was to calculate the quantity called CAPE or Convective Available Potential Energy. This method was proposed by Moncrieff and Green (1972), where they defined CAPE as

$$CAPE = g \int_{zb}^{zt} \frac{(T_{va} - T_{ve})}{T_{ve}} dz, \qquad (C.1)$$

where T_v is the virtual temperature with the subscripts a and e referring to the atmosphere and environments, respectively. The limits on the integration were for the base and top of the layer through which the parcel possessed positive buoyancy and g was the acceleration due to gravity.

CAPE represented the amount of work done per unit mass on the environment by a parcel of air rising from the level of free convection to the equilibrium level. This is a better estimate of potential instability than the LI because parcel buoyancy

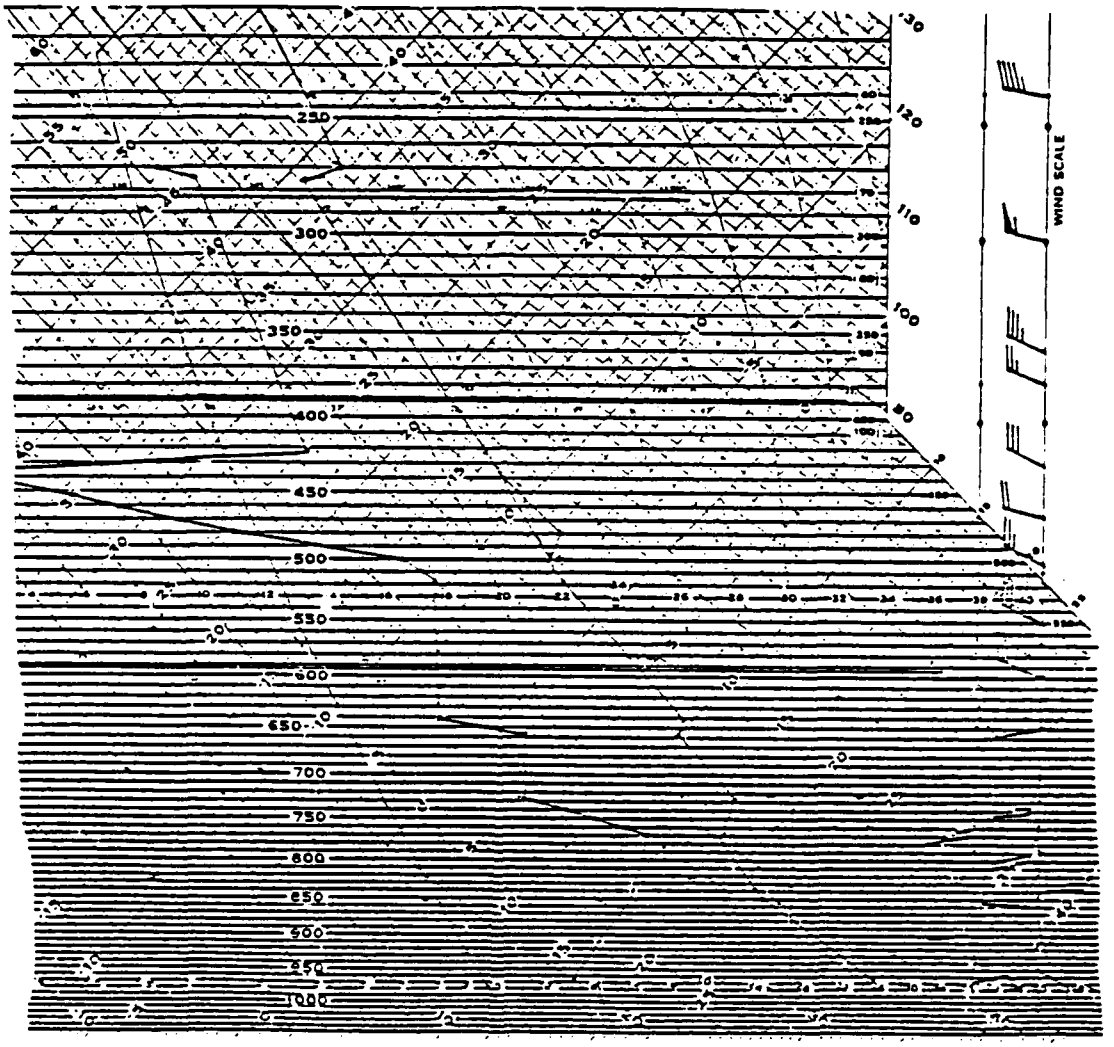

Fig. 54. The Skew-T, log P diagram at Oklahoma City for 1800 CST.

is computed for the entire column, not just the 50 kPa level.

Knowing that wind shear has an influence on convective development, Moncrieff and Green (1972) defined a convective bulk Richardson number

$$R = \frac{CAPE}{.5(\bar{U}^2 + \bar{V}^2)}, \qquad (C.2)$$

which is the ratio of CAPE to the kinetic energy found in the vertical wind shear. Stricherz (1987) has applied this technique to his work at Texas A&M University and has found favorable results. Using his implementation and the Oklahoma City sounding, CAPE was found to be approximately 2000 J kg^{-1}. The bulk Richardson number was found to be 24. This number corresponds well to the critical value for supercell development proposed by Weisman and Klemp (1982, 1984) and a value of 20 found by VBDR using a separate sounding taken by the NSSL staff.

The Surface Analysis

1800 CST

A low pressure center was located near the border of Texas and New Mexico (Fig. 55). A cold front extended into New Mexico. Also, a stationary front extended eastward through southern Oklahoma. Central Texas was being affected by an advancing dry line associated with two low pressure areas, one located near the border of Texas and Oklahoma, the other was approximately 400 km to the southwest. The dew points in central Texas and Oklahoma were near or greater than 20 deg C, whereas, behind the dry line the dew points were 10-15 deg C less. Rhea (1966) proposed the dry line as an area of highly preferred radar echo development. This was the case later in the period.

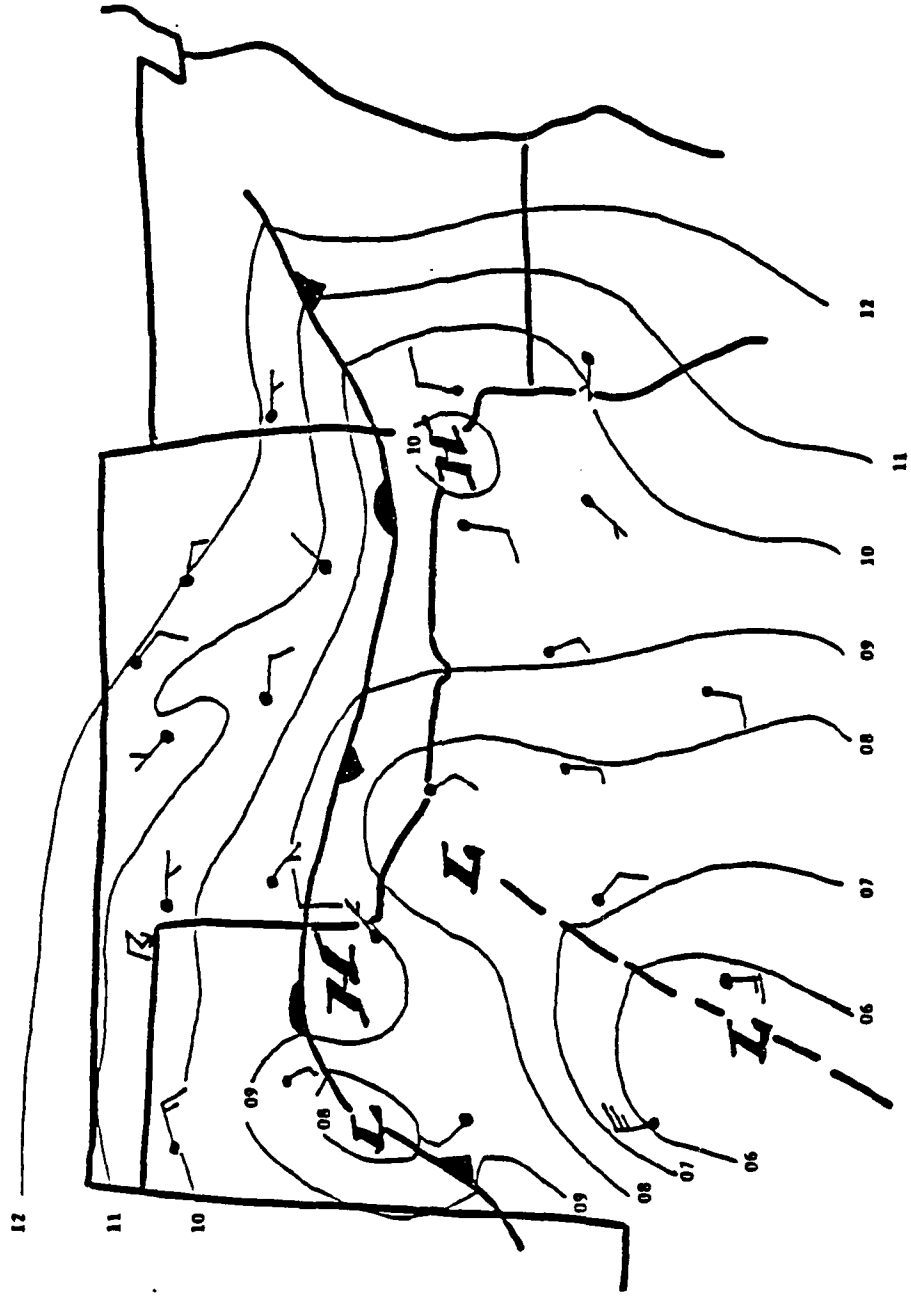

Fig. 55. The 1800 CST surface analysis.

The surface winds were southerly and normal to the stationary front on the warm air side of the boundary with the winds on the cold air side predominantly tangential to the front. Doswell (1982) identified this pattern as one which is the typical case in frontal overrunning situations.

2000 CST

At 2000 CST (Fig. 56) the low pressure area that was located in west Texas had divided and the associated cold front had moved eastward. The dry line had moved eastward also, extending southwestward from Wichita Falls, Texas. Upon examination of the NWS radar summary for 2035 CST (Fig. 57) an area of convection developed along the dry line as Rhea (1966) suggested. Also, north of the stationary front a broad area of precipitation developed as expected in typical overrunning situations. Several thunderstorms were reported at this time. The Norman, Oklahoma, Doppler weather radar reflectivity plot is shown in Fig. 58. In the vicinity of Norman, reflectivities were in excess of 50 dBZ. This particular storm developed into a supercell which produced a hook echo and 2 cm hail.

2200 CST

At this time widespread rainfall was reported over most of Oklahoma and central Texas. Surface reports in central Oklahoma near the city of Lindsay indicated 2 cm hail. In their analysis of the storm that affected Lindsay, VBDR discovered the storm produced a mesocyclone and a hook echo.

The surface analysis (not shown) indicated the frontal boundaries were nearly stationary. Many of the surface stations were reporting rain or thunderstorms at this time. Examination of the NWS radar summary plot showed many areas where

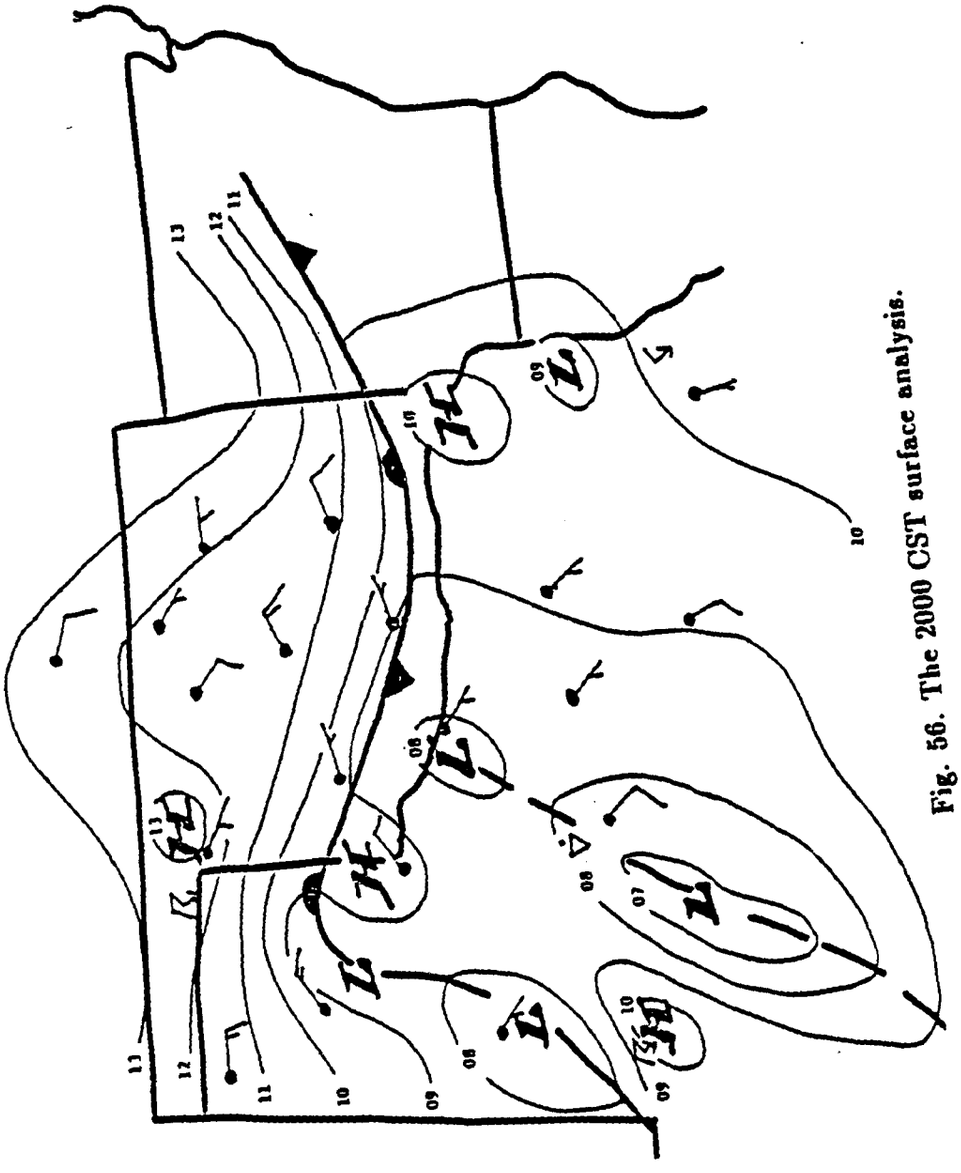

Fig. 56. The 2000 CST surface analysis.

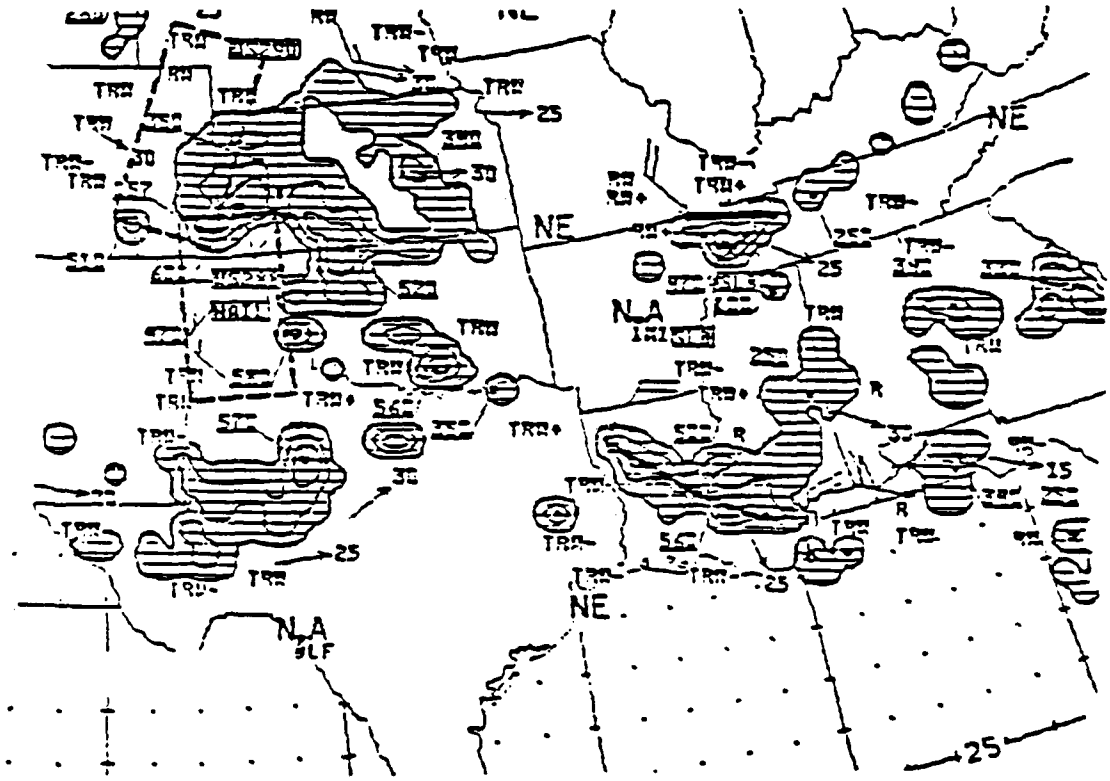

Fig. 57. The NWS radar summary for 2035 CST.

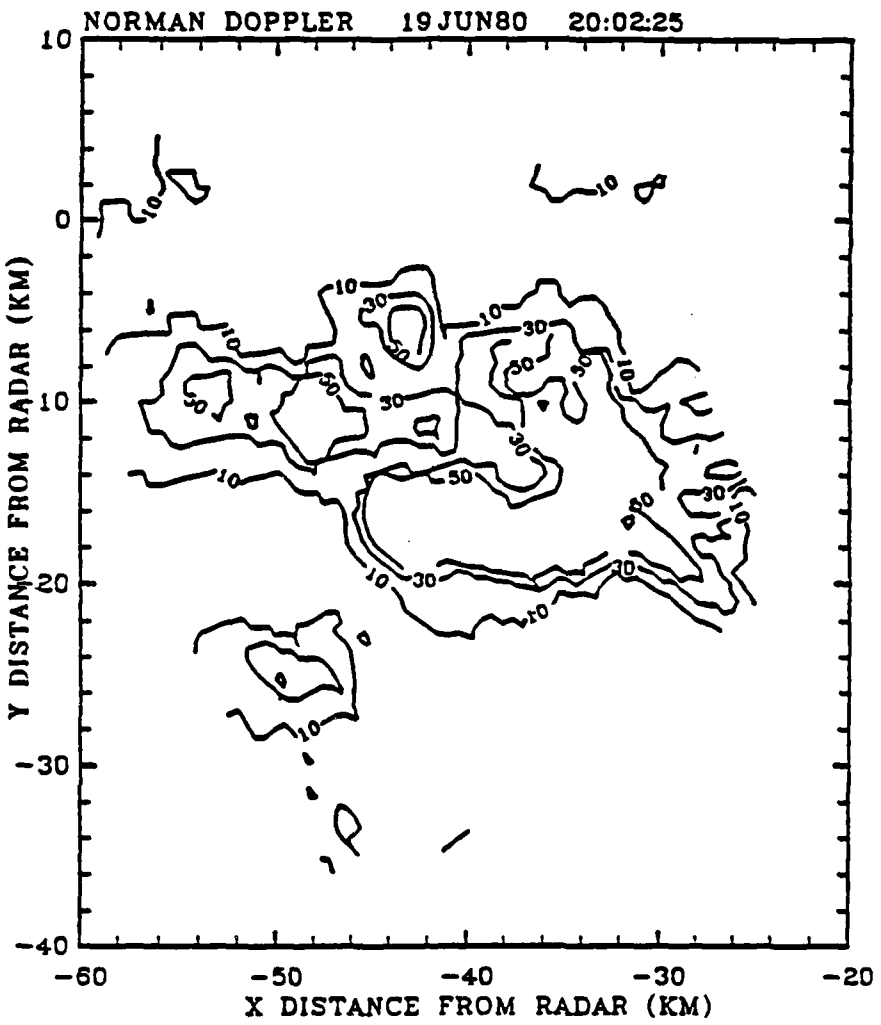

Fig. 58. The Norman Doppler radar reflectivity data for 2002 CST at 6 km AGL.

storms were in excess of 50 dBZ. The storm in the vicinity of Lindsay had developed into a thunderstorm with a maximun dBZ in excess of 60 dBZ. This was verified by the Norman Doppler radar. Fig. 59. is the radar reflectivity plot at this time. An area of greater than 10 X 10 km with greater than a 50 dBZ reflectivity could be seen, and embedded in this area were reflectivities greater than 60 dBZ.

As the storm dissipated, a gust front was produced (Klinge et al., 1987). It had a maximum radial wind of 17.5 ms^{-1}, with a minimum reflectivity along the gust front of 8.7 dBZ.

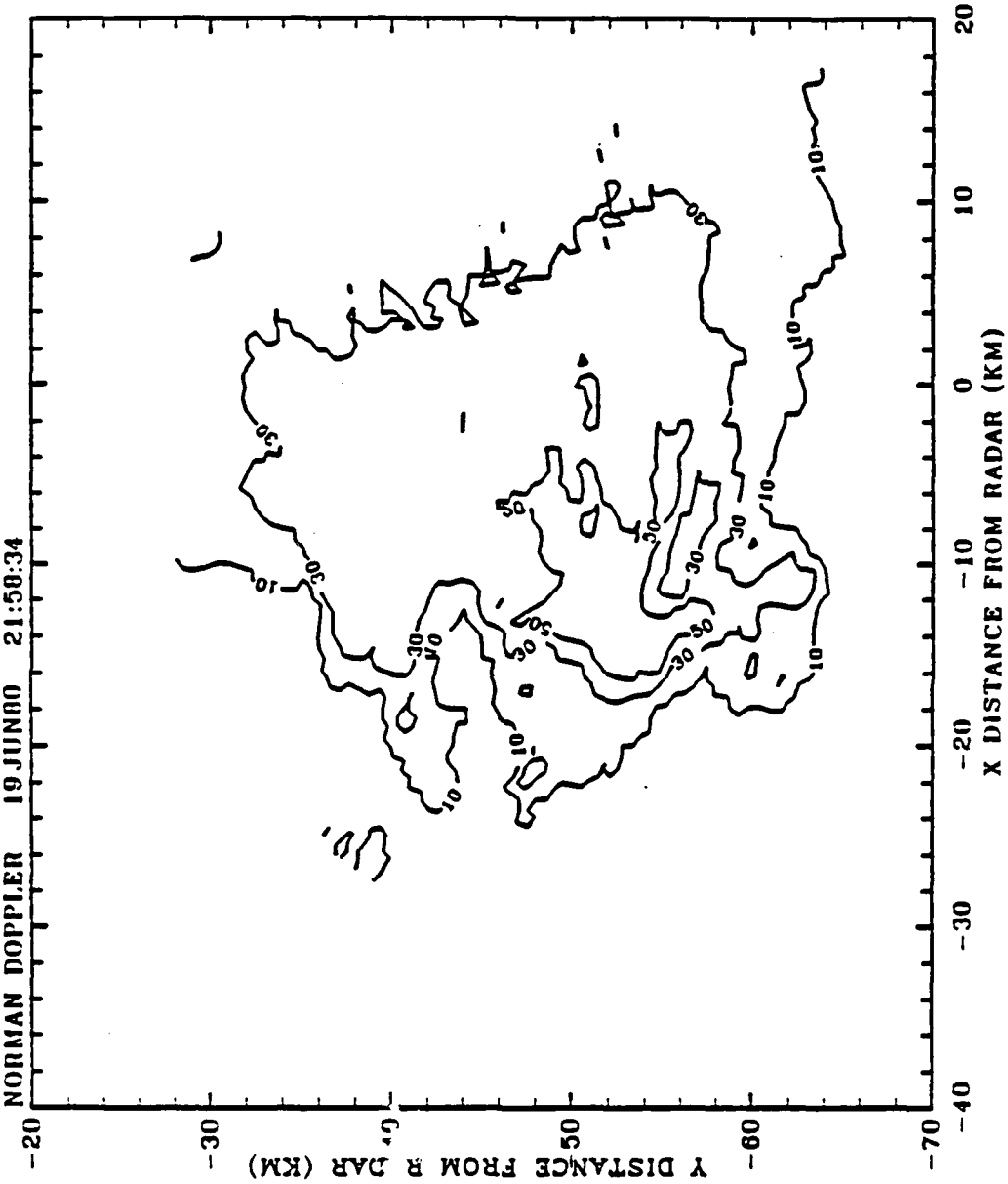

Fig. 59. As in Fig. 58, except for 2158 CST.

APPENDIX D

A COLD FRONTAL PASSAGE

Introduction

TREC was used previously to investigate the transition from a multicell to a supercell storm. The severe weather during that event was directly related to frontal overrunning. This appendix presents the results of using TREC during a cold frontal passage on 13 May 1985. The discussion will begin with a brief presentation of the mesoscale environmental conditions. Then an overview of the NOR Doppler radar data will follow. Finally, the results of the TREC analysis will be shown.

Mesoscale Environmental Conditions

The 1800 CST surface chart is shown in Fig. 60. A low pressure center was located in south central Kansas with an associated warm front extending through central Missouri. The cold front that accompanied this low pressure center extended from central Oklahoma into Texas.

The national radar summary at 1735 CST (Fig. 61) indicated a squall line approaching OKC with associated storm tops exceeding 12 km AGL. At this time central Oklahoma was under a severe weather watch till 1900 CST. The squall line was propagating southeastward with individual cells within it propagating northeastward.

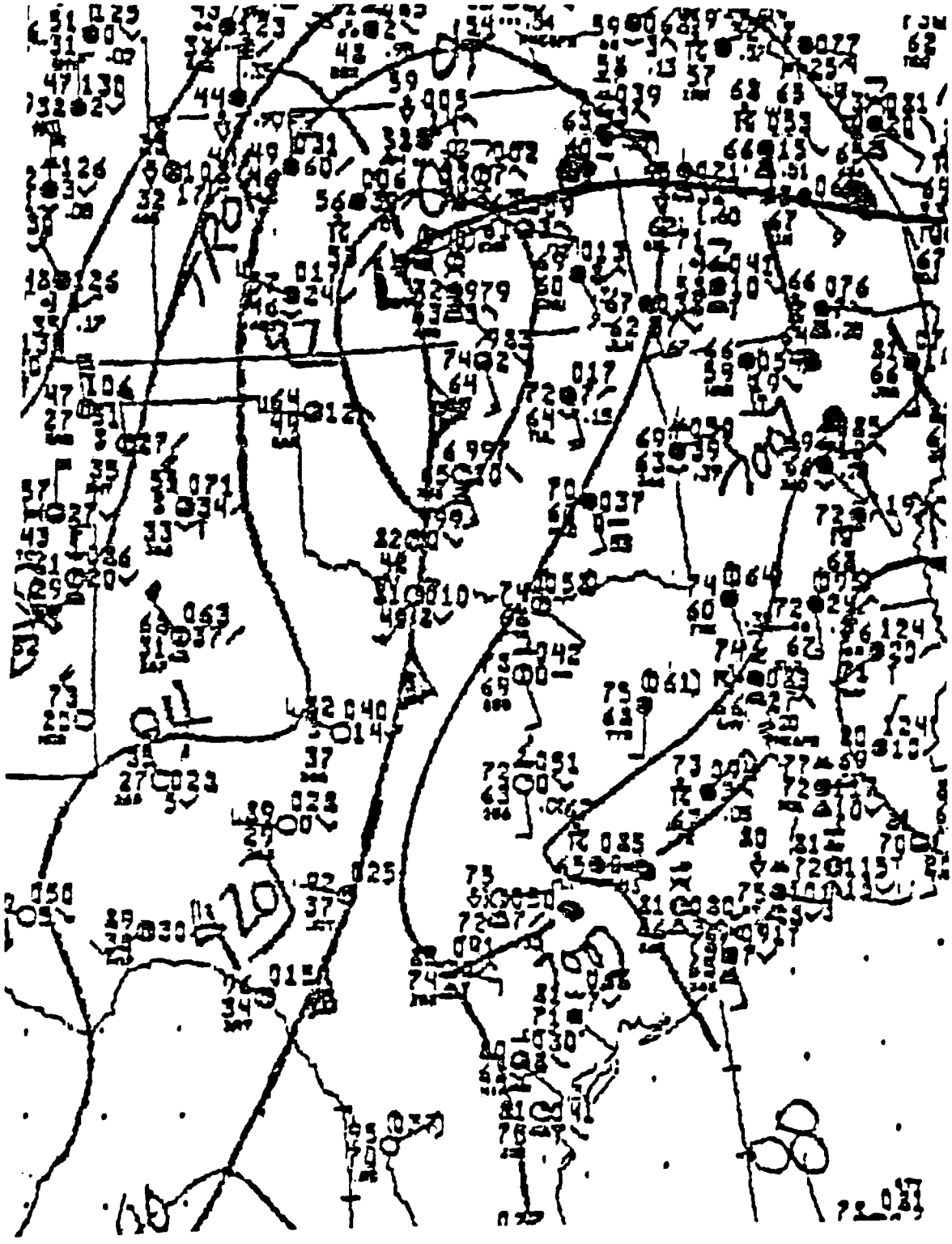

Fig. 60. The 13 May 1985, 1800 CST surface analysis.

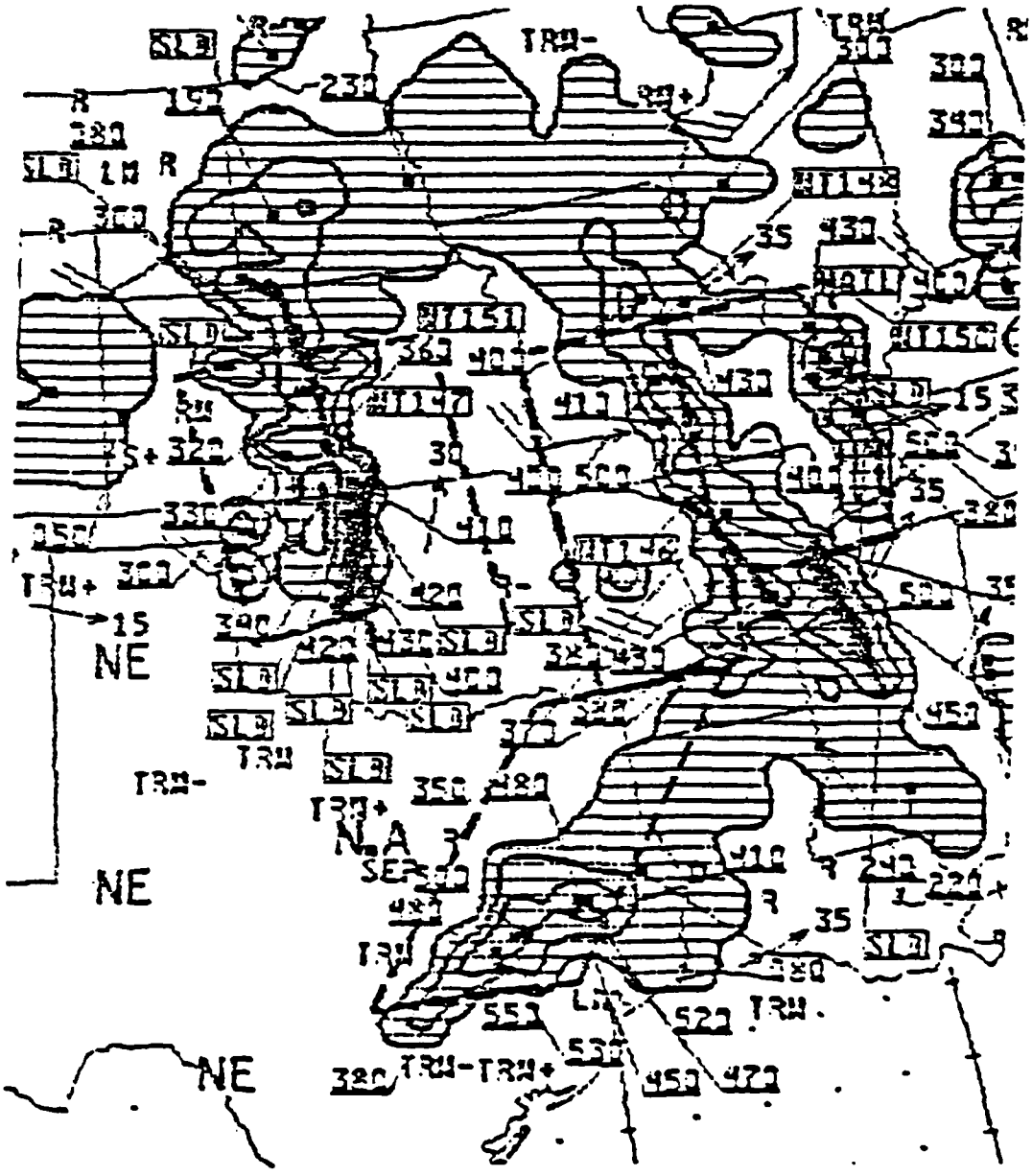

Fig. 61. The 13 May 1985, NWS radar summary for 1735 CST.

NOR Doppler Data

The Nor Doppler radar gathered data from 1700 CST to past 1900 CST; however, because the time increment between volume scans was greater than 10 min after 1740 CST, only the initial 30-40 min of data were usable for analysis. These data were gathered with a 2.5 min volume update with little interruption in data gathering. The radar scanned the northwest quadrant between azimuths 275 and 350 deg. A total of nine tilt angles were used with an average of 90 km to the leading edge of the squall line. As with the 19 June 1980 data case investigated earlier, these data were in UF and part of a dual-Doppler data set. However, for this case the CIM data were unavailable (Bumgarner, 1987). Also, these data have not been investigated by personnel at NSSL. It is a possible case to be studied later (Brandes, 1986).

Results of TREC Analyses

The 1 km AGL VMP field for 1717 CST is shown in Fig. 62. There are two major patterns, one centered at (-65,70) and the other being approximately 15 km long oriented southwest to northeast centered at (-52,86). Two smaller patterns are seen farther southwest. The largest pattern was clearly associated with a 50 dBZ cell shown in Fig. 63. The wind field in that vicinity indicated convergent flow centered at (-62,66). There was also a definite cyclonic circulation present. The wind field indicated that the primary flow feeding this region was from the south and east with a confluent area oriented northeast-southwest leaving this region apparently indicating the cell movement, which was northeast. Later time periods showed this cell tracking to the northeast.

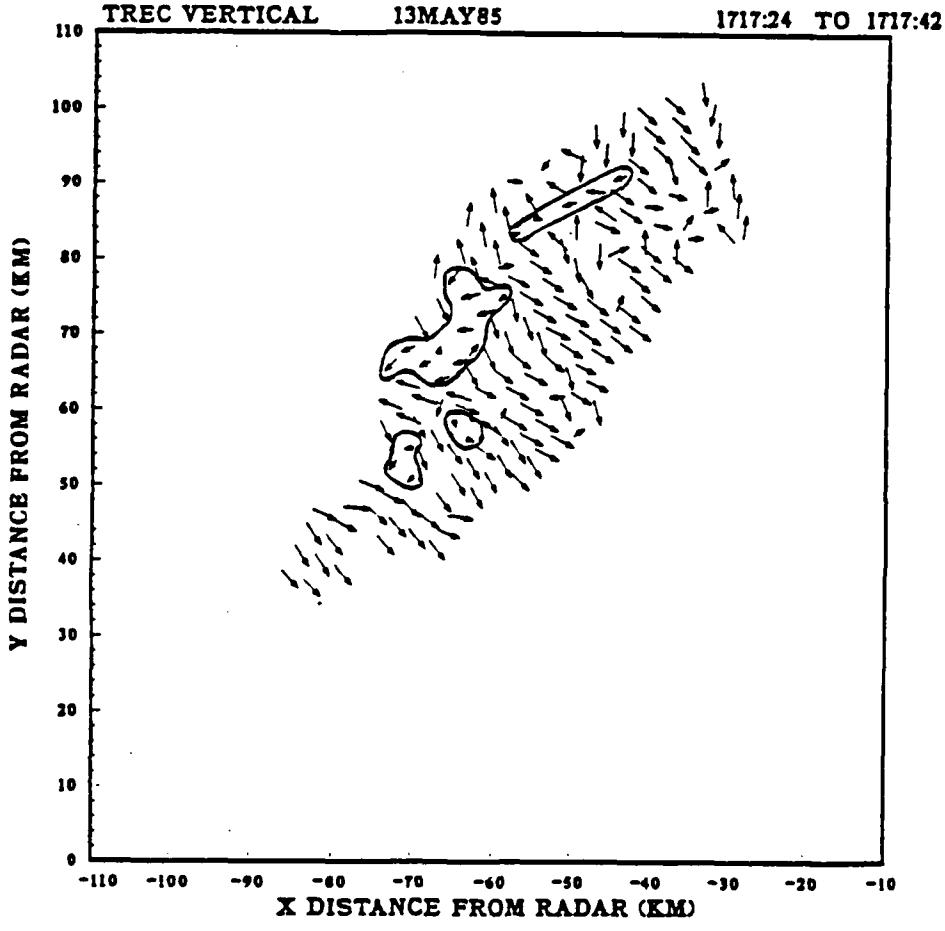

Fig. 62. The 13 May 1985, 1 km AGL VMP for 1717 CST.

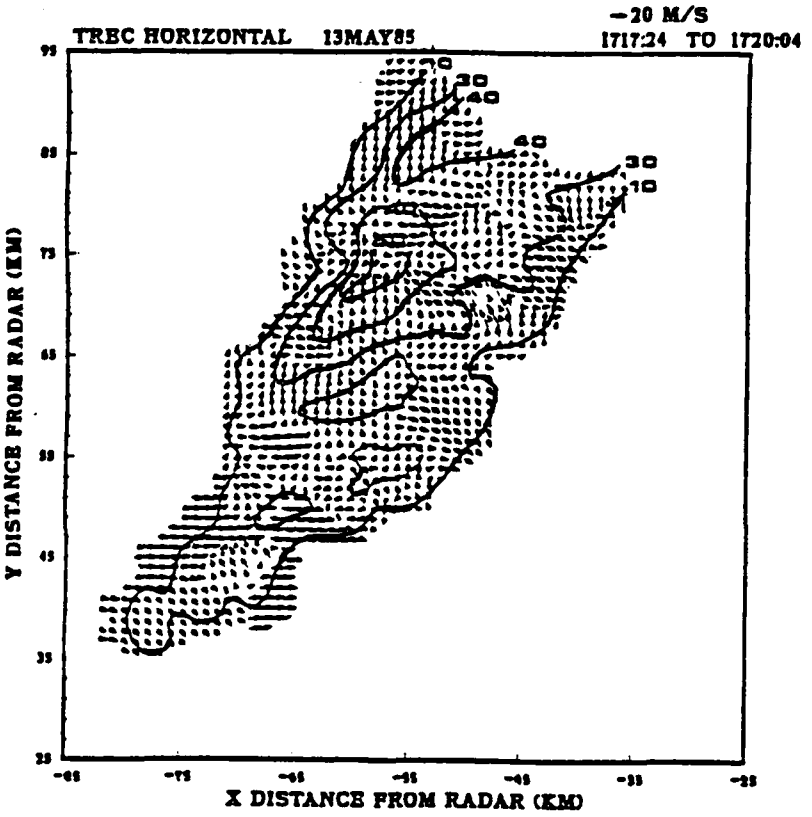

Fig. 63. The 13 May 1985, 1 km AGL horizontal wind and reflectivity fields for 1717 CST.

The two minor VMP located in the southwest were not associated with any convection at that time and were located in a region of relatively weak reflectivity. The horizontal wind field indicated confluent flow. Within 20 min that area was the site of a developing storm with a reflectivity greater than 40 dBZ.

The 6 km AGL VMP for this time period (Fig. 64) indicated that the two features discussed in the low levels were also evident at this level. The major feature associated with the 50 dBZ cell had been displaced with height to the east, whereas, the developing area to the south was located directly above the low level feature. Upon investigation of the horizontal wind field (Fig. 65) the wind flow in and around the northern VMP indicated winds up to 20 ms^{-1} feeding this storm. Also, the wind flow showed a predominant southwest flow. The developing area to the south was located in a region of 30 dBZ and 10 ms^{-1}. The wind field at this time was not very organized in this area, but changed as the storm developed.

The 6 km AGL vertical motion magnitudes (Fig. 66) indicated two maxima. Each one was associated with the two 50 dBZ cells within the derived VMP. The stronger of the two maxima was located in a confluent zone with southerly winds of 10-15 ms^{-1} converging with westerly winds of the same magnitude. Apparently, these two cells merged within 10 min, with the one located farther south overtaking the northernmost one. This new cell encompassed an area greater than 30 km^2.

A vertical cross section was constructed through the region of highest vertical velocities (Fig. 67). This area was completely under the influence of upward motion, which coincided with what was shown in Figs. 63 and 65. Also, an echo overhang had developed in the lower levels.

The VMP 10 min later had two separate areas (Fig. 68). The largest of the two was associated with the area of convection in the northern portion of the

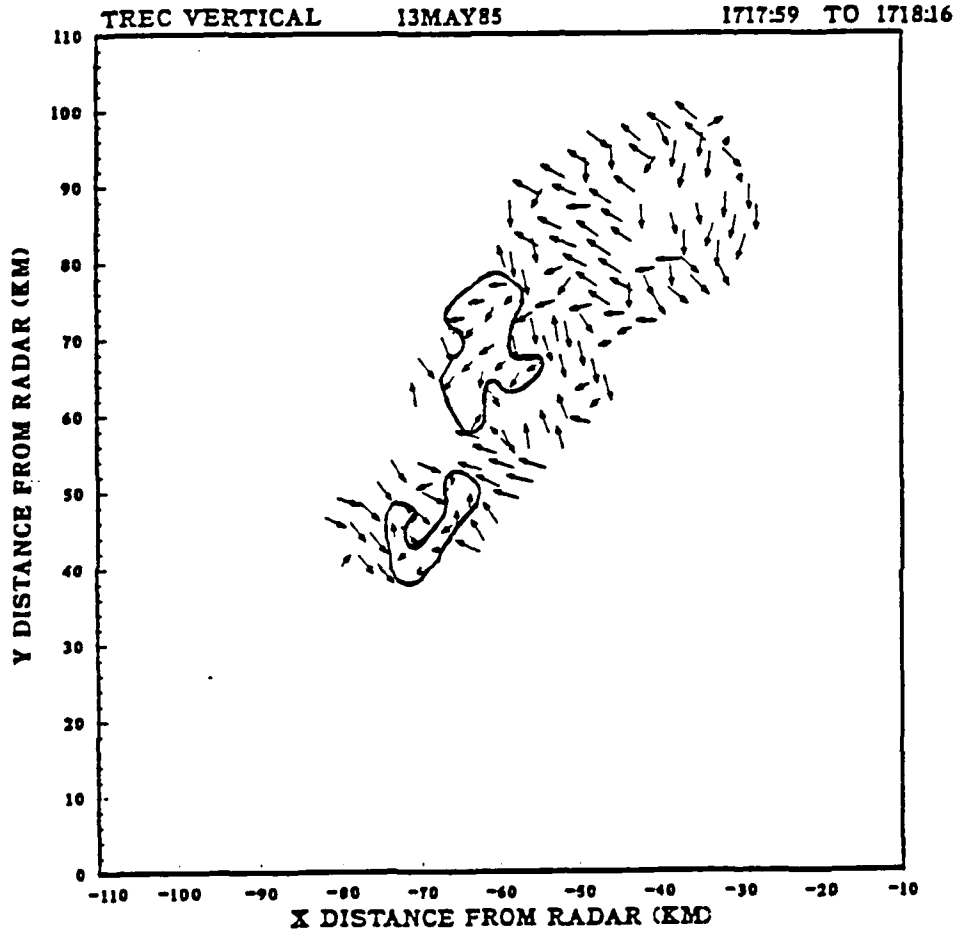

Fig. 64. As in Fig. 62, except at 6 km AGL.

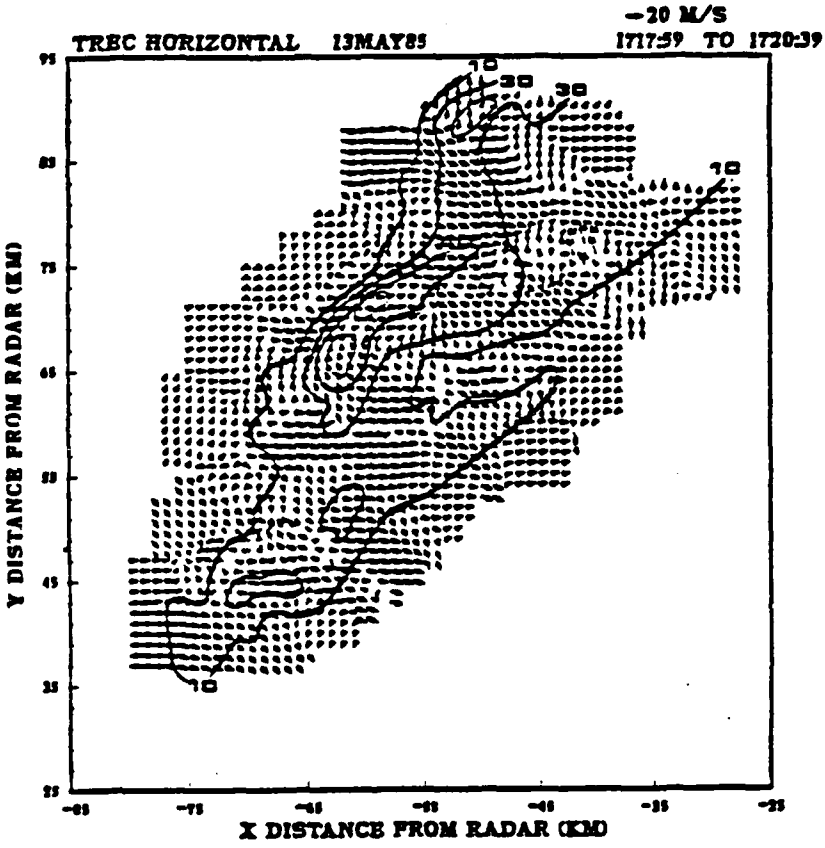

Fig. 65. As in Fig. 63, except at 6 km AGL.

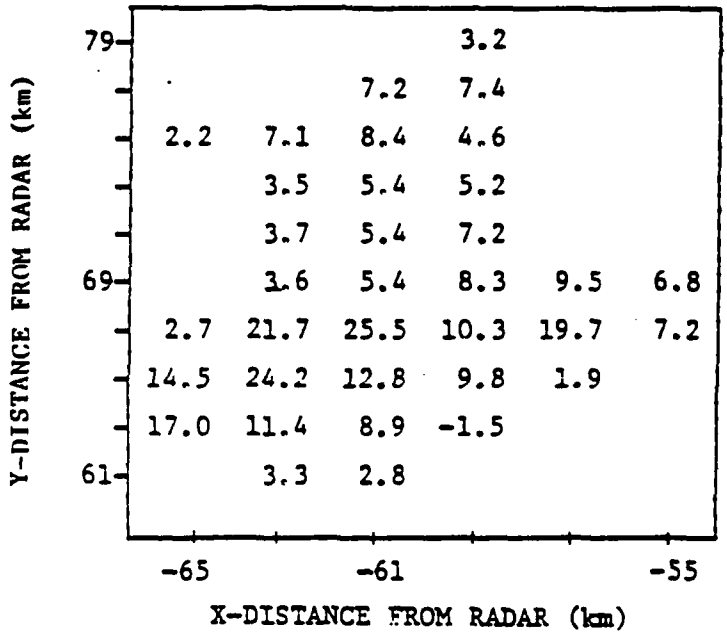

Fig. 66. The 6 km AGL TREC derived vertical motion magnitudes for 1717 CST.

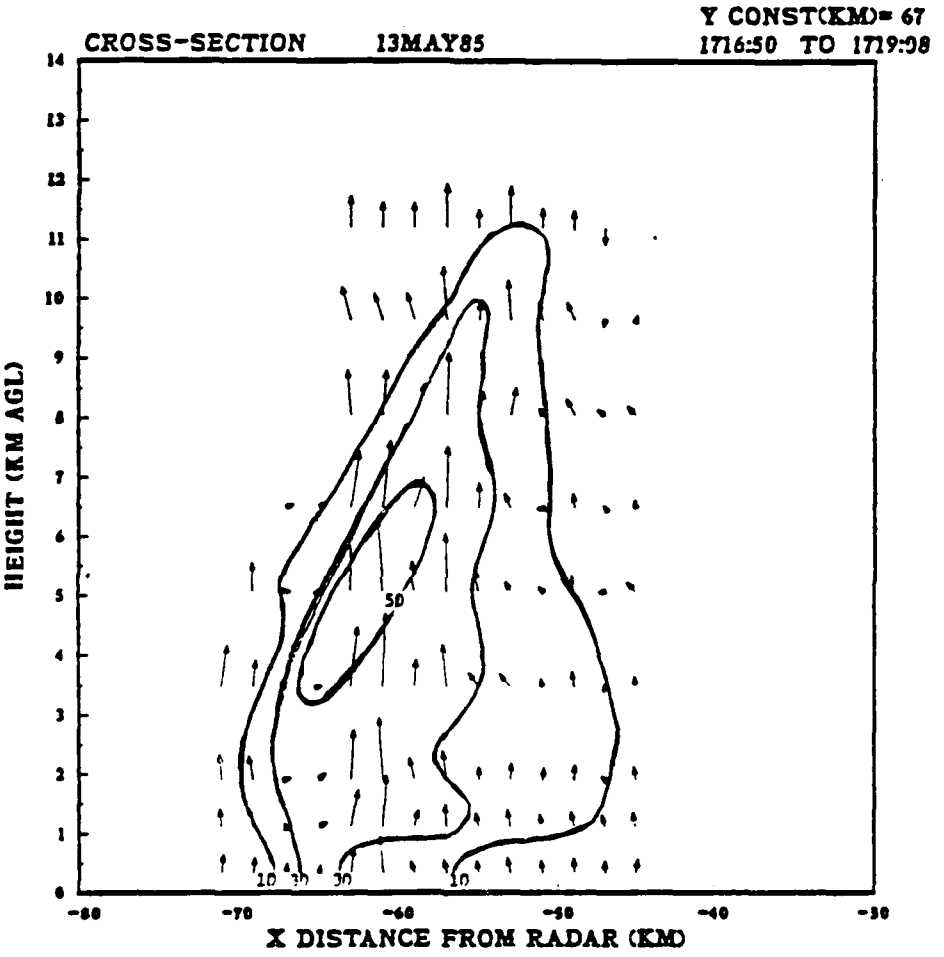

Fig. 67. Norman Doppler radar vertical cross-section and reflectivity field at y=67 km for 1717 CST.

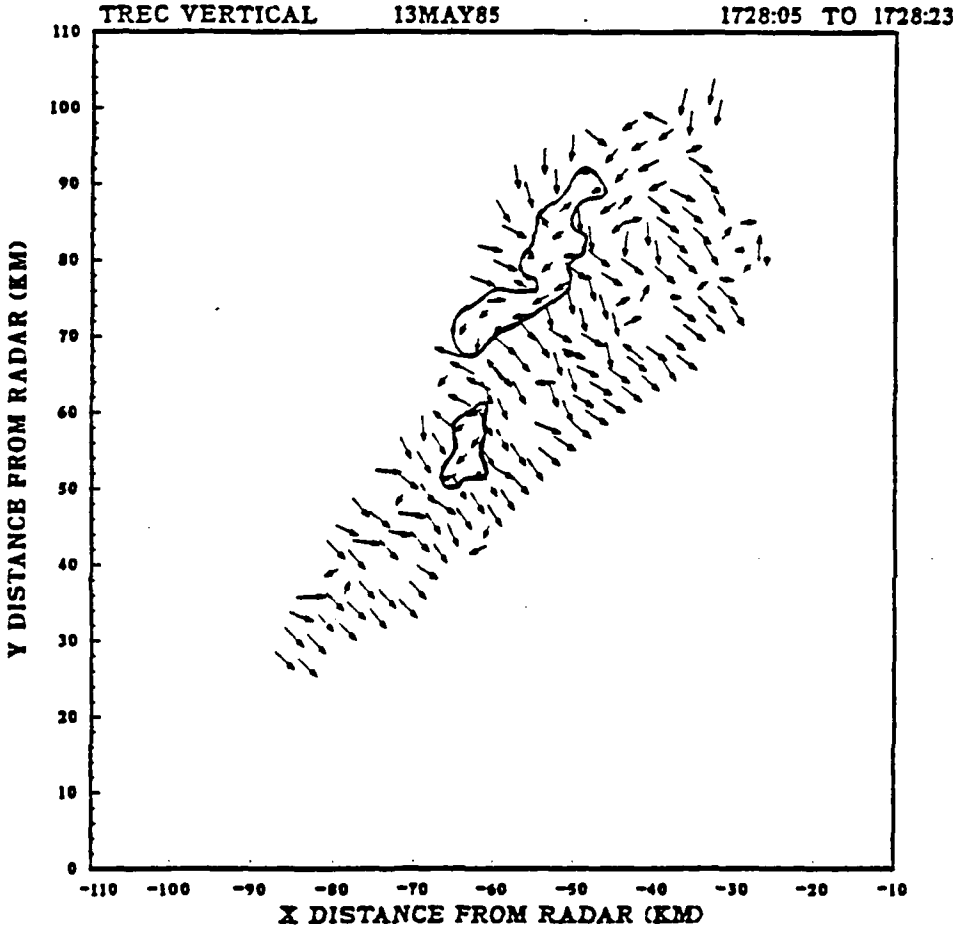

Fig. 68. As in Fig. 62, except for 1728 CST.

field, where the two 50 dBZ cells merged. The smaller of the two VMP was an indication of the vertical motion that resulted from the developing 40 dBZ cell in the southwestern portion of the squall line. These patterns were related to the horizontal wind patterns in Fig. 69. The larger of the two corresponded to deep convection centered at (-53,73). It had a shape almost identical to that of the parent storm. A definite cyclonic circulation was evident in this region. The smaller pattern centered at (-63,54) was located in a region of only 30 dBZ, but the wind field indicated a converging of the winds. In fact, the 6 km AGL wind field (Fig. 70) showed that this region had a definite convergent flow. This region had increased in intensity to over 40 dBZ. The cell associated with the largest VMP in the north had reach maturity with the 50 dBZ area encompassing over 30 km^2. It had an updraft of 20 ms^{-1}. The magnitude of the updraft for the developing cell in the southwest had reached 15 ms^{-1} and coincided with an area of convergence located at (-63,49). Another cell was developing in an area of convergence at (-59,63) and already had developed an updraft of 10 ms^{-1}. Within 20 min this area increased to a reflectivity of 40 dBZ and an updraft of 20 ms^{-1}.

At 1733 CST the VMP for the lower levels (Fig. 71) indicated several areas of possible vertical motions. One area was actually a triad of areas centered at (-46,81) that was associated with the large thunderstorm discussed earlier. The pattern presented was similar to that described by Lemon and Doswell (1979) in their Fig. 9. The couplet oriented northwest-southeast was the same in appearance as their divided updraft associated with a mesocyclone. The VMP northeast of these patterns was in the same location as their forward flank downdraft. Apparently, TREC was indicating the VMP associated with a mesocyclone.

The horizontal wind field derived by TREC for 1 km AGL is shown in Fig. 72.

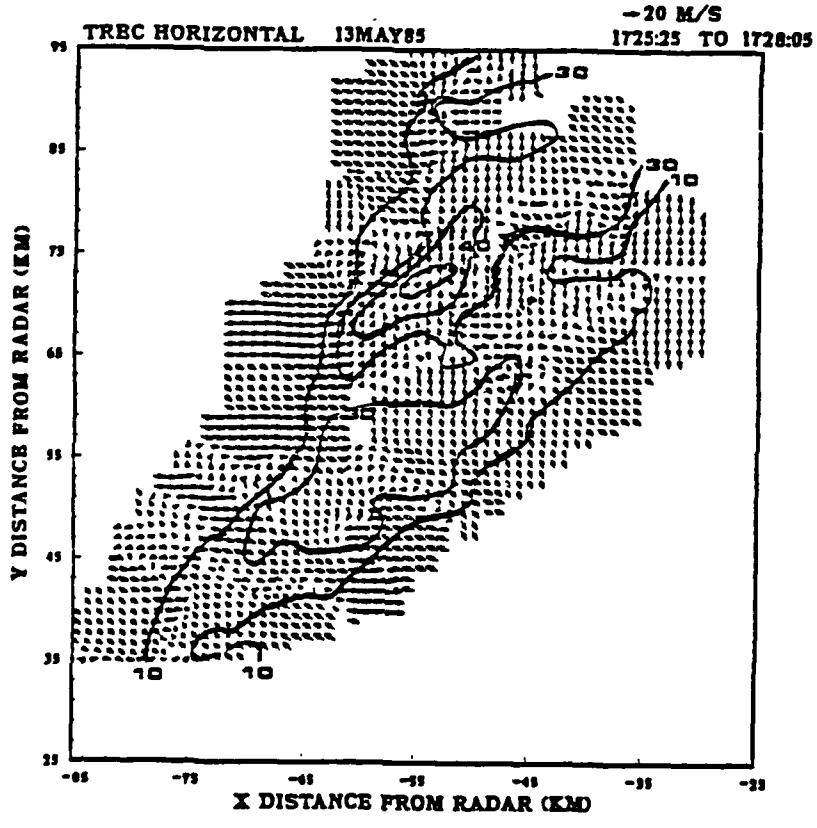

Fig. 69. As in Fig. 63, except for 1725 CST.

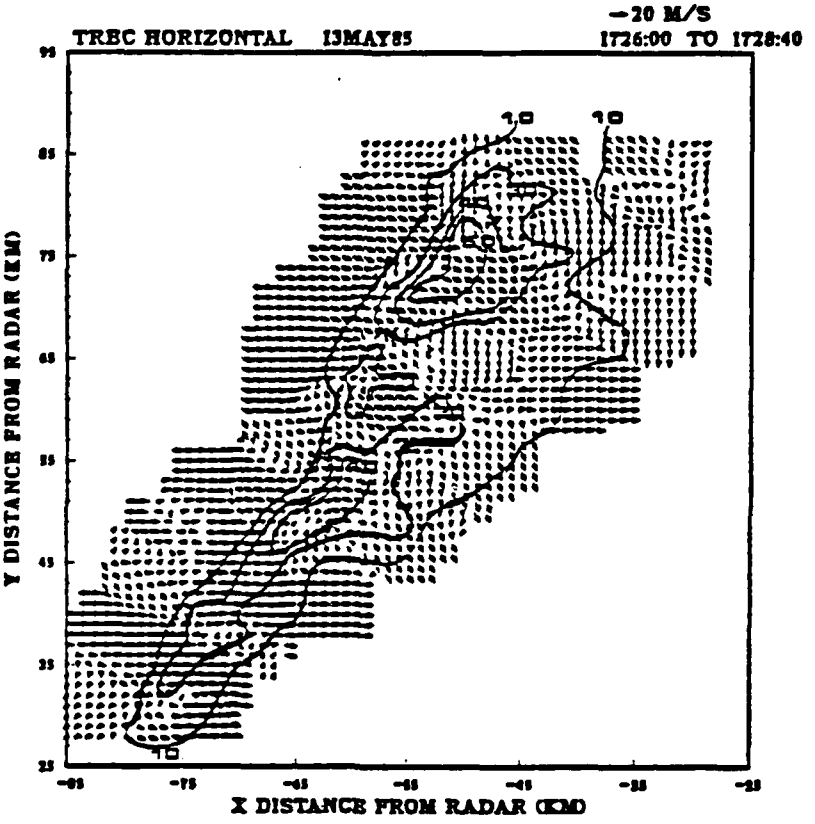

Fig. 70. As in Fig. 63, except at 6 km AGL for 1726 CST.

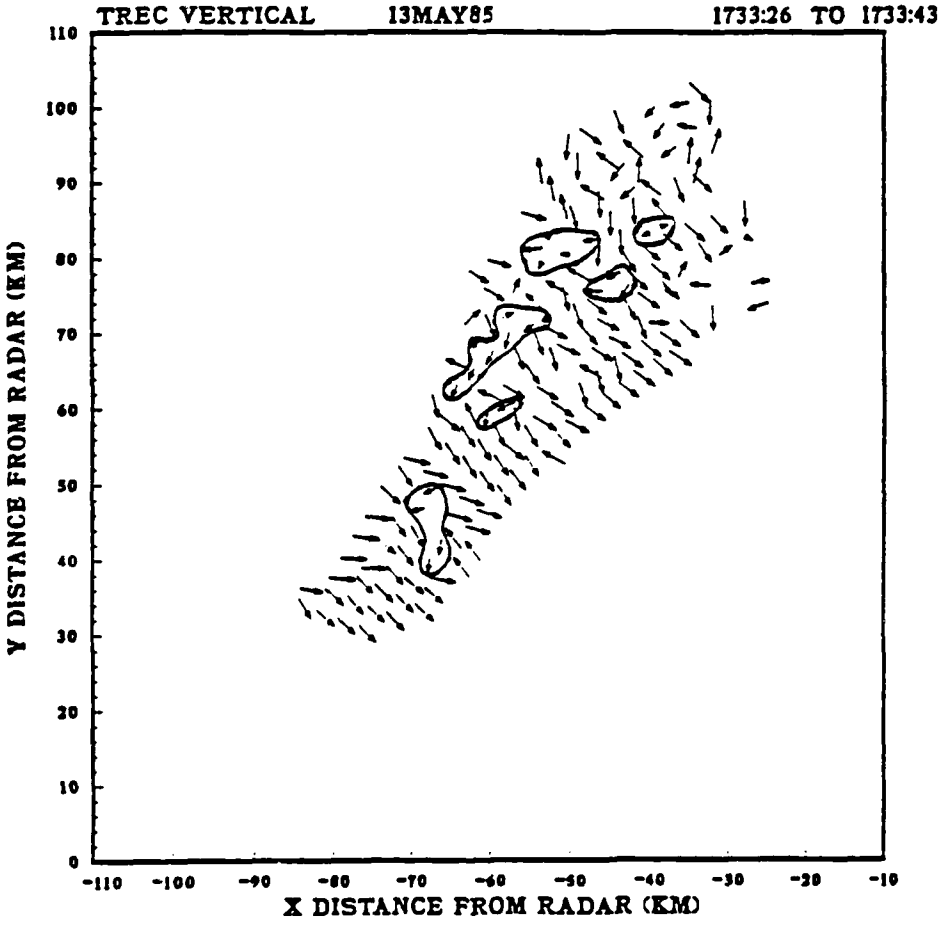

Fig. 71. As in Fig. 62, except for 1733 CST.

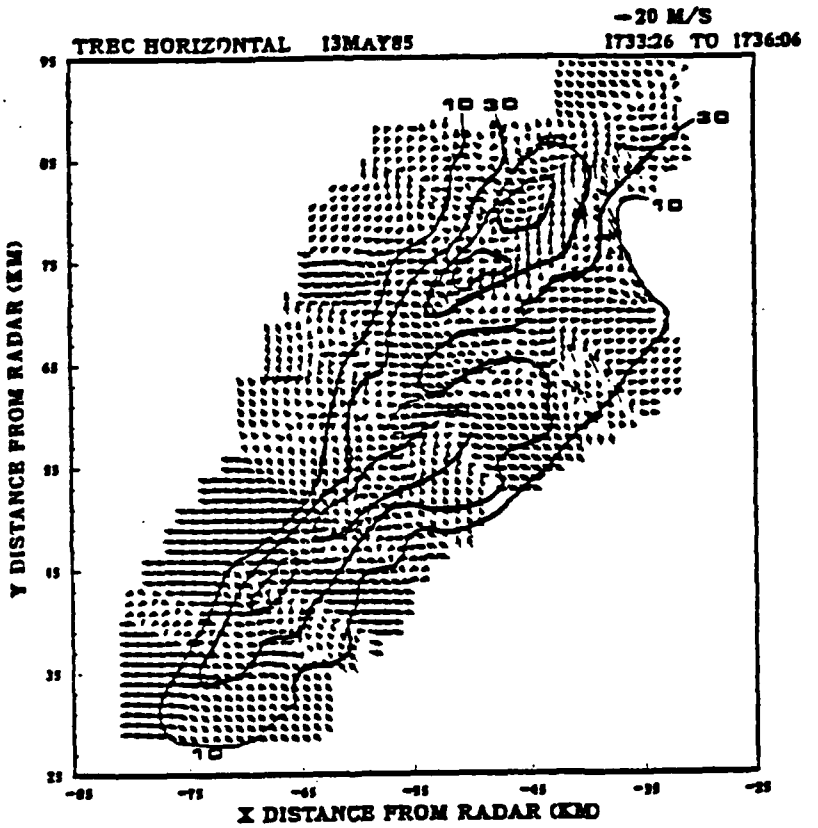

Fig. 72. As in Fig. 63, except for 1733 CST.

The wind flow in and around the large cell was similar to that described by Lemon and Doswell (1979) in their Fig. 7. Winds feeding the storm were from the the south to southeast, whereas, the wind pattern northeast of the storm flowed away in a northwest direction. The overall storm movement was to the northeast. The developing cell in the southwest did not have a definitive wind pattern at this time. TREC indicated an area of convergence that coincided with the VMP for this cell.

The 6 km AGL VMP (Fig. 73) did not indicate the divided structure noted in the lower levels for the storm in the north. It indicated two separate regions of vertical motion with one located northeast of the other. This could have been an updraft/downdraft couplet.

The horizontal wind field for 6 km AGL is shown in Fig. 74. It indicated predominantly south to southeasterly winds converging with westerly winds for the storm in the north. The winds did not veer with height as much as would be expected. This was the same problem encountered with the 19 June 1980 case, when the storm reached supercell stage.

The developing cell to the southwest did have a fair amount of vertical wind shear. This storm was still in the developmental stage and TREC was able to model the winds in a more accurate fashion. The derived vertical motion magnitudes for this area indicated that the VMP centered at (-59,49) was a downdraft of -3.5 ms^{-1}. The pattern centered at (-65,41) had a maximum updraft of 16 ms^{-1} (Fig. 75).

A cross section was constructed through the center of the updraft pattern located at y=73 km (Fig. 76). The major updraft was seen as a continuous event through the entire storm. East of the major updraft an area of downward motion was found in the middle-levels, then another updraft was seen. This downward pattern could possibly have been a wake high with the other upward pattern being

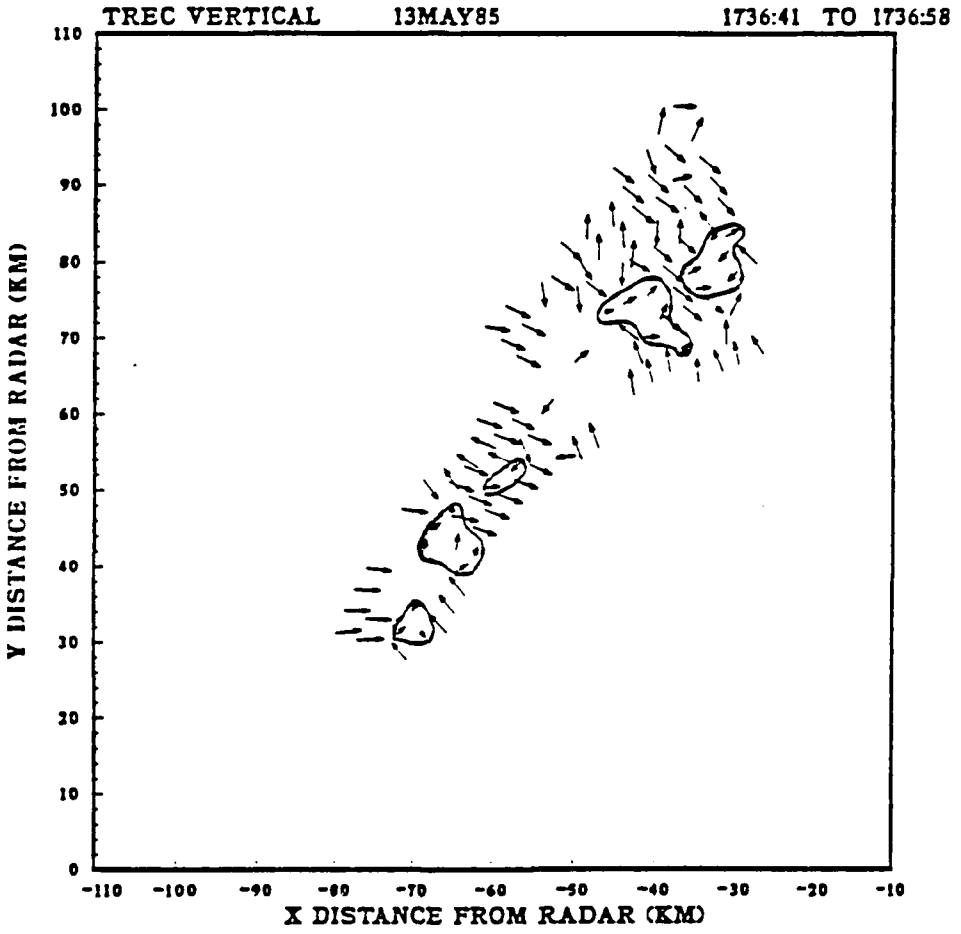

Fig. 73. As in Fig. 62, except at 6 km AGL for 1736 CST.

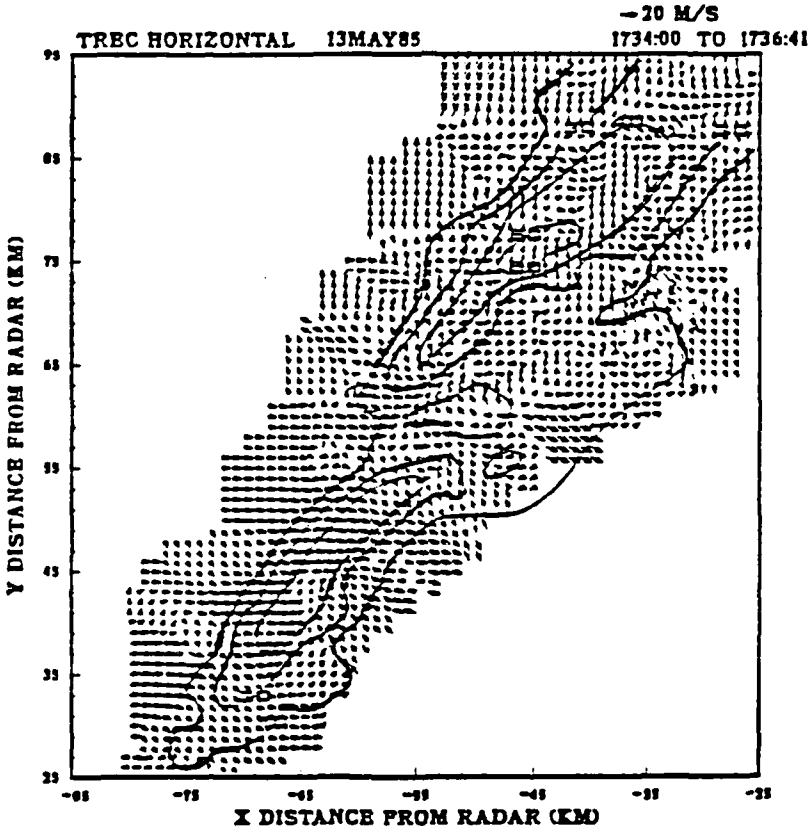

Fig. 74. As in Fig. 63, except at 6 km AGL for 1734 CST.

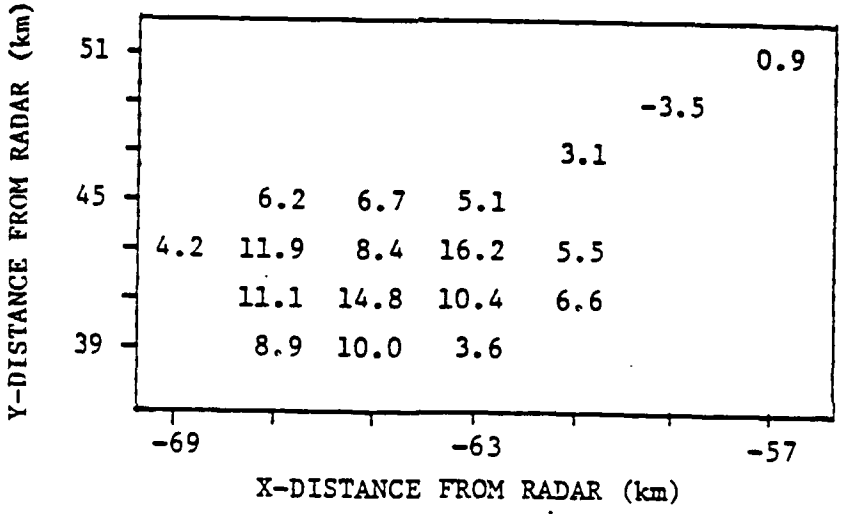

Fig. 75. As in Fig. 66, except for 1733 CST.

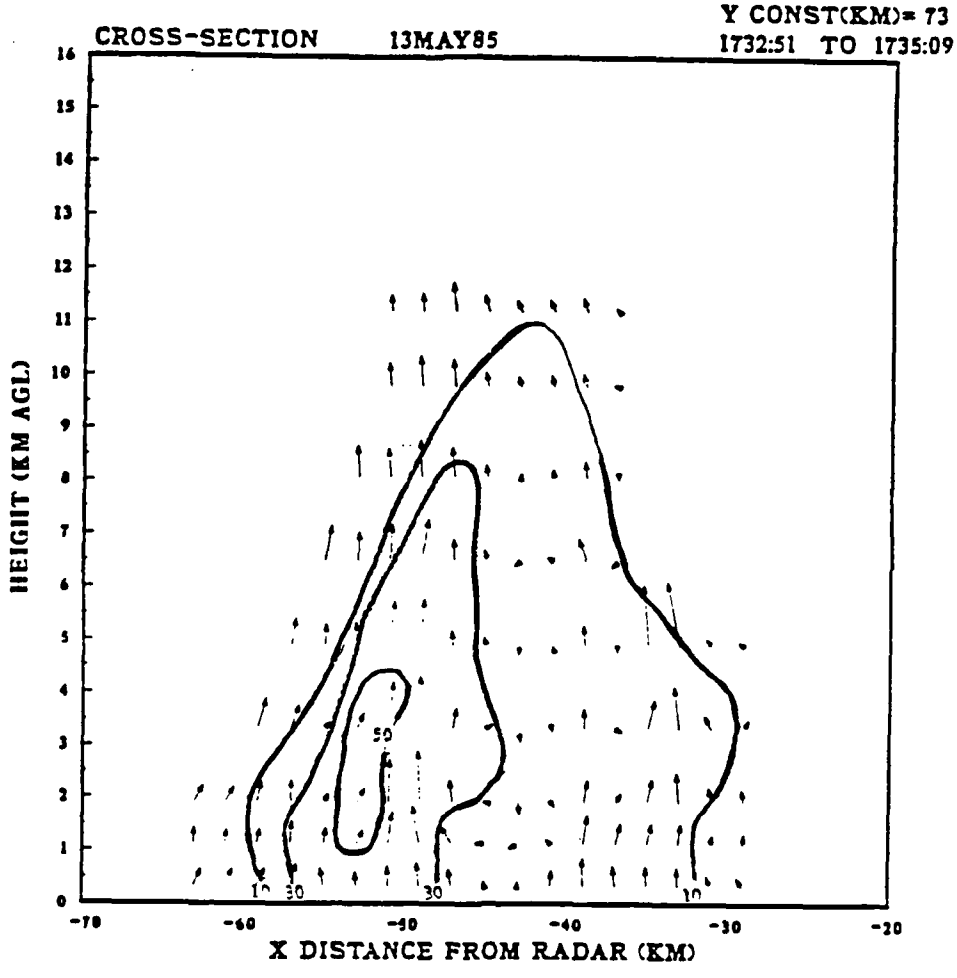

Fig. 76. As in Fig. 67, except at y=73 km for 1732 CST.

another cell developing.

After this time period the radar data were gathered with a ten min volume update. This made further analysis with TREC unwise. However, during the time periods discussed, TREC was able to model both developing and mature storms with some validity.

VITA

Robert Monroe Cox [redacted]. His parents , Mr. And Mrs. Charles N. Cox, were in the U. S. Air Force (USAF). Upon his father's retirement from the USAF in 1967 as a Chief Master Sergeant, they settled in Zephyrhills, Florida. Robert graduated from Zephyrhills High School in 1975 and began studies at the University of South Florida (USF). He earned a B.S. in Clinical Chemistry and Religious Studies in 1980 from USF. That year he married the former Rita S. Eitutis of Treasure Island, Florida, and entered the USAF. After a year of meteorology training at Saint Louis University he served as a Data Base Analyst at USAFETAC, Scott AFB, Illinois. During the time he was stationed there he earned his Master of Science degree in Meteorology from Saint Louis University. Upon graduation he served as Wing Weather Officer at Osan AB, Korea, in 1984. Next, he attended the USAF Squadron Officer School at Maxwell AFB, Alabama. In June, 1985, he entered Texas A&M University to seek the degree of Doctor of Philosophy under the Air Force Institute of Technology sponsorship. He and his wife have two children, Kyle Joshua and Sarah Grace. [redacted].